Flinders
UNIVERSITY

Fault Detection and Diagnosis Using Beard-Jones Filter

by

Rui Hou, M.Eng. (Electronics)

Supervisor: Fangpo He

Date of submission: May, 2018

Submitted to the College of Science and Engineering in partial fulfilment of the requirements for the degree of Master of Engineering (electronics) at Flinders University – Adelaide Australia

Declaration

I certify that this thesis does not incorporate without acknowledgment any material previously submitted for a degree or diploma in any university, and that to the best of my knowledge and belief it does not contain any material previously published or written by another person except where due reference is made in the text.

Date: July, 2018

Acknowledgement

First, I'd like to say thank you to my supervisor, Fangpo He, I'm inspired by her encouraging persistence and dedicated work style. I really appreciate her valuable help and encouragement to my project.

And I'm thankful to ph.D. student Peng Zhang, for his kindness in helping me during the project.

Also, I want to say thank you to all related staff that helped a lot in many ways, thank you for your patience and kindness.

Finally, special thanks to my wife, thanks for your selfless support all the way from China to Australia.

Abstract

It is well known that, for many engineering systems, such as aircrafts and vehicles, there is a high demand for maintaining a system's safety during its operation. A fault in a system may lead to a complete break-down of the system operation. The detection and the handling of faults therefore play an important role in the design and operation of an engineering system.

In this project, a fault detection and diagnosis system using the concept of the Beard-Jones (BJ) filter is designed and demonstrated for a Multi-Input Multi-Output (MIMO) mechanical plate structure. The structure includes a top plate, a base plate, a disturance transducer, and three pairs of co-located sensors and actuators that bond the top and base plates together. Structural vibrations introduced by the disturbance transducer at the base plate are controlled by the three sensor-actuator pairs, such that the top plate can remain stationary despite the constant vibration excitation induced from the base plate. The main goal of the fault detection and diagnosis system is to detect and identify each actuator fault that may occur during the operation of the MIMO control system.

A transfer function representation of the plate structure is constructed through dedicated theoretical analysis and physical experiment. The theoretical analysis aims to derive the general mathematical expression of the transfer function model while the physical experiment, using the ModalVIEW software, aims to produce the parameters (such as mode shapes, damping ratios, and natural frequencies) of the transfer function model. For the purpose of fault detection, a state-space representation of the system with a defined dimension representing a pre-selected frequency range of concern is developed based on the identified transfer function representation of the system.

A fault detection process is constructed using the BJ filter detection theory that offers a set of straightforward design and implementation properties with a wide range of applicability. Essentially, a BJ filter acts as a state observer and produces the estimated output of a system under no-fault operation conditions. When a fault vector $\boldsymbol{f_i}$ is introduced into the system, the output difference between the fault system and the BJ filter will produce a specific directional residual associated with the fault such that the value of the output residual is stable and proportional to $\mathbf{C}\boldsymbol{f_i}$ (where $\mathbf{C}$ is the output matrix of the system). The key in designing the BJ filter is therefore to construct the detection gain matrix $\mathbf{L}$ based on a set of design criteria and

restrictions. In particular, for a multiple-fault detection, two restrictions, namely the mutual detectability and the output separability, will need to be checked in priority.

In order to validate the BJ filter design principle and procedure, a random system with pre-defined fault vectors is first tested via simulation in MATLAB SIMULINK. A conceptual BJ filter structure for the underlying plate control system is then designed (assuming the satisfaction of the design restrictions) and tested in MATLAB SIMULINK via different configurations (namely, SISO configuration – considering one pair of the inputs and outputs of the real system only, 2I2O configuration – considering two pairs of the inputs and outputs of the real system only, and MIMO configuration – considering all three pairs of the inputs and outputs of the real system, respectively). Simulation results confirm that the designed conceptual BJ filters are able to detect the pre-defined faults in the both the random and the real plate systems successfully.

Upon the validation of the conceptual BJ filter design principle and procedure, an operable BJ filter is designed specifically for actuator fault detection of the given plate control system in real-time operations. Considering that the initial state-space model of the given plant does not meet the output separability requirement of the BJ filter design, an extended model of the system is proposed where the derivative of each output is included in the system output vector, thus extending the existing system from 3I3O to 3I6O. Such an arrangement guarantees that the extended system, while keeping the features of the original plate control system, provides a revised form of the system output matrix that satisfies the output separability requirement. The corresponding extended version of the BJ filter, capable of performing real-time actuator fault detection and diagnosis of the given plate control system, is then designed and validated via simulation in MATLAB SIMULINK.

The designed real-time BJ filter is finally tested via experiment. For effective actuator fault detection and diagnosis, a dual BJ filter configuration is implemented where one BJ filter acts as an online observer of the given plate system by producing the extended system output from the truncated model of the true plant, and another BJ filter acts as a fault detector and identifier by producing the required residual proportional to $\mathbf{C}\boldsymbol{f_i}$ (where $\mathbf{C}$ is the output matrix of the extended system). This arrangement takes into account the inevitable modelling errors between the real plant and the modelled plant used for the BJ filter design purpose, and increases the accuracy of the fault detection and identification in practice. A set of experimental data is

obtained that verifies the design and implementation of the proposed BJ fault detection and diagnosis system for real-time operation of the given MIMO plate control structure.

List of Figures

Contents

Chapter 1 : Introduction

In this chapter, the project background is introduced in the first section to briefly state the aims and motivation of this thesis and the second section outlines the structure of the thesis.

1.1 Project Background

Control systems have been integrated into multiple aspects of modern life. They appear in cars, washing machines, and elevators as well as modern engineering systems such as aircraft, mass transit vehicles, and ships, which have all become more complex and automated in order to meet increasing demands for better performance and cost efficiency. This has in turn increased demand for guarantees of operational safety and reliability in these systems. A fault in a control system is caused by an unallowable deviation from the normal operating condition of the system and will usually appear without any indication [1, 2 and 3]. Due to the unpredictability of such events, faults are often difficult to be detected in a timely manner and may not be amenable to protective measures. A fault may not only lead to declines in a control system's performance, but also the possible collapse of the entire control system. A very small fault in a control system with strict requirements for system safety, such as in an airplane, can cause a catastrophe with significant casualties and economic losses. Several examples of such serious disasters are given below:

Case 1: On 26 April 1986, reactor No.4 at the Chernobyl nuclear power plant exploded, and a large amount of radioactive material was leaked. Serious radiation resulted in 31 deaths within three months of the accident, and, in all, over 60000 people had died of side effects of nuclear radiation after 15 years. This disaster was the biggest accident since the beginning of the nuclear power Era, and the main reason for the disaster was a lack of fault detection and poor handling techniques [4].

Case 2: On July 4, 1996, the Ariane 5 rocket exploded 77 seconds after launch. The reason was an abnormal transmission of information in the Inertial Reference Unit, which provided incorrect altitude and tracking information to the control systems [5].

Case 3: On May 25, 1979, a McDonnell-Douglas DC-10 aircraft (AMERICAN AIRLINES flight 191) crashed at Chicago O'Hare International Airport. At that time, 271 passengers on the airplane and 2 persons on the ground died [6]. This was caused by a malfunction in the leading-edge slat assembly.

These massive disasters have caused people to think about what can be done to prevent such things from happening. Although the occurrence of a failure is rarely completely preventable, analysis of accident results indicates that the most serious consequences of such failures can be avoided, and that casualties and property losses can be minimized or mitigated. If fault information can be detected quickly enough, it is possible to ensure the safe operation of a control system, to gain enough time for the system to stop safely and for maintenance to be implemented. In Case 1, a safety shutdown should have been added to the system so that such reactions could be stopped immediately, before the risk of explosion. In Case 2, the incorrect information from the Inertial Reference Unit could have been detected if there had been sufficient redundancy in the system (another sensor) so that the tracking information could be compared with the expected data. In Case 3, a backup control system to control the aircraft in the case of jammed components was required.

All these examples illustrate the increasing demand for fault detection, fault diagnosis, and fault-tolerant controls to maximize the safety and reliability of a control system's real-time operation. This is thus the motivation of this thesis, which mainly focuses on the fault detection and fault diagnosis of a mechanical plate structure.

1.2 Outline of This Thesis

In this thesis, a fault detection and diagnosis system using the concept of the Beard-Jones (BJ) filter is designed and demonstrated for a Multi-Input Multi-Output (MIMO) mechanical plate structure with three pairs of sensors and actuators. The outline of this thesis is as follows:

In Chapter 2, an overall literature review is presented. System identification and fault classification methods are introduced in detail. Different fault detection approaches, as well as their applications, are analyzed and compared.

In Chapter 3, the feature and characteristics of the MIMO mechanical plate structure used in this study are described. Based on the theoretical analysis and physical experiment, the procedure of building the mathematical model of the plate is illustrated in detail.

In Chapter 4, as the core of the fault detection approach adopted in this thesis, the Beard-Jones filter is discussed in detail. The structure of the Beard-Jones (BJ) filter which forms the basic concept in the fault detection approach is introduced firstly. The BJ filter fault detection theory which applied to one-fault and multiple-fault situations are, respectively, discussed, and the BJ

filter design principle and design procedure are validated using a random system with pre-defined fault vectors in MATLAB SIMULINK.

In Chapter 5, a conceptual BJ filter structure for the underlying plate control system is designed (assuming the satisfaction of the design restrictions) and validated in MATLAB SIMULINK via different configurations (namely, SISO configuration – considering one pair of the inputs and outputs of the real system only, 2I2O configuration – considering two pairs of the inputs and outputs of the real system only, and MIMO configuration – considering all three pairs of the inputs and outputs of the real system, respectively).

In Chapter 6, an operable BJ filter is discussed specifically for actuator fault detections of the given plate control system, and is tested in real-time experiment.

In Chapter 7, meaningful conclusions from the studies presented in this thesis are drawn based on which future works are suggested.

Chapter 2 : Literature Review

In this chapter, an overall literature related to fault detection and diagnosis is reviewed. System identification is firstly discussed to explain the system modelling approaches, followed by fault classification. Different fault detection approaches, as well as their applications, are then analyzed and compared, which leads to the main approach, the Beard-Jones filter approach used in this thesis.

2.1 System Identification

In general, system identification acts as a link connecting the measured input and output data of a system with a simplified model of known or unknown parameters. The purpose of this is to construct a mathematical model of a dynamic system by using the observed input and output data. With the help of a mathematical model, a suitable control system for the actual system can be designed, and the performance of the overall system can be assessed and monitored. Dynamic systems are ubiquitous, so the application of system identification can be divided into many aspects, such as system modelling, prediction, fault detection, and diagnosis [7, 8, 9, and 10].

There are three main properties of system identification, as listed below [11]:

- The validity of the models (obtained by system identification) may be limited. For example, they may only fit to certain situations or certain types of outputs.
- The models may not offer physical insights of the systems, if the model parameters have no distinct physical relationships with the real systems. Most of the parameters only act as mirrors to express the primary behaviors of the overall systems of concern.
- The most significant advantage of system identification is that the models, if good enough, will be useful for system analysis and design. A compromise between precision of modelling results and simplicity of a model must be made, so that some physical properties, such as negligible interference sources and unnecessary nonlinear parameters, could be ignored.

As representations of the physical systems by mathematical models using system identification vary to some extent, there are three key methods of constructing these mathematical models: numerical analysis, theoretical analysis, and physical experimentation [12].

- Numerical analysis is the most efficient and useful method in mathematical modelling due to the rapid advances in computer technologies. The invention of specific software tools, such as ANSYS and MATLAB, have made numerical analysis much easier and more effective. The accuracy of the models depends on the accuracy established in those specific software programs. This thesis mainly focuses on modelling a laboratory model using this method [13].
- Theoretical analysis is implemented by considering the physical properties and characteristics of a real system. Taking the advantage of theoretical derivations, a mathematical model of a system can be obtained precisely. However, in most instances, it is difficult to carry out an effective theoretical analysis because of the complexity of the structure of a real system.
- Physical experiment is the most dependable way to deduce a mathematical model. By conducting real-time experiments, obtained data can be used to reflect the dynamics of the system under examination to the maximum extent. However, it may be tricky to use the obtained data to construct a mathematical model that is appropriate for system analysis and design purposes.

For an engineering system, a valid model of a system is vital for the system dynamic analysis and controller design purposes. The more accurate a mathematical model of the system, the more reliable the results of the final system solution. Mathematical models can be represented by different forms of mathematical equations, based on an intended use [11]. There are two major forms used to express these mathematical models, namely, transfer function representation, and state space representation.

Transfer Function Representation

Transfer function representation is commonly applied to characterize the I/O relationships of physical systems; the definition of this type of systems is that the system under examination can be expressed by a time-invariant, linear, differential equation. The process of obtaining the transfer function mainly relies on the Laplace transformations that transform the differential equation in the time domain into a ratio between the output and the input of the system in the s-domain.

Assume a time-invariant, linear, differential equation of the form:

$$a_0 y^n + a_1 y^{n-1} + \cdots + a_{n-1}\dot{y} + a_n y = b_0 x^m + b_1 x^{m-1} + \cdots + b_{m-1}\dot{x} + b_m x \qquad (2.1)$$

where *x* and *y* indicate the input and output of the system. Based on the principle of the transfer function, (2.1) can be transferred into the s-domain as:

$$\text{Transfer function} = G(s) = \frac{Y(s)}{X(s)} = \frac{b_0 s^m + b_1 s^{m-1} + \cdots + b_{m-1} s + b_m}{a_0 s^n + a_1 s^{n-1} + \cdots + a_{n-1} s + a_n} \tag{2.2}$$

where $G(s)$ is the transfer function between $Y(s)$ and $X(s)$ in the s-domain.

The main properties of a transfer function are listed below [14]:

1) The nature of a transfer function is a mathematical model, that uses the operational derivation to express the differential equation in term of the input and output of a system.

2) A transfer function shows the characteristics of the corresponding system itself, which are not related to the input properties or any disturbances in the outside world.

3) The elements contained in a transfer function can only represent the relation between the input and output of the current corresponding system. In most cases, the elements do not have any physical meanings, which means that two physical structures may be represented by an identical transfer function form.

4) Based on a known transfer function of a system, the output and response of the system can be studied using different forms of inputs.

5) When a system transfer function is not known, introducing a known input in an experiment setting to study the output of the system can help establish the transfer function.

State Space Representation

With the development of the modern control theory, modern engineering systems have become even more complex, and the required system accuracy is also increasing. Such systems often involve multiple inputs and outputs (MIMO), and possess complicated design requirements. This type of system is better presented by a state space representation that was established for effective analysis and design of modern control systems [14]. For simplicity, the general state space representation concerning a linear, time-invariant system can be shown as:

$$\begin{cases} \dot{\boldsymbol{X}}(\boldsymbol{t}) = \mathbf{A}\boldsymbol{X}(\boldsymbol{t}) + \mathbf{B}\boldsymbol{U}(\boldsymbol{t}) \\ \boldsymbol{Y}(\boldsymbol{t}) = \mathbf{C}\boldsymbol{X}(\boldsymbol{t}) + \mathbf{D}\boldsymbol{U}(\boldsymbol{t}) \end{cases} \tag{2.3}$$

where $\boldsymbol{U}(\boldsymbol{t})$ and $\boldsymbol{Y}(\boldsymbol{t})$ are the input and output vectors, respectively, and $\boldsymbol{X}(\boldsymbol{t})$ is the state vector.

Alongside convenient and simple data processing when dealing with complex systems, another advantage of state space is that the choice of state variables does not need to take the physical meaning of the system into consideration; this freedom allows designers to construct the state space representation in a much simpler way.

2.2 Fault Classification

Faults in a modern control system are events which may happen without any indication and may lead to any form of the unexpected deviation of the system parameters or characteristics. During the process of the system operation, faults can influence the performance of sensors, actuators, or other system components [15 and 16]:

- Sensor faults: These faults are related to inaccurate sensor readings within the control system. Sensor faults can be classified into two types, partial faults, and total faults. The information provided by a total sensor fault is not related to the physical parameters being measured; such situations may occur because of broken wires. Partial sensor faults provide readings that may be in some way related to the measured parameters, but these readings may have a gain reduction or other bias in the measurement [17].
- Actuator faults: Actuator faults lead to situations in which correct control commands cannot be applied to the system [18]. As with sensor faults, actuator faults can also be divided into total and partial types. Total actuator fault may occur due to a stuck actuator, which cannot produce any actuation, while actuators with partial faults such as fuel leakage may provide a proportion of the normal operation.
- Component faults: In general, these faults belong to the plant itself, and cover anything that cannot be classified as a sensor or actuator fault. Component faults refer to deviations in the parameters of physical systems; these parameters can be related to mass or shape or be related to the plate structure. In this thesis, component faults will not be taken into consideration, as the basic assumption is that the plate structure will not be changed and that any mathematical model constructed based on the system identification will thus always be valid.

As with system identification of a plate structure, faults occurring in the system also need to be modelled. According to the mathematical treatment of faults, faults are classified as additive faults and multiplicative faults [19].

Multiplicative faults commonly refer to parameter changes in the system, as shown in Figure 2.1a. When introducing the multiplicative faults into the state space model, the system mathematical model is modified as:

$$\begin{cases} \dot{\boldsymbol{X}}(\boldsymbol{t}) = (\mathbf{A} + \Delta\mathbf{A})\boldsymbol{X}(\boldsymbol{t}) + (\mathbf{B} + \Delta\mathbf{B})\boldsymbol{U}(\boldsymbol{t}) \\ \boldsymbol{Y}(\boldsymbol{t}) = (\mathbf{C} + \Delta\mathbf{C})\boldsymbol{X}(\boldsymbol{t}) + (\mathbf{D} + \Delta\mathbf{D})\boldsymbol{U}(\boldsymbol{t}) \end{cases} \tag{2.4}$$

where $\Delta\mathbf{A}$, $\Delta\mathbf{B}$, $\Delta\mathbf{C}$, and $\Delta\mathbf{D}$ represent parameter changes. From the above equation, multiplicative faults multiply themselves with the state and input vectors, which makes this type of fault harder to handle than additive faults [20]. Another difficulty when dealing with multiplicative faults is that parameter changes may influence the stability and controllability of the entire plate structure. A further disadvantage of multiplicative faults is the limitation of representing only sensor and actuator faults. Therefore, as multiplicative faults can be expressed using additive faults, this thesis mainly focuses on studying additive faults.

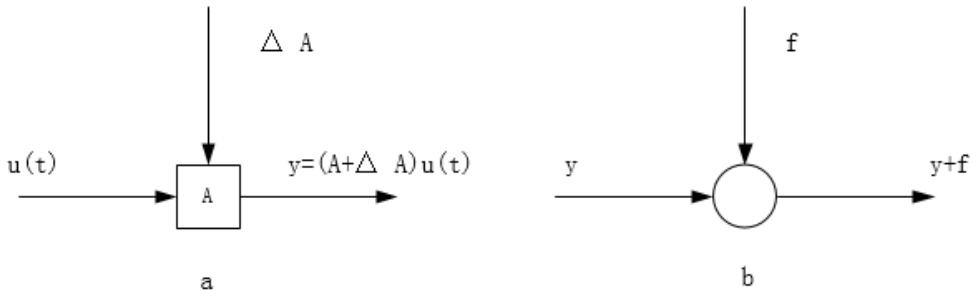

Figure 2.1a is for multiplicative fault, 2.1b is for additive fault

Additive fault can be regarded as external inputs to the system, as shown in Figure 2.1b. When introducing additive faults into the state space model, the system mathematical model is modified as:

$$\begin{cases} \dot{\boldsymbol{X}}(\boldsymbol{t}) = \mathbf{A}\boldsymbol{X}(\boldsymbol{t}) + \mathbf{B}\boldsymbol{U}(\boldsymbol{t}) + \boldsymbol{f_1}(\boldsymbol{t}) \\ \boldsymbol{Y}(\boldsymbol{t}) = \mathbf{C}\boldsymbol{X}(\boldsymbol{t}) + \mathbf{D}\boldsymbol{U}(\boldsymbol{t}) + \boldsymbol{f_2}(\boldsymbol{t}) \end{cases} \tag{2.5}$$

where $\boldsymbol{f_1}(\boldsymbol{t})$ and $\boldsymbol{f_2}(\boldsymbol{t})$ represent the fault models caused by additive faults. This form can be applied to the modelling of all three types of faults previously defined. Due to this advantage, additive fault modelling is more suitable for designing fault detection algorithms, especially in terms of the application of state space representation [17].

2.3 Fault Detection Approaches

2.3.1 Hardware Redundancy and Analytical Redundancy

With the increasing popularity of automatic controls in modern engineering systems, fault detection now plays a very important role in indicating abnormal or undesired process states, thus allowing the system to take proper actions to maintain degraded but acceptable operation to prevent accidents prior to maintenance [21]. Two main fault detection methods are utilized in control systems: hardware redundancy and analytical redundancy. The basic operational processes are shown in Figure 2.2 [22].

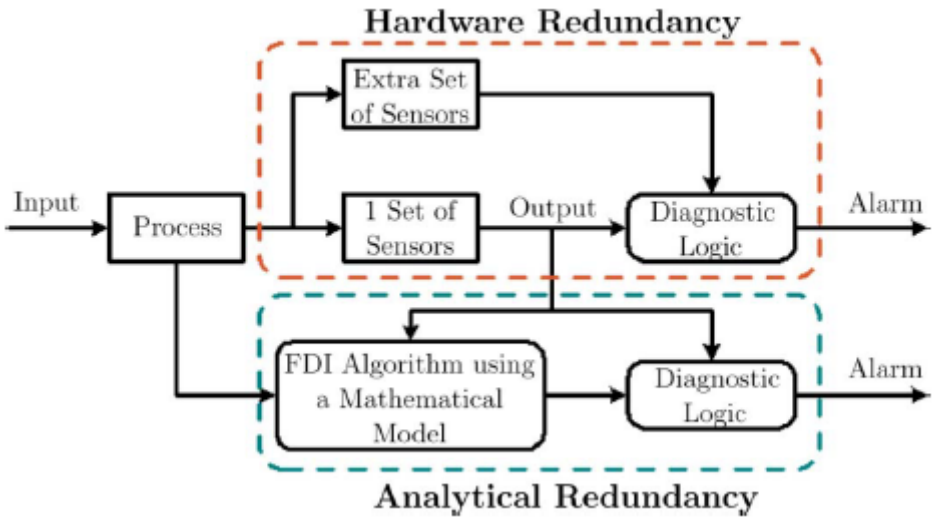

Figure 2.2 Hardware redundancy vs analytical redundancy

Hardware Redundancy

In general, the traditional method for fault detection is based on hardware redundancy. Hardware redundancy adds spare components (such as multiple sensors, actuators, and components) to the system in order to measure possible output deviations. A continued operation can thus be accomplished by isolating a fault component and switching to the use of the spare component [23]. A voting technique is a typical approach in hardware redundancy, and this can identify the time and location of faults among all the redundant components. However, this technique has three limitations [24]:

- The outputs of the sensors must be algebraically related to the nominal condition.
- The detection law does not have the ability to distinguish a failure location between the system component and the sensors that indicate the outputs of the components.

- As the detection law has no memory, it is difficult for the voting technique to detect the "soft" failures.

The appealing advantage of hardware redundancy is its simplicity in terms of design process and implementation. In addition, in most cases, there is no need to adjust parameters in other parts of the system in order to achieve compatibility with spare components. Thus, no additional logical operation is required for this type of fault detection. However, in the fundamental parts of the modern control systems, many faults cannot be simply detected and localized prior to the failure of the entire system. Some types of failures, such as pressure losses and stuck actuators, can be detected and localized immediately. However, in complex cases, the detection task must be done by grouping several components into one unit. This approach makes it easy to implement fault detection, but causes the use of hardware to become inefficient due to the loss of normal operating components. The performance of hardware redundancy can be improved by using all spare components simultaneously with the primary components, instead of retaining all of the spare components as idle before a fault occurs. This arises because, when considering sensor performance in the system, using several sensors (primary and redundant) to measure the same parameter can produce a much more precise result than using only one sensor. When considering actuator performance in the system, several actuators (primary and redundant) can also produce the same total output (sum of each actuator output) with less effort than one primary actuator, which results in a higher saturation level and longer average lifetime for each device [25].

However, there are other limitations to the hardware redundancy method. The most important limitation is that it cannot deal with performance degradation caused by changes in operating parameters such as environmental changes, as in most cases such environmental changes are unknown and cannot be predicted ahead.

Although hardware redundancy is a reliable method to guarantee the normal operation of systems, its limitation and cost make it an imperfect method for many systems. Therefore, this thesis will mainly focus on analytical redundancy.

Analytical Redundancy

Due to the limitations of hardware redundancy as explained above, analytical redundancy was developed to provide systems with more effective methods for dealing with deviations in the systems and their environment, to make full use of redundancy. Analytical redundancy uses a

specific algorithm to construct a mathematical model, and it is thus usually regarded as a model-based method of fault detection.

Figure 2.3 shows a general structure for analytical redundancy in detail for a Fault Detection and Identification (FDI) system. The process for an FDI system can be separated into three stages [22]. The first stage is to produce a set of variables, normally known as residuals, utilizing residual generation methods. The number of generations depends on the FDI system, as several residual generations may run in parallel for fault detection. The generated residuals must be ideally 0 under normal operating conditions. To ensure the residuals can be applied to practical applications, they must be insensitive to outside disturbance and model uncertainties as well as being sensitive to corresponding faults to the maximum extent. The second stage is to decide whether there are faults occurring in the control system; the location of faults is based on the information extracted from the residuals by the decision filter. This step can usually be implemented by mathematical calculation and statistical methods based on the fault model and will detect any deviation compared with the normal operating system (zero). Finally, the last stage is to reconfigure the controller to maintain the operation of the system.

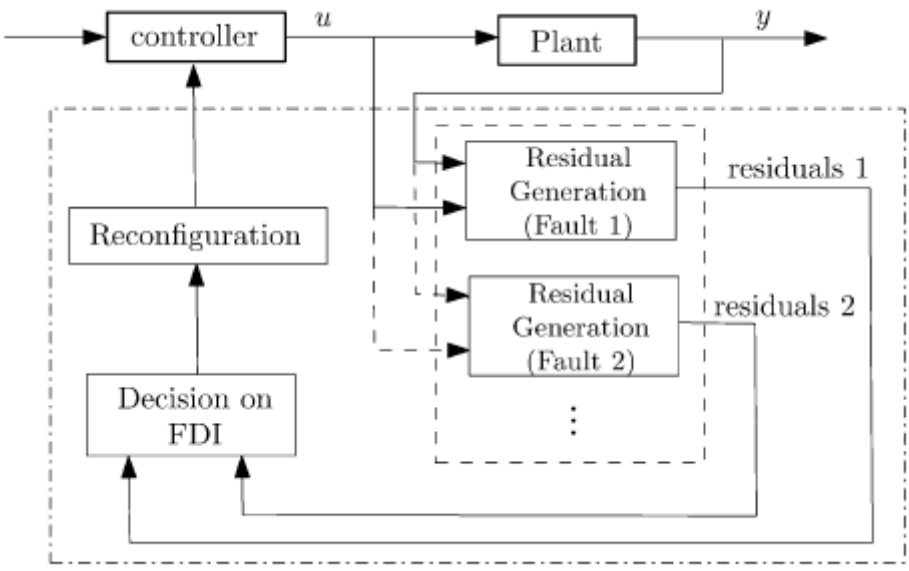

Figure 2.3 Fault detection, isolation, and reconfiguration system using analytical redundancy

In the analytical redundancy method, the residuals are always obtained based on the system's mathematical models. These mathematical models can be developed based on different principles, such as Newton's law of motion in mechanical systems, or past experience and observations. This approach makes it difficult for mathematical models to represent the behaviors of real systems precisely because of modelling errors and uncertainties along with

noise and disturbances; the generated residuals can be nonzero under normal operating conditions in reality. This problem can be overcome by using two approaches [22]

- Robust residual generation: This method designs a robust filter which can produce residuals that are not sensitive to outside noise and disturbance while remaining sensitive to corresponding faults.
- Robust residual evaluation: This method develops the hypothesis detecting algorithm in order to estimate the residuals. The main idea behind this method is to test changes in the system parameters which are related to faults.

The main properties and advantages of analytical redundancy are shown below [26]:

- Faults can be detected and diagnosed much earlier in cases of both abrupt or slow behaviour. This means that the detection delay can be minimized, which allows the system enough time to react, such as by implementing reconfiguration, a fix, or other mitigating operations. The method used to achieve earlier detection can be based on input-output relationships derived from mathematical models.
- It has the ability to distinguish between different types of failures, such as sensor, actuator, and component faults. This ability enables the system to act to deal with failures in order to maintain a normal system operation.
- No spare hardware components are needed to implement fault detection, as computer software is used for fault detection [27].
- It can monitor system process in every transient state.
- Advances in analytical redundancy lay the basis for fault-tolerant control.
- It maintains good robustness while dealing with various noise impacts.
- It displays a high level of sensitivity to faults.
- It can achieve in-depth fault diagnosis with close-loop fault detection.

2.3.2 Major Approaches in Analytical Redundancy

As the analytical redundancy method has several advantages, as illustrated above, compared to hardware redundancy, this method is generally more cost efficient. However, analytical redundancy still has several problems that must be solved. There is, in particular, a need to focus on meeting the requirements of robustness when faced with modelling uncertainties and environmental disturbances. Thus, in recent decades, many scholars have been devoted to the research of algorithms in analytical redundancy, and several effective and practical algorithms

have been successfully implemented; these are state estimation, parity relation, parameter estimation, and Kalman filter [35].

Parameter Estimation

The parameter estimation approach is suitable for the conditions where the system faults are associated with parameter deviation in the mathematical model, making it suitable for multiplicative faults. In general, the model parameters do not need to be measured, the parameter estimation approach estimates the model parameters recursively to minimize the computational requirements. An appropriate mathematical model must be constructed to meet the first principle, which relates the model parameters to system parameters with physical meanings. The setting of thresholds normally relies on the differences between the model parameters and the parameter estimation [28].

There are five main steps for implementing the parameter estimation approach [29].

1) Constructing a mathematical model for the input variable u and output variable y using conservation equations and operational relationships. This model relates each physical parameter p and input variable u to the output variable y.
2) Making assumption or gathering physical parameters together to construct a new observable parameter q that can be uniquely detected. By means of this process, the new re-defined parameter can linearly enter the mathematical model, which can simplify the parameter estimation approach.
3) Estimating the new parameter q by measuring the current and past input and output variables, and obtaining q' which is the estimated q used in the process [30].
4) Based on q', calculating the corresponding p', which is an estimation of the physical parameter p.
5) Comparing the physical parameter p with the estimated p' by computing their difference; if the result is non-zero and exceeds a pre-set threshold, then faults are detected.

As the parameter estimation approach mainly focuses on the system which has time-varying parameters and multiplicative faults, this thesis will not cover this approach in detail [31].

Kalman Filter

The basic principle of the Kalman filter is the use of a recursive algorithm for estimating states. The Kalman filter method can be treated as a special situation in stochastic optimization. This method was firstly developed by Mehra and Peschon to generate residuals for fault detection

and isolation [32]. Faults can be detected through statistical testing based on the covariance and mean of residuals. Basseville and Benveniste have proven that the fault isolation process can be implemented by applying a bank of Kalman filters associated with all possible deviations which may occur in the system [33].

Although Kalman filter approach can achieve successful and effective fault detection as a simple residual based algorithm, its ability to identify faults is relatively limited [33]. In addition, when dealing with multiple models (especially where the number of faulty modes is very high), the Kalman filter is much more complex than observer estimation. Thus, this thesis will not utilize this approach.

Parity Relation

The parity relation approach generates residuals which represent the differences between the real system output and the mathematical model output. Then, a linear transformation is applied to the generated residuals, which makes them much easier to identify. These two steps form the basic function of the residual generation filter that produces the desired fault detection properties. Various schemes can be applied to construct a residual generator that satisfies the requirements of the response feature. Generally, the purpose of the residual generator is to enhance fault detection and isolation in order to improve its ability to identify fault occurrences and locations. In addition, several properties such as robustness to noise and disturbance can be improved [34].

The main features of the parity relation approach are shown below [35].

- Model parameters and model structure are known precisely and adapt to the process well.
- Suitable for additive faults.
- When dealing with additive faults, input signal need not be changed.
- The linear parity relation can be transformed to observer representation [36].

Several researchers have pointed out the relationship between the parity relation approach and the observer estimation approach [37, 38]. Chen and Patton investigated this issue in detail and their result showed that the parity relation approach was equivalent to the observer estimation method (dead-beat observer) [39]. However, compared with the observer estimation approach, the parity relation approach has few design flexibilities [39], and this thesis will thus mainly focus on the observer estimation approach.

Observer Estimation

The basic idea of the observer estimation approach is the use of Luenberger observers or specific filters to estimate the output value of the system based on measurements. The error obtained from output estimation is regarded as residual. The general process of observer estimation is that if all the sensors in the system are good and the mathematical model of the system is precisely known, the estimated state vectors will match the real state vectors quickly. In contrast, if one sensor is faulty, the difference between the real and estimated state vector can be used to identify the faulty sensor [40].

The observer estimation approach is especially suitable for detecting changes in sensors and actuators, which means that it is most suitable for additive faults. The required mathematical model is generally based on the First Principle; thus, the state vectors retain physical meanings, which improves fault isolation capacity [29].

The key features of the observer estimation approach are shown below [35].

- Model parameters and model structure must be known precisely and be well-adapted to the process.
- Fast response to sudden faults.
- The ability to detect small faults such as additive faults and gains.
- The ability to achieve on-line real-time fault detection.

The advantages of using observer estimation lie in its freedom and flexibility in terms of choosing the detection gain, which enables this approach to adapt to a variety of situations. This thesis will mainly focus on one of the most important observer estimation approaches, the Beard-Jones (BJ) filter, because of its excellent ability to deal with MIMO systems [41].

2.3.3 Beard-Jones Filter

The Beard-Jones (BJ) filter was firstly proposed by Beard, before being developed by Jones. The development of this filter not only contributed to the application of observer theory but also created the basis for an observer-based fault detection and isolation framework [42]. The BJ filter has attracted significant attention because of its properties, including an ability to identify faults in a system that does not depend on the mode of faults [43]. The main process used by the BJ filter is to divide the output error signal (residual) into several subspaces. In each subspace, the signal transmission from one fault is designed to be maximized, while the signal transmission from other faults is designed to be minimized. Based on this characteristic,

once a nonzero residual is detected, the fault can be detected and isolated by placing this residual into subspaces [18].

The mathematical model of the BJ filter can be expressed as:

$$\dot{\widehat{\boldsymbol{X}}}(\boldsymbol{t}) = \mathbf{A}\widehat{\boldsymbol{X}}(\boldsymbol{t}) + \mathbf{B}\boldsymbol{U}(\boldsymbol{t}) + \mathbf{L}(\boldsymbol{Y}(\boldsymbol{t}) - \mathbf{C}\widehat{\boldsymbol{X}}(\boldsymbol{t})) \tag{2.6}$$

where $\widehat{\boldsymbol{X}}(\boldsymbol{t})$ is the estimated state of the true state $\boldsymbol{X}(\boldsymbol{t})$, **L** is the detection gain, and **A**, **B**, and **C** are system matrix, input matrix and output matrix, respectively. Based on (2.6), the state error $\varepsilon(\boldsymbol{t})$ and the output error $\hat{\varepsilon}(\boldsymbol{t})$ can be expressed as:

$$\begin{cases} \varepsilon(\boldsymbol{t}) = \boldsymbol{X}(\boldsymbol{t}) - \widehat{\boldsymbol{X}}(\boldsymbol{t}) \\ \hat{\varepsilon}(\boldsymbol{t}) = \boldsymbol{Y}(\boldsymbol{t}) - \mathbf{C}\widehat{\boldsymbol{X}}(\boldsymbol{t}) \end{cases} \tag{2.7}$$

The key to designing a BJ filter is to select a proper value for **L** so that the output error has directional properties associated with the corresponding fault. The advantages of the BJ filter and the reasons why a designer might use a BJ filter as the fault detection approach, as in this thesis, are illustrated below [43].

1) By using subspace concepts, the output error of a BJ filter has directional properties associated with the corresponding fault. This special property enables a BJ filter to implement fault detection and fault isolation simultaneously.
2) BJ filters can be tractable to detecting the system with high order models. When dealing with vibration cancelations, most continuous systems (including those for beams and plates) must be considered as high-order models rather than order-reduced models to maintain accuracy.
3) A BJ filter can deal with a D-term (that is generated to account for the errors in the mathematical model of a system due to a necessary model-order reduction in the system identification process).

Due to time constraints, this thesis mainly focuses on the first advantage of the BJ filter. The remaining two features (higher-order and D-term applications) are thus suggested as directions for future research work. More details about the BJ filter in light of the first factor will be discussed in Chapter 4.

Chapter 3 : System Identification of Plate Structure

As a link between a dynamic system and a simplified mathematical model, system identification plays an important role in analysing and controlling a modern engineering system. In this chapter, the procedure of building such a mathematical model is illustrated in detail. Firstly, the feature and characteristics of a MIMO mechanical plate structure are described. A transfer function representation of the plate structure is then constructed through dedicated theoretical analysis and physical experiment. The theoretical analysis aims to derive the general mathematical expression of the transfer function model whereas the physical experiment, using the ModalVIEW software, aims to generate the Frequency Response Function (FRF) curves of the mechanical plate structure and to produce the useful parameters of the transfer function model, such as the mode shapes, damping ratios and natural frequencies. Finally, for the purpose of fault detection, a state-space representation of the mechanical plate structure with a defined dimension representing a pre-selected frequency range of concern is developed based on the identified transfer function representation of the system.

3.1 Characteristics of Plate Structure

The MIMO mechanical plate structure used in this project is shown in Figure 3.1, which is used to demonstrate the fault detection problem in a MIMO control system. This structure includes a top plate, a base plate, a disturance transducer, and three pairs of co-located sensors and actuators that bond the top and base plates together. The disturbance transducer is utilized to generate structural vibrations to the base plate, and transducer 1, 2 and 3 which are mounted with the top plate by screws are treated as sensors and actuators to control the structural vibrations such that the top plate can remain stationary despite the constant vibration excitation induced from the base plate. From Figure 3.1, it is seen that the disturbance signal generated from the disturbance transducer passes through the base board to the other three transducers and then through sensing and actuating, finally transfers onto the top plate. From a control point of view, since transducer 1, 2 and 3 are utilized as sensors as well as actuators, this control system can be regarded as a MIMO control system with three-inputs and three-outputs. Three input signals come from three actuators which are used to generate the vibration forces into three transducers, and three output signals come from three sensors which are used to sense the vibration amplitudes which are right above the corresponding transducers on the top plate.

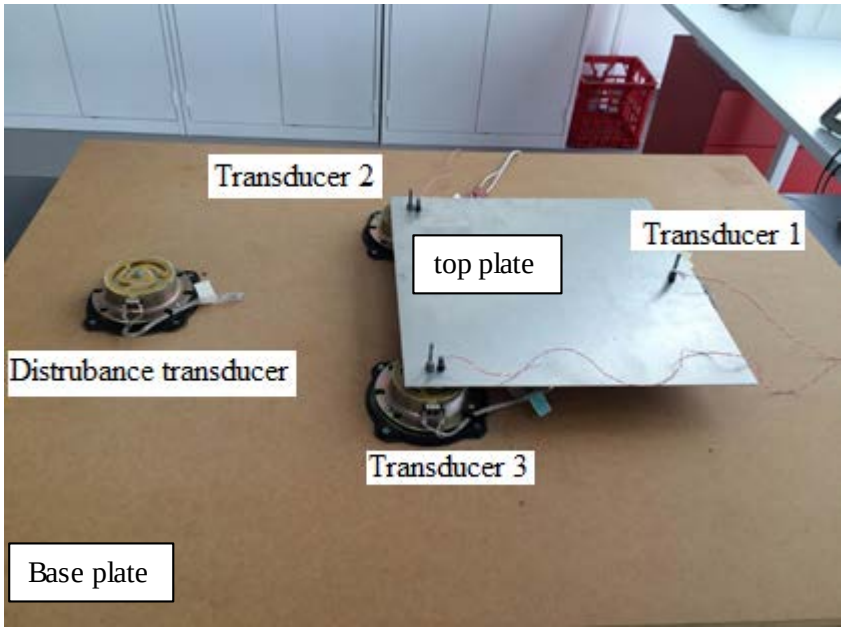

Figure 3.1 The MIMO mechanical plate structure

The general transfer function representation for the open-loop physical system can be expressed as:

$$\boldsymbol{Y}(s) = \boldsymbol{G}(s) \times \boldsymbol{U}(s) \tag{3.1}$$

where $\boldsymbol{Y}(s)$ represents the output signal of the system, $\boldsymbol{U}(s)$ represents the input signal of the system and $\boldsymbol{G}(s)$ represents the transfer matrix of the plate structure. As explained above, this physical system is regarded as a MIMO control system with three-inputs and three-outputs, so the system can be expressed as:

$$\begin{bmatrix} Y_1(s) \\ Y_2(s) \\ Y_3(s) \end{bmatrix} = \begin{bmatrix} G_{11}(s) & G_{12}(s) & G_{13}(s) \\ G_{21}(s) & G_{22}(s) & G_{23}(s) \\ G_{31}(s) & G_{32}(s) & G_{33}(s) \end{bmatrix} \times \begin{bmatrix} U_1(s) \\ U_2(s) \\ U_3(s) \end{bmatrix} \tag{3.2}$$

where $Y_i(s)$ (i = 1, 2, 3) are three output signals of the system, $U_j(s)$ (j = 1, 2, 3) are three input signals of the system, and $G_{ij}(s)$ (i = 1, 2, 3 and j= 1, 2, 3) represents the element of $\boldsymbol{G}(s)$ that is related to the i^{th} output (output of transducer i) and the j^{th} input (input of transducer j). The plate layout related to the open-loop system modelling is shown in Figure 3.2 [46].

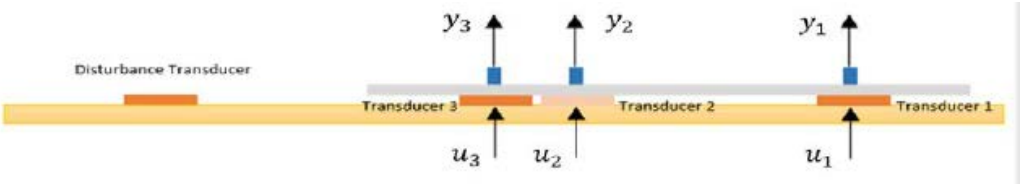

Figure 3.2 Plate layout for open-loop system

From (3.2), it can be concluded that the transfer matrix $\boldsymbol{G}(s)$ of this MIMO control system can be represented by a 3×3 transfer function matrix, and every element $G_{ij}(s)$ of this transfer matrix stands for the dynamics between transducers i and j. Based on (3.2), the block diagram which represents the current MIMO control system is shown in Figure 3.3.

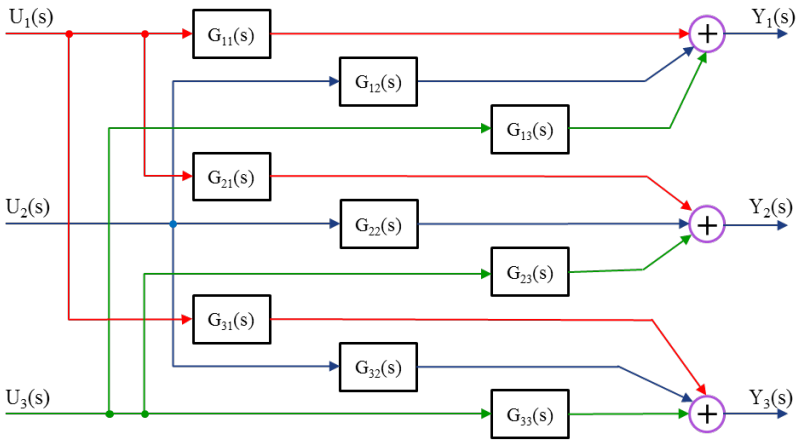

Figure 3.3 MIMO control system block diagram

Based on the above study and analysis, a clear conclusion can be drawn that each input signal will impact on three output signals at the same time, and similarly each output signal will be influenced by three input signals at the same time. After clearly understanding the feature and characteristics of the given plate structure, the next section will briefly explain the theoretical analysis in order to derive the general mathematical expression of the transfer matrix $\boldsymbol{G}(s)$.

3.2 Theoretical Analysis of Transfer Function Model

In general, fundamental physics theory is needed to generate the mathematical model of the flexible plate structure. In order to determine the mathematical model, partial different equation which is normally called PDE is introduced to better represent the flexible plate structure by cancelling the vibrations resonant in multiple modes [44]. In addition, the plate structure can be determined by a two-dimensional mathematical model using PDE in this project [45]. The two-dimensional PDE is shown as [12]:

$$\mathcal{L}[\varphi(x,y,t)] + \mathcal{C}\left[\frac{d\varphi(x,y,t)}{dt}\right] + \mathcal{M}\left[\frac{d^2\varphi(x,y,t)}{dt^2}\right] = \mathcal{F}(x,y,t) \tag{3.3}$$

where $\mathcal{L}$, $\mathcal{C}$ and $\mathcal{M}$ represent the linear homogeneous differential stiffness, mass and damping operator, respectively. (x,y) represents the spatial coordinate, $\varphi(x,y,t)$ represents the eigenvector (mode shape) at position (x,y) and $\mathcal{F}(x,y,t)$ represents the random input force at position (x,y).

The solution of PDE will create one set of orthogonal eigenfunctions which enable the flexible plate structure to be represented by the sum of infinite decoupled 2nd order ordinary differential equation, and each ordinary differential equation is related to a certain mode of vibration. Because this thesis focuses on the BJ filter fault detection, the derivation process of PDE can refer to [12] in detail. Finally, the transfer function model of the flexible plate structure is shown as:

$$G(x,y,s) = \sum_{k=1}^{\infty} \frac{\varphi^k(x,y)\varphi^k(x1,y1)}{s^2+2\varsigma^k(x,y,x1,y1)w^k{}_{(x,y,x1,y1)}s+w^{k\,2}(x,y,x1,y1)} \tag{3.4}$$

where $\varphi^k(x,y)$ and $\varphi^k(x1,y1)$ represent mode shape related to point (x,y) and $(x1,y1)$ at nth mode, respectively. $\varsigma^k(x,y,x1,y1)$ represents damping ratio between point (x,y) and $(x1,y1)$ at kth mode. $w^k(x,y,x1,y1)$ represents natural frequency between point (x,y) and $(x1,y1)$ at kth mode. Based on the general representation of the flexible plate structure, the modified transfer function equation which fits into this project is given as:

$$G_{ij}(s) = \sum_{k=1}^{\infty} \frac{\varphi_i^k \varphi_j^k}{s^2+2\varsigma_{ij}^k w_{ij}^k s+w_{ij}^{k\,2}} = \sum_{k=1}^{\infty} \frac{\varphi_{ij}^k}{s^2+2\varsigma_{ij}^k w_{ij}^k s+w_{ij}^{k\,2}} \tag{3.5}$$

where i is the position of the i^{th} actuator (output of transducer) and j is the position of the j^{th} sensor (input of transducer). φ_i^k and φ_j^k represent mode shape related to the i^{th} actuator and the j^{th} sensor, respectively, at kth mode, and φ_i^k and φ_j^k can be integrated into φ_{ij}^k . ς_{ij}^k represents damping ratio between the i^{th} actuator and the j^{th} sensor at kth mode. w_{ij}^k represents natural frequency between the i^{th} actuator and the j^{th} sensor at kth mode.

So far, (3.5) shows that the transfer function model can be determined by three parameters which are mode shape, damping ratio and natural frequency, and these three parameters can be obtained by the physical experiment using ModalVIEW software, which will be explained in the next section.

3.3 Physical Experiment of Transfer Function Model

In this section, the physical experiment is conducted to produce system parameters required in the transfer function model. There are mainly four steps described in the following sections to perform the analysis using ModalVIEW and MATLAB software:

- Perform FRF measurement.
- Perform curve fitting method to produce system parameters.

- Validate the transfer function model of the system.
- Validate the truncated model of the system.

3.3.1 Perform Frequency Response Function (FRF) Measurement.

The arrangement of the physical system and the block diagram of the experimental setup are shown in Figure 3.4 and Figure 3.5, respectively. For the analysis of an open-loop system identification, points A and A' should be open in Figure 3.5. A sinusoidal sweep signal whose frequency is from 20 *Hz* to 200 *Hz* is generated by a signal generator and then, is inserted into transducer 1, 2, and 3 (T1, T2, and T3), respectively, as the input signal u_j (j = 1, 2, 3) after amplification [46]. When this sinusoidal sweep signal is inserted into each input signal alone, three accelerometers are used to measure three output signals y_{ij} (i = 1, 2, 3) simultaneously, and these four signals are recorded by the data acquisition system (NI DAQ) and sent to ModalVIEW software simultaneously in order to produce the corresponding measured FRF of the system:

$$G_{ij}(s) = \frac{y_{ij}}{u_j} \qquad (i = 1,2,3) \tag{3.6}$$

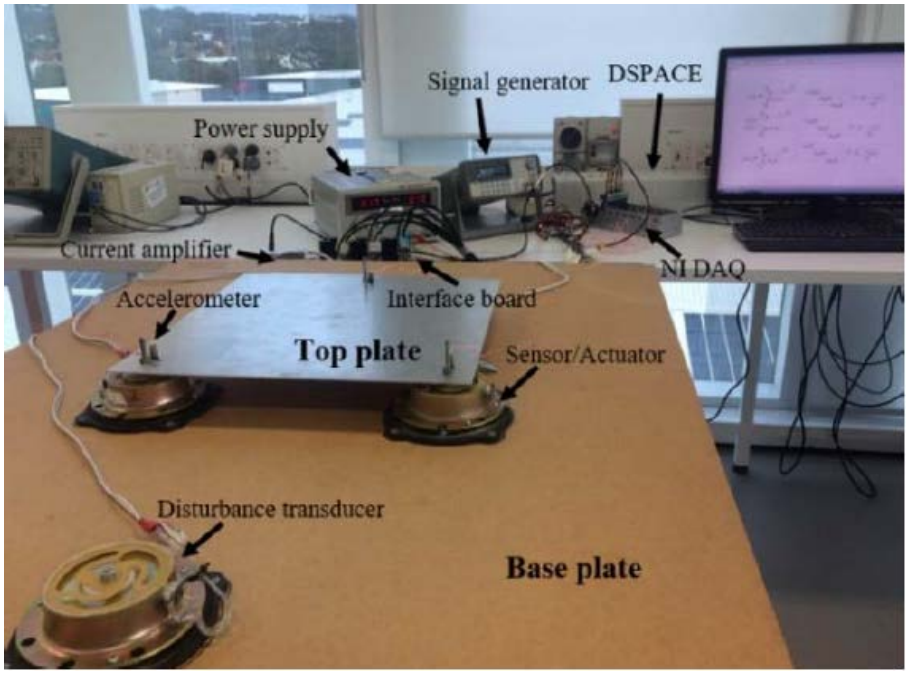

Figure 3.4 The arrangement of the physical system

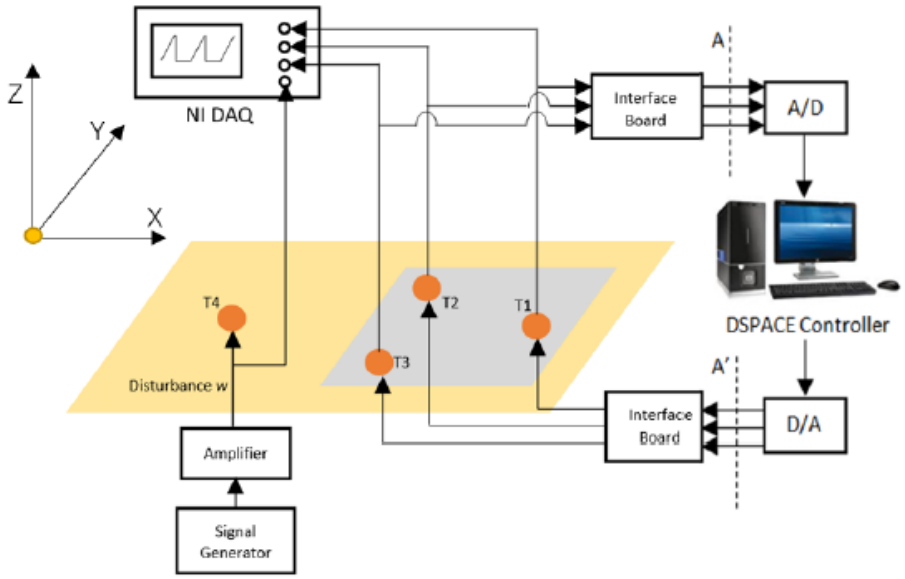

Figure 3.5 The block diagram of the experimental setup

Finally, nine measured FRF curves, $G_{ij}(s)$ $(i,\ j = 1, 2, 3)$, for the open-loop system are generated through ModalVIEW software and plotted in Figure 3.6.

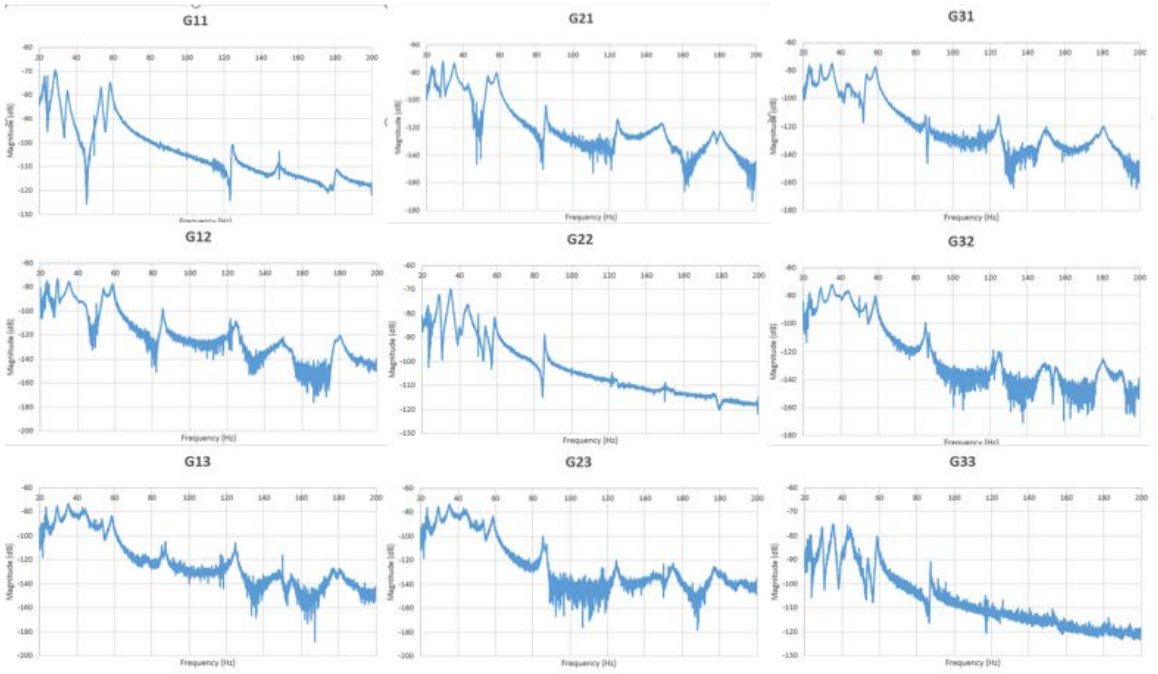

Figure 3.6 Measured FRF curves for the open-loop real system

3.3.2 Perform Curve Fitting Method to Produce System Parameters.

To model the physical system mathematically, the ModalVIEW software provides a Multiple Degree of Freedom (MDOF) polynomial curve fitting method which can be applied into each

measured FRF curve to produce the estimated parameters (such as mode shapes, damping ratios, and natural frequencies) of the transfer function model.

The results of curve fitting method for each measured FRF curve are shown in Figure 3.7 where the precision of this method is demonstrated such that results of curve fitting (red curve) match the measured FRF curves (blue curve) precisely enough.

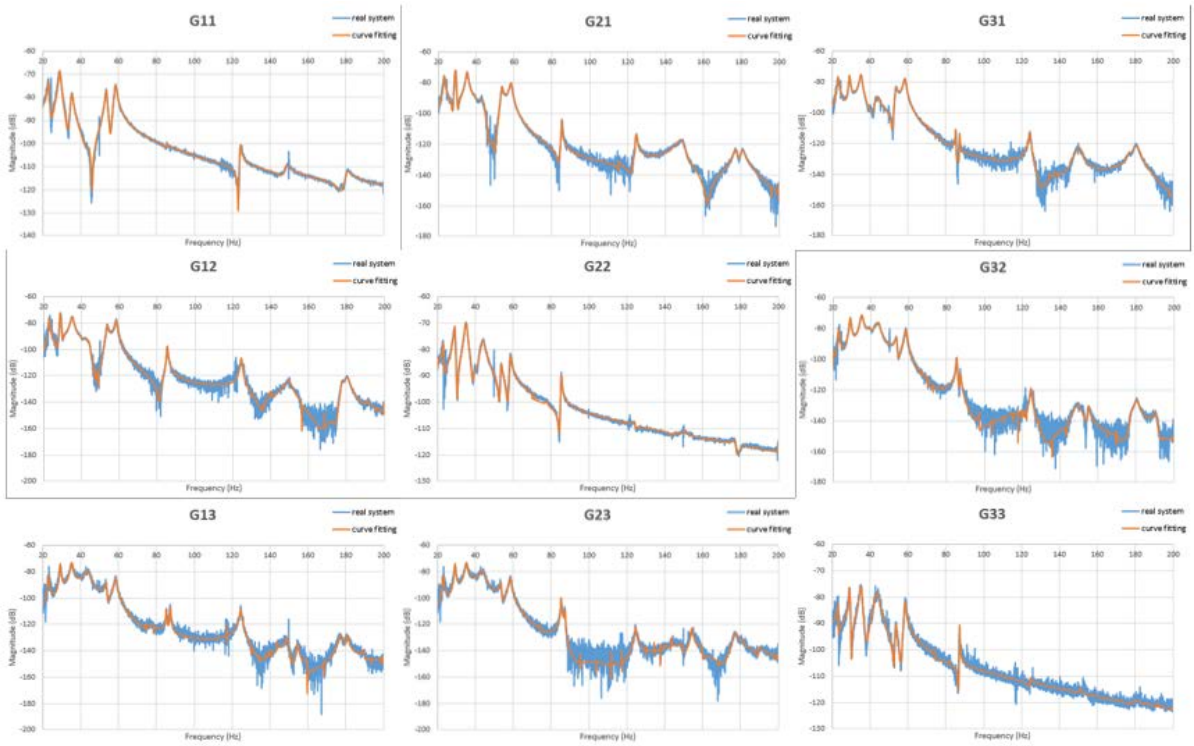

Figure 3.7 Results of curve fitting (red) vs. measured FRF curves (blue)

The corresponding transfer function, $G_{ij}(s)$, is expressed as:

$$G_{ij}(s) = \sum_{k=1}^{N}\left(\frac{\varphi_{ij}^{k}}{s^2 + 2\zeta_{ij}^{k} w_{ij}^{k} s + w_{ij}^{k\,2}}\right) = \sum_{k=1}^{N}\left(\frac{m_{ij}^{k}}{s-\mu_{ij}^{k}} + \frac{m_{ij}^{k\,*}}{s-\mu_{ij}^{k\,*}}\right) \tag{3.7}$$

where m_{ij}^{k} is the magnitude measured by curve fitting method, N is the number of estimated mode, $\mu_{ij}^{k} = -\zeta_{ij}^{k} w_{ij}^{k} + j w_{ij}^{k}\sqrt{1-\zeta_{ij}^{k\,2}}$ and $\mu_{ij}^{k\,*} = -\zeta_{ij}^{k} w_{ij}^{k} - j w_{ij}^{k}\sqrt{1-\zeta_{ij}^{k\,2}}$. Natural frequencies, w_{ij}^{k}, damping ratios, ζ_{ij}^{k}, and magnitudes, m_{ij}^{k} can be acquired directly from the curve fitting method, while the mode shapes, φ_{ij}^{k}, require to be calculated by [46]:

$$\varphi_{ij}^{k} = m_{ij}^{k} \times 2 w_{ij}^{k}\sqrt{1-\zeta_{ij}^{k\,2}} \tag{3.8}$$

Finally, all parameters of the transfer function model can be obtained and only first three modes are displayed in Table 3.1.

Table 3.1 All parameters of the transfer function model (first three modes)

$G_{11}(s)$			
Mode	Natural frequency (rad/s)	Damping ratio	Mode shape
1	145.907272	0.01893171	0.15363842
2	182.852866	0.01653821	0.41430841
3	222.785222	0.01802016	0.19853058
$G_{21}(s)$			
Mode	Natural frequency (rad/s)	Damping ratio	Mode shape
1	146.334548	0.017293	0.11828148
2	184.371104	0.0102591	0.18811558
3	221.993378	0.01584925	0.34159332
$G_{31}(s)$			
Mode	Natural frequency (rad/s)	Damping ratio	Mode shape
1	146.302265	0.01737686	0.10027307
2	183.906556	0.01125181	0.1920355
3	221.994835	0.01641266	0.27221838
$G_{12}(s)$			
Mode	Natural frequency (rad/s)	Damping ratio	Mode shape
1	146.205623	0.01208586	0.07290046
2	181.912795	0.0090579	0.17558329
3	221.391273	0.02018604	0.34610302
$G_{22}(s)$			
Mode	Natural frequency (rad/s)	Damping ratio	Mode shape
1	145.738971	0.01225517	0.05076275
2	183.839301	0.01036957	0.18305818
3	221.280048	0.01988154	0.61395187
$G_{32}(s)$			
Mode	Natural frequency (rad/s)	Damping ratio	Mode shape
1	145.757852	0.01229378	0.04862492

2	183. 606333	0. 01063791	0. 15373242
3	221. 295643	0. 01994371	0. 51509689
$G_{13}(s)$			
Mode	Natural frequency (rad/s)	Damping ratio	Mode shape
1	145. 234739	0. 0108145	0. 04698852
2	184. 634413	0. 00769278	0. 07202531
3	222. 570149	0. 01680347	0. 18801199
$G_{23}(s)$			
Mode	Natural frequency (rad/s)	Damping ratio	Mode shape
1	145. 234739	0. 0108145	0. 03451708
2	184. 634413	0. 00769278	0. 10226404
3	222. 570149	0. 01680347	0. 35679415
$G_{33}(s)$			
Mode	Natural frequency (rad/s)	Damping ratio	Mode shape
1	144. 835311	0. 00939594	0. 02300727
2	184. 843744	0. 00754164	0. 07687854
3	222. 45161	0. 01651211	0. 25701579

3.3.3 Validate Transfer Function Model of The System.

Since all parameters of the transfer function model have be obtained, the transfer function model (red curve), $G_{ij}(s)$, can be plotted in MATLAB and is compared with each of the measured FRF curves (blue curve) as shown in Figure 3.8.

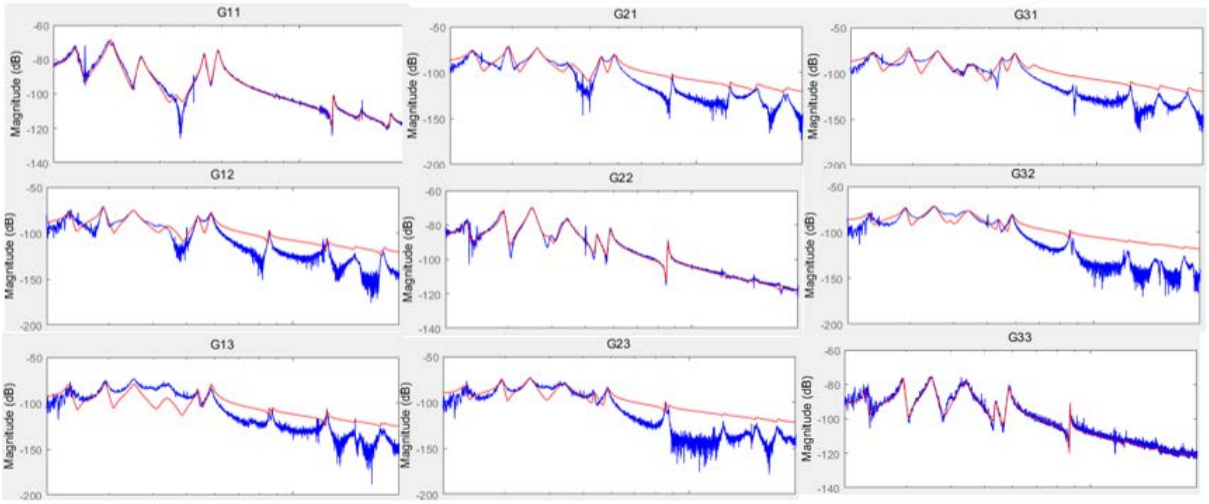

Figure 3.8 Simulated transfer function models (red) vs. measured FRF curves (blue)

It can be seen from Figure 3.8 that simulated transfer function models are able to match measured FRF curves especially when comparing magnitudes of each mode. Therefore, the obtained transfer function model is an acceptable mathematical model to represent the physical system.

3.3.4 Validate Truncated Model of The System.

As the first three modes have the dominant impact on the system performance due to the reason that the real influence on the plate is based on $amplitude/frequency^2$, a truncated model is thus applied to represent the physical system [46]. The truncated model (red curve) is plotted in MATLAB and is compared with each of the measured FRF curves (blue curve) as shown in Figure 3.9.

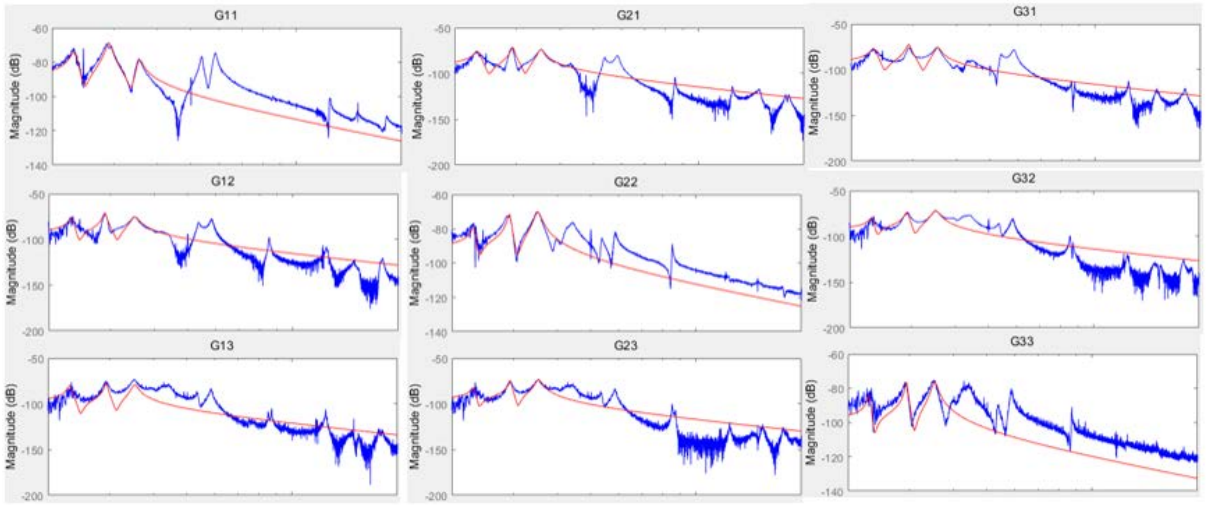

Figure 3.9 Simulated truncated model (red) vs. measured FRF curves (blue)

It is seen from Figure 3.9 that the truncated model relatively matches especially when comparing magnitudes of first three modes. Therefore, the truncated model can be regarded as a valid simplified mathematical model of the physical system.

3.4 Construction of State Space Representation

For the purpose of fault detection, a state space representation of the system is developed from the transfer function representation and the construction procedure is discussed in this section in detail. As the last section indicates that the truncated model can well represent the physical system, the transfer function model can be rewritten as:

$$G_{ij}(s) = \sum_{k=1}^{3} \frac{\varphi_i^k \varphi_j^k}{s^2 + 2\zeta_{ij}^k w_{ij}^k s + w_{ij}^{k\,2}} \tag{3.9}$$

Before building the state space representation, the transfer matrix of the mathematical model should be derived in detail. According to (3.2) and Figure 3.3, this MIMO control system has three inputs and three outputs, and the coupling effect leads to the interaction between them. Therefore, one output is determined by three inputs, and the transfer function representation for each output can be expressed as below in terms of three different modes.

MODE 1:

The transfer function representation for output 1, 2 and 3 at mode 1 is shown in (3.10), (3.11) and (3.12), respectively.

$$Y_1^1(s) = Y_{11}^1(s) + Y_{12}^1(s) + Y_{13}^1(s) = \frac{\varphi_{11}^1}{s^2 + 2\zeta_{11}^1 w_{11}^1 s + w_{11}^{1\,2}} U_1(s) + \frac{\varphi_{12}^1}{s^2 + 2\zeta_{12}^1 w_{12}^1 s + w_{12}^{1\,2}} U_2(s) + \frac{\varphi_{13}^1}{s^2 + 2\zeta_{13}^1 w_{13}^1 s + w_{13}^{1\,2}} U_3(s) \tag{3.10}$$

$$Y_2^1(s) = Y_{21}^1(s) + Y_{22}^1(s) + Y_{23}^1(s) = \frac{\varphi_{21}^1}{s^2 + 2\zeta_{21}^1 w_{21}^1 s + w_{21}^{1\,2}} U_1(s) + \frac{\varphi_{22}^1}{s^2 + 2\zeta_{22}^1 w_{22}^1 s + w_{22}^{1\,2}} U_2(s) + \frac{\varphi_{23}^1}{s^2 + 2\zeta_{23}^1 w_{23}^1 s + w_{23}^{1\,2}} U_3(s) \tag{3.11}$$

$$Y_3^1(s) = Y_{31}^1(s) + Y_{32}^1(s) + Y_{33}^1(s) = \frac{\varphi_{31}^1}{s^2 + 2\zeta_{31}^1 w_{31}^1 s + w_{31}^{1\,2}} U_1(s) + \frac{\varphi_{32}^1}{s^2 + 2\zeta_{32}^1 w_{32}^1 s + w_{32}^{1\,2}} U_2(s) + \frac{\varphi_{33}^1}{s^2 + 2\zeta_{33}^1 w_{33}^1 s + w_{33}^{1\,2}} U_3(s) \tag{3.12}$$

where $Y_i^1(s)$ (i=1, 2 and 3) represents the i^{th} output of mode 1. $Y_{ij}^1(s)$ (i, j=1, 2 and 3) represents the i^{th} output which caused by the j^{th} input of mode 1. φ_{ij}^1 represents the mode shape related to the i^{th} output and the j^{th} input of mode 1. ς_{ij}^1 represents the damping ratio between the i^{th} output and the j^{th} input of mode 1. w_{ij}^1 represents the natural frequency between the i^{th} output and the j^{th} input of mode 1.

MODE 2:

The transfer function representation for output 1, 2 and 3 at mode 2 is shown in (3.13), (3.14) and (3.15), respectively.

$$Y_1^2(s) = Y_{11}^2(s) + Y_{12}^2(s) + Y_{13}^2(s) = \frac{\varphi_{11}^2}{s^2+2\varsigma_{11}^2 w_{11}^2 s+w_{11}^{2\,2}} U_1(s) + \frac{\varphi_{12}^2}{s^2+2\varsigma_{12}^2 w_{12}^2 s+w_{12}^{2\,2}} U_2(s) + \frac{\varphi_{13}^2}{s^2+2\varsigma_{13}^2 w_{13}^2 s+w_{13}^{2\,2}} U_3(s) \quad (3.13)$$

$$Y_2^2(s) = Y_{21}^2(s) + Y_{22}^2(s) + Y_{23}^2(s) = \frac{\varphi_{21}^2}{s^2+2\varsigma_{21}^2 w_{21}^2 s+w_{21}^{2\,2}} U_1(s) + \frac{\varphi_{22}^2}{s^2+2\varsigma_{22}^2 w_{22}^2 s+w_{22}^{2\,2}} U_2(s) + \frac{\varphi_{23}^2}{s^2+2\varsigma_{23}^2 w_{23}^2 s+w_{23}^{2\,2}} U_3(s) \quad (3.14)$$

$$Y_3^2(s) = Y_{31}^2(s) + Y_{32}^2(s) + Y_{33}^2(s) = \frac{\varphi_{31}^2}{s^2+2\varsigma_{31}^2 w_{31}^2 s+w_{31}^{2\,2}} U_1(s) + \frac{\varphi_{32}^2}{s^2+2\varsigma_{32}^2 w_{32}^2 s+w_{32}^{2\,2}} U_2(s) + \frac{\varphi_{33}^2}{s^2+2\varsigma_{33}^2 w_{33}^2 s+w_{33}^{2\,2}} U_3(s) \quad (3.15)$$

where $Y_i^2(s)$ (i=1, 2 and 3) represents the i^{th} output of mode 2. $Y_{ij}^2(s)$ (i, j=1, 2 and 3) represents the i^{th} output which caused by the j^{th} input of mode 2. φ_{ij}^2 represents the mode shape related to the i^{th} output and the j^{th} input of mode 2. ς_{ij}^2 represents the damping ratio between the i^{th} output and the j^{th} input of mode 2. w_{ij}^2 represents the natural frequency between the i^{th} output and the j^{th} input of mode 2.

MODE 3:

The transfer function representation for output 1, 2 and 3 at mode 3 is shown in (3.16), (3.17) and (3.18), respectively.

$$Y_1^3(s) = Y_{11}^3(s) + Y_{12}^3(s) + Y_{13}^3(s) = \frac{\varphi_{11}^3}{s^2+2\zeta_{11}^3 w_{11}^3 s+w_{11}^{3\,2}} U_1(s) + \frac{\varphi_{12}^3}{s^2+2\zeta_{12}^3 w_{12}^3 s+w_{12}^{3\,2}} U_2(s) + \frac{\varphi_{13}^3}{s^2+2\zeta_{13}^3 w_{13}^3 s+w_{13}^{3\,2}} U_3(s) \quad (3.16)$$

$$Y_2^3(s) = Y_{21}^3(s) + Y_{22}^3(s) + Y_{23}^3(s) = \frac{\varphi_{21}^3}{s^2+2\zeta_{21}^3 w_{21}^3 s+w_{21}^{3\,2}} U_1(s) + \frac{\varphi_{22}^3}{s^2+2\zeta_{22}^3 w_{22}^3 s+w_{22}^{3\,2}} U_2(s) + \frac{\varphi_{23}^3}{s^2+2\zeta_{23}^3 w_{23}^3 s+w_{23}^{3\,2}} U_3(s) \quad (3.17)$$

$$Y_3^3(s) = Y_{31}^3(s) + Y_{32}^3(s) + Y_{33}^3(s) = \frac{\varphi_{31}^3}{s^2+2\zeta_{31}^3 w_{31}^3 s+w_{31}^{3\,2}} U_1(s) + \frac{\varphi_{32}^3}{s^2+2\zeta_{32}^3 w_{32}^3 s+w_{32}^{3\,2}} U_2(s) + \frac{\varphi_{33}^3}{s^2+2\zeta_{33}^3 w_{33}^3 s+w_{33}^{3\,2}} U_3(s) \quad (3.18)$$

where $Y_i^3(s)$ (i=1, 2 and 3) represents the i^{th} output of mode 3. $Y_{ij}^3(s)$ (i, j=1, 2 and 3) represents the i^{th} output which caused by the j^{th} input of mode 3. φ_{ij}^3 represents the mode shape related to the i^{th} output and the j^{th} input of mode 3. ζ_{ij}^3 represents the damping ratio between the i^{th} output and the j^{th} input of mode 3. w_{ij}^3 represents the natural frequency between the i^{th} output and the j^{th} input of mode 3.

As this state-space modelling method needs a common denominator for each mode, the common damping ratios and natural frequencies need to be selected. For damping ratios, select the largest value of 9 sets of data in one mode. For natural frequencies, calculate the average frequencies in one mode. Therefore, the 9 different sets of ζ_{ij}^1、ζ_{ij}^2 and ζ_{ij}^3 can be merged into ζ^1、ζ^2 and ζ^3, and the 9 different sets of w_{ij}^1、w_{ij}^2 and w_{ij}^3 can be merged into w^1、w^2 and w^3.

After this modification, the transfer function representation can be simplified, and the results are shown below:

MODE 1:

$$Y_1^1(s) = Y_{11}^1(s) + Y_{12}^1(s) + Y_{13}^1(s) = \frac{\varphi_{11}^1 U_1(s)+\varphi_{12}^1 U_2(s)+\varphi_{13}^1 U_3(s)}{s^2+2\zeta^1 w^1 s+w^{1\,2}} \quad (3.19)$$

$$Y_2^1(s) = Y_{21}^1(s) + Y_{22}^1(s) + Y_{23}^1(s) = \frac{\varphi_{21}^1 U_1(s)+\varphi_{22}^1 U_2(s)+\varphi_{23}^1 U_3(s)}{s^2+2\zeta^1 w^1 s+w^{1\,2}} \quad (3.20)$$

$$Y_3^1(s) = Y_{31}^1(s) + Y_{32}^1(s) + Y_{33}^1(s) = \frac{\varphi_{31}^1 U_1(s) + \varphi_{32}^1 U_2(s) + \varphi_{33}^1 U_3(s)}{s^2 + 2\zeta^1 w^1 s + w^{1^2}} \quad (3.21)$$

MODE 2:

$$Y_1^2(s) = Y_{11}^2(s) + Y_{12}^2(s) + Y_{13}^2(s) = \frac{\varphi_{11}^2 U_1(s) + \varphi_{12}^2 U_2(s) + \varphi_{13}^2 U_3(s)}{s^2 + 2\zeta^2 w^2 s + w^{2^2}} \quad (3.22)$$

$$Y_2^2(s) = Y_{21}^2(s) + Y_{22}^2(s) + Y_{23}^2(s) = \frac{\varphi_{21}^2 U_1(s) + \varphi_{22}^2 U_2(s) + \varphi_{23}^2 U_3(s)}{s^2 + 2\zeta^2 w^2 s + w^{2^2}} \quad (3.23)$$

$$Y_3^2(s) = Y_{31}^2(s) + Y_{32}^2(s) + Y_{33}^2(s) = \frac{\varphi_{31}^2 U_1(s) + \varphi_{32}^2 U_2(s) + \varphi_{33}^2 U_3(s)}{s^2 + 2\zeta^2 w^2 s + w^{2^2}} \quad (3.24)$$

MODE 3:

$$Y_1^3(s) = Y_{11}^3(s) + Y_{12}^3(s) + Y_{13}^3(s) = \frac{\varphi_{11}^3 U_1(s) + \varphi_{12}^3 U_2(s) + \varphi_{13}^3 U_3(s)}{s^2 + 2\zeta^3 w^3 s + w^{3^2}} \quad (3.25)$$

$$Y_2^3(s) = Y_{21}^3(s) + Y_{22}^3(s) + Y_{23}^3(s) = \frac{\varphi_{21}^3 U_1(s) + \varphi_{22}^3 U_2(s) + \varphi_{23}^3 U_3(s)}{s^2 + 2\zeta^3 w^3 s + w^{3^2}} \quad (3.26)$$

$$Y_3^3(s) = Y_{31}^3(s) + Y_{32}^3(s) + Y_{33}^3(s) = \frac{\varphi_{31}^3 U_1(s) + \varphi_{32}^3 U_2(s) + \varphi_{33}^3 U_3(s)}{s^2 + 2\zeta^3 w^3 s + w^{3^2}} \quad (3.27)$$

Then, the transfer matrix of mathematical model can be built as:

$$\mathbf{Y(s)} = \begin{bmatrix} Y_1(s) \\ Y_2(s) \\ Y_3(s) \end{bmatrix} = \begin{bmatrix} Y_1^1(s) + Y_1^2(s) + Y_1^3(s) \\ Y_2^1(s) + Y_2^2(s) + Y_2^3(s) \\ Y_3^1(s) + Y_3^2(s) + Y_3^3(s) \end{bmatrix} =$$

$$\begin{bmatrix} \frac{\varphi_{11}^1 U_1(s) + \varphi_{12}^1 U_2(s) + \varphi_{13}^1 U_3(s)}{s^2 + 2\zeta^1 w^1 s + w^{1^2}} + \frac{\varphi_{11}^2 U_1(s) + \varphi_{12}^2 U_2(s) + \varphi_{13}^2 U_3(s)}{s^2 + 2\zeta^2 w^2 s + w^{2^2}} + \frac{\varphi_{11}^3 U_1(s) + \varphi_{12}^3 U_2(s) + \varphi_{13}^3 U_3(s)}{s^2 + 2\zeta^3 w^3 s + w^{3^2}} \\ \frac{\varphi_{21}^1 U_1(s) + \varphi_{22}^1 U_2(s) + \varphi_{23}^1 U_3(s)}{s^2 + 2\zeta^1 w^1 s + w^{1^2}} + \frac{\varphi_{21}^2 U_1(s) + \varphi_{22}^2 U_2(s) + \varphi_{23}^2 U_3(s)}{s^2 + 2\zeta^2 w^2 s + w^{2^2}} + \frac{\varphi_{21}^3 U_1(s) + \varphi_{22}^3 U_2(s) + \varphi_{23}^3 U_3(s)}{s^2 + 2\zeta^3 w^3 s + w^{3^2}} \\ \frac{\varphi_{31}^1 U_1(s) + \varphi_{32}^1 U_2(s) + \varphi_{33}^1 U_3(s)}{s^2 + 2\zeta^1 w^1 s + w^{1^2}} + \frac{\varphi_{31}^2 U_1(s) + \varphi_{32}^2 U_2(s) + \varphi_{33}^2 U_3(s)}{s^2 + 2\zeta^2 w^2 s + w^{2^2}} + \frac{\varphi_{31}^3 U_1(s) + \varphi_{32}^3 U_2(s) + \varphi_{33}^3 U_3(s)}{s^2 + 2\zeta^3 w^3 s + w^{3^2}} \end{bmatrix} \quad (3.28)$$

Since the mode shape φ_{ij}^k is the product of φ_i^k and φ_j^k as explained in the theoretical analysis, the transfer matrix can be modified as:

$$\mathbf{Y}(\mathbf{s}) = \begin{bmatrix} Y_1(s) \\ Y_2(s) \\ Y_3(s) \end{bmatrix} = \begin{bmatrix} Y_1^1(s) + Y_1^2(s) + Y_1^3(s) \\ Y_2^1(s) + Y_2^2(s) + Y_2^3(s) \\ Y_3^1(s) + Y_3^2(s) + Y_3^3(s) \end{bmatrix} =$$

$$\begin{bmatrix} \frac{\varphi_1^1(\varphi_1^1 U_1(s)+\varphi_2^1 U_2(s)+\varphi_3^1 U_3(s))}{s^2+2\zeta^1 w^1 s+w^{1^2}} + \frac{\varphi_1^2(\varphi_1^2 U_1(s)+\varphi_2^2 U_2(s)+\varphi_3^2 U_3(s))}{s^2+2\zeta^2 w^2 s+w^{2^2}} + \frac{\varphi_1^3(\varphi_1^3 U_1(s)+\varphi_2^3 U_2(s)+\varphi_3^3 U_3(s))}{s^2+2\zeta^3 w^3 s+w^{3^2}} \\ \frac{\varphi_2^1(\varphi_1^1 U_1(s)+\varphi_2^1 U_2(s)+\varphi_3^1 U_3(s))}{s^2+2\zeta^1 w^1 s+w^{1^2}} + \frac{\varphi_2^2(\varphi_1^2 U_1(s)+\varphi_2^2 U_2(s)+\varphi_3^2 U_3(s))}{s^2+2\zeta^2 w^2 s+w^{2^2}} + \frac{\varphi_2^3(\varphi_1^3 U_1(s)+\varphi_2^3 U_2(s)+\varphi_3^3 U_3(s))}{s^2+2\zeta^3 w^3 s+w^{3^2}} \\ \frac{\varphi_3^1(\varphi_1^1 U_1(s)+\varphi_2^1 U_2(s)+\varphi_3^1 U_3(s))}{s^2+2\zeta^1 w^1 s+w^{1^2}} + \frac{\varphi_3^2(\varphi_1^2 U_1(s)+\varphi_2^2 U_2(s)+\varphi_3^2 U_3(s))}{s^2+2\zeta^2 w^2 s+w^{2^2}} + \frac{\varphi_3^3(\varphi_1^3 U_1(s)+\varphi_2^3 U_2(s)+\varphi_3^3 U_3(s))}{s^2+2\zeta^3 w^3 s+w^{3^2}} \end{bmatrix} \quad (3.29)$$

From (3.29), it can be seen that there are common parts in the transfer matrix for each mode, so the following definition can be made:

$$P_1(s) = \frac{\varphi_1^1 U_1(s)+\varphi_2^1 U_2(s)+\varphi_3^1 U_3(s)}{s^2+2\zeta^1 w^1 s+w^{1^2}} = \frac{\begin{bmatrix}\varphi_1^1 & \varphi_2^1 & \varphi_3^1\end{bmatrix}\begin{bmatrix}U_1(s) \\ U_2(s) \\ U_3(s)\end{bmatrix}}{s^2+2\zeta^1 w^1 s+w^{1^2}} \quad (3.30)$$

$$P_2(s) = \frac{\varphi_1^2 U_1(s)+\varphi_2^2 U_2(s)+\varphi_3^2 U_3(s)}{s^2+2\zeta^2 w^2 s+w^{2^2}} = \frac{\begin{bmatrix}\varphi_1^2 & \varphi_2^2 & \varphi_3^2\end{bmatrix}\begin{bmatrix}U_1(s) \\ U_2(s) \\ U_3(s)\end{bmatrix}}{s^2+2\zeta^2 w^2 s+w^{2^2}} \quad (3.31)$$

$$P_3(s) = \frac{\varphi_1^3 U_1(s)+\varphi_2^3 U_2(s)+\varphi_3^3 U_3(s)}{s^2+2\zeta^3 w^3 s+w^{3^2}} = \frac{\begin{bmatrix}\varphi_1^3 & \varphi_2^3 & \varphi_3^3\end{bmatrix}\begin{bmatrix}U_1(s) \\ U_2(s) \\ U_3(s)\end{bmatrix}}{s^2+2\zeta^3 w^3 s+w^{3^2}} \quad (3.32)$$

where $P_i(s)$ (i=1, 2 and 3) represents the intermediate output of this system for each mode. Based on the above definition, the transfer matrix can be modified as:

$$\mathbf{Y}(\mathbf{s}) = \begin{bmatrix} Y_1(s) \\ Y_2(s) \\ Y_3(s) \end{bmatrix} = \begin{bmatrix} \varphi_1^1 P_1(s) + \varphi_1^2 P_2(s) + \varphi_1^3 P_3(s) \\ \varphi_2^1 P_1(s) + \varphi_2^2 P_2(s) + \varphi_2^3 P_3(s) \\ \varphi_3^1 P_1(s) + \varphi_3^2 P_2(s) + \varphi_3^3 P_3(s) \end{bmatrix} = \begin{bmatrix} \varphi_1^1 & \varphi_1^2 & \varphi_1^3 \\ \varphi_2^1 & \varphi_2^2 & \varphi_2^3 \\ \varphi_3^1 & \varphi_3^2 & \varphi_3^3 \end{bmatrix} \begin{bmatrix} P_1(s) \\ P_2(s) \\ P_3(s) \end{bmatrix} \quad (3.33)$$

In order to build the state space form, some transformation need to be done. Apply the inverse Laplace transform to (3.30), the time domain equation is shown as:

$$s^2 P_1(s) + 2\zeta^1 w^1 s P_1(s) + w^{1^2} P_1(s) = \begin{bmatrix}\varphi_1^1 & \varphi_2^1 & \varphi_3^1\end{bmatrix}\begin{bmatrix}U_1(s) \\ U_2(s) \\ U_3(s)\end{bmatrix}$$

$$\ddot{p_1} + 2\zeta^1 w^1 \dot{p_1} + w^{1^2} p_1 = \begin{bmatrix}\varphi_1^1 & \varphi_2^1 & \varphi_3^1\end{bmatrix}\begin{bmatrix}u_1 \\ u_2 \\ u_3\end{bmatrix} \quad (3.34)$$

Based on (3.34) and the state-space theory, this second order differential equation can be converted into two first order differential equations which are displayed in state-space form according to Figure 3.10.

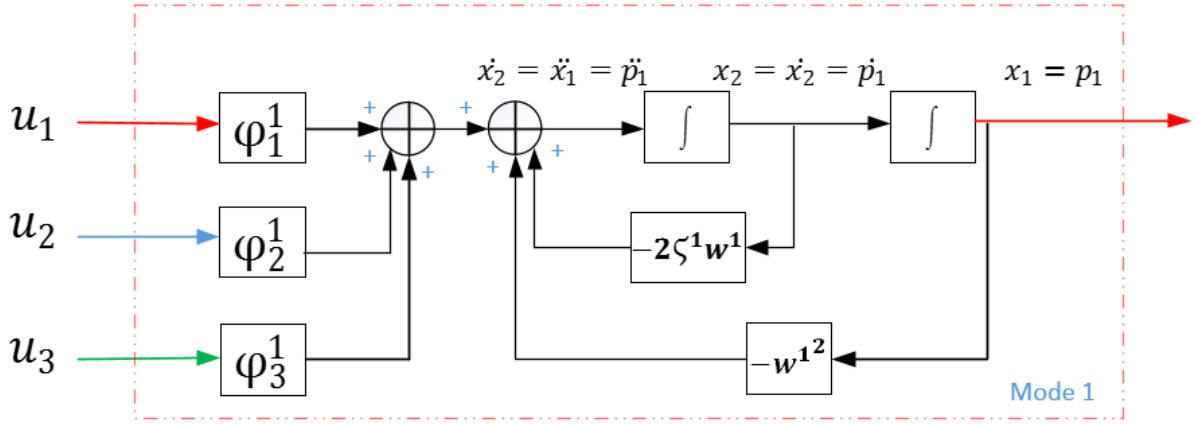

Figure 3.10 The block diagram of the state space representation for p_1

The state space representation for p_1 is shown as:

$$\begin{cases} \dot{x}_1 = x_2 \\ \dot{x}_2 = [\varphi_1^1 \quad \varphi_2^1 \quad \varphi_3^1]\begin{bmatrix} u_1 \\ u_2 \\ u_3 \end{bmatrix} - 2\zeta^1 w^1 x_2 - w^{1^2} x_1 \end{cases}$$

$$\begin{bmatrix} \dot{x}_1 \\ \dot{x}_2 \end{bmatrix} = \begin{bmatrix} 0 & 1 \\ -w^{1^2} & -2\zeta^1 w^1 \end{bmatrix}\begin{bmatrix} x_1 \\ x_2 \end{bmatrix} + \begin{bmatrix} 0 & 0 & 0 \\ \varphi_1^1 & \varphi_2^1 & \varphi_3^1 \end{bmatrix}\begin{bmatrix} u_1 \\ u_2 \\ u_3 \end{bmatrix} \tag{3.35}$$

where x_1 is a variable which is defined as p_1 and x_2 is a variable which is defined as $\dot{p}_1$.

Apply the inverse Laplace transform to (3.31), the time domain equation is shown as:

$$s^2 P_2(s) + 2\zeta^2 w^2 s P_2(s) + w^{2^2} P_2(s) = [\varphi_1^2 \quad \varphi_2^2 \quad \varphi_3^2]\begin{bmatrix} U_1(s) \\ U_2(s) \\ U_3(s) \end{bmatrix}$$

$$\ddot{p}_2 + 2\zeta^2 w^2 \dot{p}_2 + w^{2^2} p_2 = [\varphi_1^2 \quad \varphi_2^2 \quad \varphi_3^2]\begin{bmatrix} u_1 \\ u_2 \\ u_3 \end{bmatrix} \tag{3.36}$$

Based on (3.36) and the state-space theory, this second order differential equation can be converted into two first order differential equations which are displayed in the state-space form according to Figure 3.11.

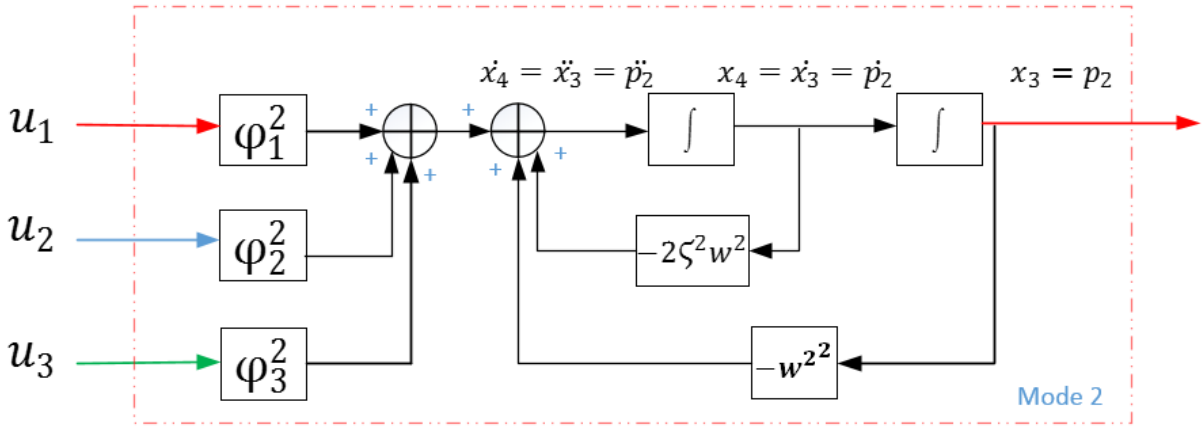

Figure 3.11 The block diagram of the state space representation for p_2

The state space representation for p_2 is shown as:

$$\begin{cases} \dot{x}_3 = x_4 \\ \dot{x}_4 = [\varphi_1^2 \quad \varphi_2^2 \quad \varphi_3^2]\begin{bmatrix} u_1 \\ u_2 \\ u_3 \end{bmatrix} - 2\zeta^2 w^2 x_4 - w^{2^2} x_3 \end{cases}$$

$$\begin{bmatrix} \dot{x}_3 \\ \dot{x}_4 \end{bmatrix} = \begin{bmatrix} 0 & 1 \\ -w^{2^2} & -2\zeta^2 w^2 \end{bmatrix}\begin{bmatrix} x_3 \\ x_4 \end{bmatrix} + \begin{bmatrix} 0 & 0 & 0 \\ \varphi_1^2 & \varphi_2^2 & \varphi_3^2 \end{bmatrix}\begin{bmatrix} u_1 \\ u_2 \\ u_3 \end{bmatrix} \tag{3.37}$$

where x_3 is a variable which is defined as p_2 and x_4 is a variable which is defined as $\dot{p}_2$.

Apply the inverse Laplace transform to (3.32), the time domain equation is shown as:

$$s^2 P_3(s) + 2\zeta^3 w^3 s P_3(s) + w^{3^2} P_3(s) = [\varphi_1^3 \quad \varphi_2^3 \quad \varphi_3^3]\begin{bmatrix} U_1(s) \\ U_2(s) \\ U_3(s) \end{bmatrix}$$

$$\ddot{p}_3 + 2\zeta^3 w^3 \dot{p}_3 + w^{3^2} p_3 = [\varphi_1^3 \quad \varphi_2^3 \quad \varphi_3^3]\begin{bmatrix} u_1 \\ u_2 \\ u_3 \end{bmatrix} \tag{3.38}$$

Based on (3.38) and the state-space theory, this second order differential equation can be converted into two first order differential equations which are displayed in the state-space form according to Figure 3.12.

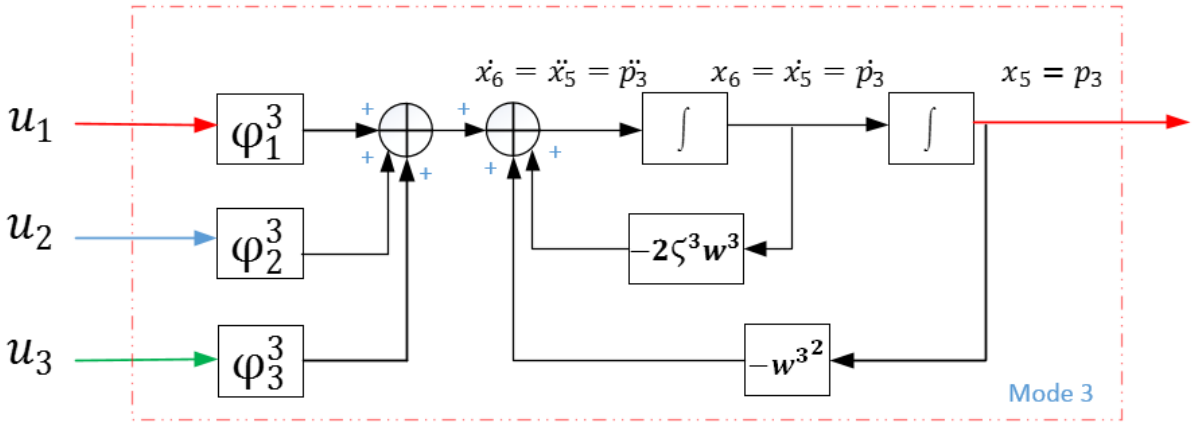

Figure 3.12 The block diagram of the state space representation for p_3

The state space representation for p_3 is shown as:

$$\begin{cases} \dot{x}_5 = x_6 \\ \dot{x}_6 = [\varphi_1^3 \quad \varphi_2^3 \quad \varphi_3^3]\begin{bmatrix} u_1 \\ u_2 \\ u_3 \end{bmatrix} - 2\varsigma^3 w^3 x_6 - w^{3^2} x_5 \end{cases}$$

$$\begin{bmatrix} \dot{x}_5 \\ \dot{x}_6 \end{bmatrix} = \begin{bmatrix} 0 & 1 \\ -w^{3^2} & -2\varsigma^3 w^3 \end{bmatrix}\begin{bmatrix} x_5 \\ x_6 \end{bmatrix} + \begin{bmatrix} 0 & 0 & 0 \\ \varphi_1^3 & \varphi_2^3 & \varphi_3^3 \end{bmatrix}\begin{bmatrix} u_1 \\ u_2 \\ u_3 \end{bmatrix} \tag{3.39}$$

where x_5 is a variable which is defined as p_3 and x_6 is a variable which is defined as $\dot{p}_3$.

Finally, based on the obtained (3.35), (3.37) and (3.39), the state representation of the physical system can be obtained in (3.40). In addition, the output equation can also be obtained based on (3.33) and the relation between p_i and x_i.

$$\begin{cases} \dot{\boldsymbol{X}}(\boldsymbol{t}) = \mathbf{A}\boldsymbol{X}(\boldsymbol{t}) + \mathbf{B}\boldsymbol{U}(\boldsymbol{t}) \\ \boldsymbol{Y}(\boldsymbol{t}) = \mathbf{C}\boldsymbol{X}(\boldsymbol{t}) \end{cases} \tag{3.40}$$

where $\boldsymbol{X}(\boldsymbol{t}) = \begin{bmatrix} x_1 \\ x_2 \\ x_3 \\ x_4 \\ x_5 \\ x_6 \end{bmatrix}$ $\boldsymbol{Y}(\boldsymbol{t}) = \begin{bmatrix} y_1 \\ y_2 \\ y_3 \end{bmatrix}$ $\mathbf{A} = \begin{bmatrix} 0 & 1 & & & & \\ -w^{1^2} & -2\varsigma^1 w^1 & & & & \\ & & 0 & 1 & & \\ & & -w^{2^2} & -2\varsigma^2 w^2 & & \\ & & & & 0 & 1 \\ & & & & -w^{3^2} & -2\varsigma^3 w^3 \end{bmatrix}$

$$\mathbf{B} = \begin{bmatrix} 0 & 0 & 0 \\ \varphi_1^1 & \varphi_2^1 & \varphi_3^1 \\ 0 & 0 & 0 \\ \varphi_1^2 & \varphi_2^2 & \varphi_3^2 \\ 0 & 0 & 0 \\ \varphi_1^3 & \varphi_2^3 & \varphi_3^3 \end{bmatrix} \quad \mathbf{C} = \begin{bmatrix} \varphi_1^1 & 0 & \varphi_1^2 & 0 & \varphi_1^3 & 0 \\ \varphi_2^1 & 0 & \varphi_2^2 & 0 & \varphi_2^3 & 0 \\ \varphi_3^1 & 0 & \varphi_3^2 & 0 & \varphi_3^3 & 0 \end{bmatrix}$$

All parameters of the state space representation are listed in Table 3.2, and they are all based on the selection method explained before.

Table 3.2 All parameters of the state space representation

Mode 1		Mode 2		Mode 3	
ς^1	0.02677	ς^2	0.02533	ς^3	0.02419
w^1	142.3048	w^2	182.434	w^3	218.9208
φ_1^1	0.3639	φ_1^2	0.7229	φ_1^3	0.4552
φ_2^1	0.2821	φ_2^2	0.4803	φ_2^3	0.8414
φ_3^1	0.2384	φ_3^2	0.4456	φ_3^3	0.758

The block diagram of the physical system in the state space form is shown in Figure 3.13. The physical meanings of the parameters of the system are important and useful when dealing with the real system, especially in the experimental process. In this project, three outputs (y_1, y_2 and y_3) are measured by three sensors which produce the corresponding displacement of the plate. Three inputs (u_1, u_2 and u_3) are generated by three actuators, which are injected into the plate in the form of acceleration. The mode shape φ_i^k which connects with three outputs are regarded as the sensor gains and these gains represent the corresponding proportional relation between p_i and y_i^k. The mode shape φ_j^k which connects with three inputs are regarded as the actuator gains and these gains represent the proportion of inputs that can be inject into the system.

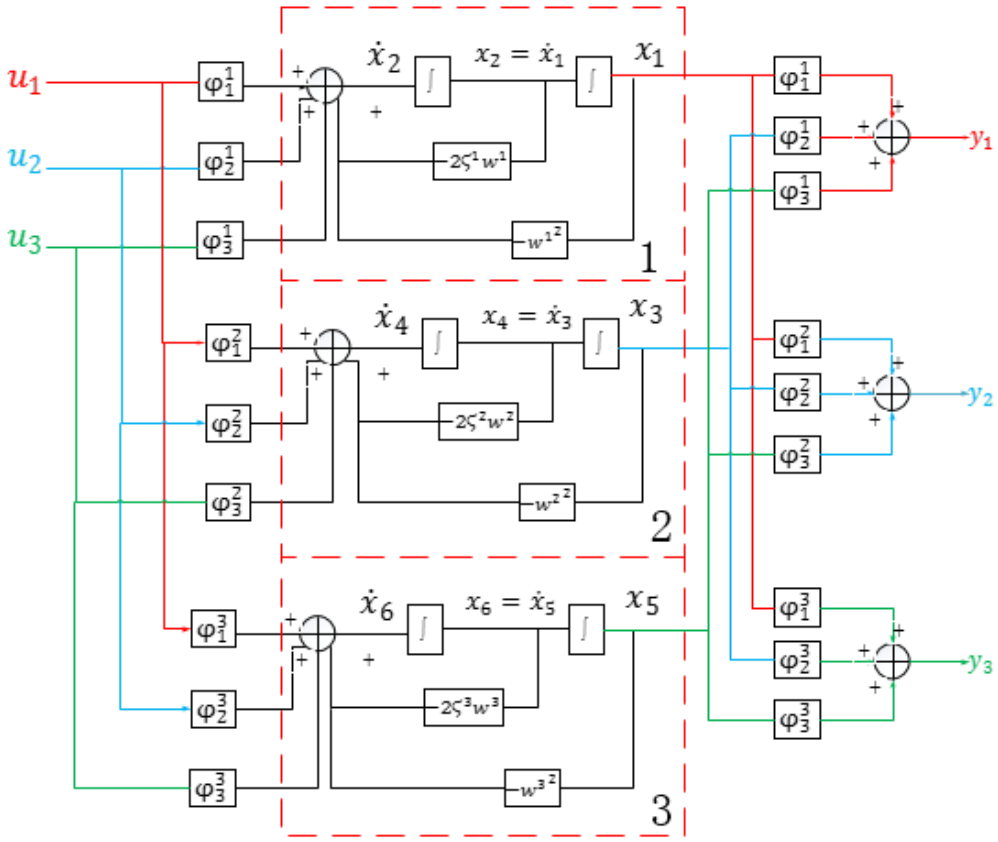

Figure 3.13 The block diagram of the physical system in state space form

Chapter 4 : Beard-Jones Filter

In this chapter, the Beard-Jones (BJ) filter will be discussed in detail as the core of the fault detection approach. Firstly, the structure of the BJ filter which forms the basic concept in the fault detection approach is introduced in section 4.1. Then in section 4.2, the BJ filter fault detection theory for one-fault situation and multiple-fault situation are introduced. In section 4.3, a random system with pre-defined fault vectors is laid out to validate the BJ filter design principle and procedure. Finally, through simulation, the feature of the BJ filter as a fault detection tool is validated.

4.1 The Structure of Beard-Jones (BJ) Filter

The fault detection problem using BJ filter mainly depends on the reference mathematical model (structure of BJ filter) method which is related to the observer and state estimation theory. There are three mathematical models need to be taken into consideration, which are normal operation system mathematical model, failure system mathematical model and reference mathematical model [24]. The relation between these three mathematical models will be discussed in detail in this section, and the dynamic changes in this relation caused by faults will lead to the key point in designing the BJ filter, which is the selection of a proper detection gain.

The normal operation system mathematical model is described firstly. The system considered in the project is restricted to linear and time invariant system, and this system can be perfectly characterized by the relation between the control signal $\boldsymbol{U(t)}$ and output signal $\boldsymbol{Y(t)}$. The state space representation of this system is shown as:

$$\begin{cases} \dot{\boldsymbol{X}}(\boldsymbol{t}) = \mathbf{A}\boldsymbol{X}(\boldsymbol{t}) + \mathbf{B}\boldsymbol{U}(\boldsymbol{t}) \\ \boldsymbol{Y}(\boldsymbol{t}) = \mathbf{C}\boldsymbol{X}(\boldsymbol{t}) \end{cases} \tag{4.1}$$

where $\boldsymbol{X(t)}$ is a n×1 state vector, $\boldsymbol{U(t)}$ is a r×1 control input vector and $\boldsymbol{Y(t)}$ is a m×1 output vector. Matrices **A**, **B** and **C** are corresponding coefficient matrices which have the dimension of n×n, n×r and m×n, respectively. With the knowledge of the structure and parameters of the existing system, the state space representation of the BJ filter (reference mathematical model) can be constructed as [47]:

$$\begin{cases} \dot{\widehat{\boldsymbol{X}}}(\boldsymbol{t}) = \mathbf{A}\widehat{\boldsymbol{X}}(\boldsymbol{t}) + \mathbf{B}\boldsymbol{U}(\boldsymbol{t}) + \mathbf{L}(\boldsymbol{Y}(\boldsymbol{t}) - \widehat{\boldsymbol{Y}}(\boldsymbol{t})) \\ \boldsymbol{Y}(\boldsymbol{t}) = \mathbf{C}\widehat{\boldsymbol{X}}(\boldsymbol{t}) \end{cases} \tag{4.2}$$

where $\widehat{\boldsymbol{X}}(\boldsymbol{t})$ is a n×1 estimated state vector, $\widehat{\boldsymbol{Y}}(\boldsymbol{t})$ is a m×1 estimated output vector and **L** is a n×m detection gain matrix. This reference mathematical model is intended to estimate the normal operation of the system, which can be used to compare with the real system. The reason for using $\mathbf{L}(\boldsymbol{Y}(\boldsymbol{t}) - \widehat{\boldsymbol{Y}}(\boldsymbol{t}))$ is to deal with the initial condition (because the initial condition for the system is normally unknown). One design criterion for choosing matrix **L** is to enable the estimate state vector to trace the real state vector within a required period of time. This process should be stable and fast. Based on (4.1) and (4.2), the state error and the output error can be derived from the difference between the real system model and the reference model when there is no fault in the system.

$$\begin{aligned}
&\dot{\varepsilon}(\boldsymbol{t}) = \dot{\boldsymbol{X}}(\boldsymbol{t}) - \dot{\widehat{\boldsymbol{X}}}(\boldsymbol{t}) \\
&= \mathbf{A}\boldsymbol{X}(\boldsymbol{t}) + \mathbf{B}\boldsymbol{U}(\boldsymbol{t}) - \mathbf{A}\widehat{\boldsymbol{X}}(\boldsymbol{t}) - \mathbf{B}\boldsymbol{U}(\boldsymbol{t}) - \mathbf{L}(\boldsymbol{Y}(\boldsymbol{t}) - \widehat{\boldsymbol{Y}}(\boldsymbol{t})) \\
&= \mathbf{A}\boldsymbol{X}(\boldsymbol{t}) + \mathbf{B}\boldsymbol{U}(\boldsymbol{t}) - \mathbf{A}\widehat{\boldsymbol{X}}(\boldsymbol{t}) - \mathbf{B}\boldsymbol{U}(\boldsymbol{t}) - \mathbf{L}(\boldsymbol{C}\boldsymbol{X}(\boldsymbol{t}) - \boldsymbol{C}\widehat{\boldsymbol{X}}(\boldsymbol{t})) \\
&= (\mathbf{A} - \mathbf{LC})\boldsymbol{X}(\boldsymbol{t}) - (\mathbf{A} - \mathbf{LC})\widehat{\boldsymbol{X}}(\boldsymbol{t}) \\
&= (\mathbf{A} - \mathbf{LC})\varepsilon(\boldsymbol{t}) \qquad (4.3)
\end{aligned}$$

$$\begin{aligned}
&\hat{\varepsilon}(\boldsymbol{t}) = \boldsymbol{Y}(\boldsymbol{t}) - \widehat{\boldsymbol{Y}}(\boldsymbol{t}) \\
&= \mathbf{C}\boldsymbol{X}(\boldsymbol{t}) - \mathbf{C}\widehat{\boldsymbol{X}}(\boldsymbol{t}) \\
&= \mathbf{C}\varepsilon(\boldsymbol{t}) \qquad (4.4)
\end{aligned}$$

where $\varepsilon(\boldsymbol{t})$ is a n×1 state error vector and $\hat{\varepsilon}(\boldsymbol{t})$ is a m×1 output error vector. These two equations lead to another design criterion for choosing matrix **L** such that the output error (residual) will have a fixed direction associated with certain failure. The block diagram of the fault detection system using the BJ filter is present in Figure 4.1.

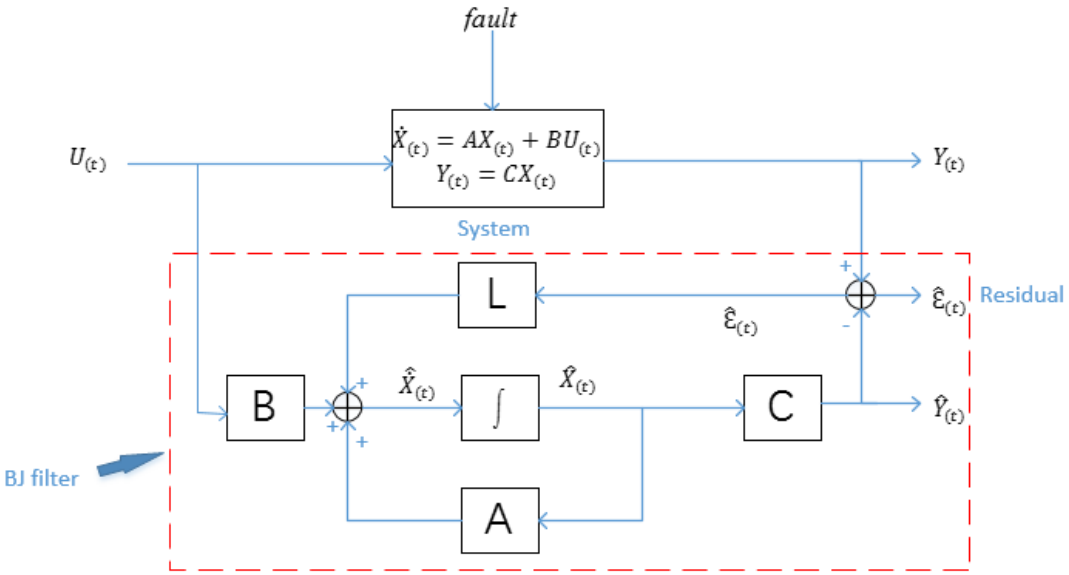

Figure 4.1 The block diagram of fault detection system using the BJ filter

In this project, only additive faults are taken into consideration, which mainly consist of sensor faults and actuator faults. In the present of faults in a control system, failure system mathematical model can be developed from the normal operation system mathematical model.

The system of (4.1) with actuator faults can commonly be modelled by adding a single fault component to the state equation of (4.1) to form:

$$\begin{cases} \dot{\boldsymbol{X}}(\boldsymbol{t}) = \mathbf{A}\boldsymbol{X}(\boldsymbol{t}) + \mathbf{B}\boldsymbol{U}(\boldsymbol{t}) + \boldsymbol{f_i}\boldsymbol{\mu_i} \\ \boldsymbol{Y}(\boldsymbol{t}) = \mathbf{C}\boldsymbol{X}(\boldsymbol{t}) \end{cases} \tag{4.5}$$

where $\boldsymbol{f_i}$ is a n×1 failure vector which is associated with the i^{th} actuator fault and $\boldsymbol{\mu_i}$ represents a time-varying scalar which normally is a function of $\boldsymbol{U}(\boldsymbol{t})$. It is not necessary to actually know the value of $\boldsymbol{\mu_i}$, because the design of the BJ filter does not need the knowledge of this function, and the selection of $\boldsymbol{\mu_i}$ can be arbitrary. However, in the case that the directions of faults are hard to be distinguished, the knowledge of the fault magnitude which can be set by applying different values of $\boldsymbol{\mu_i}$ can be very useful [48]. Based on (4.2) and (4.5), the state error and the output error can be derived from the difference between the failure system model and the reference model when there exists the i^{th} actuator fault in the system.

$$\begin{aligned} &\dot{\varepsilon}(\boldsymbol{t}) = \dot{\boldsymbol{X}}(\boldsymbol{t}) - \hat{\dot{\boldsymbol{X}}}(\boldsymbol{t}) \\ &= \mathbf{A}\boldsymbol{X}(\boldsymbol{t}) + \mathbf{B}\boldsymbol{U}(\boldsymbol{t}) + \boldsymbol{f_i}\boldsymbol{\mu_i} - \mathbf{A}\hat{\boldsymbol{X}}(\boldsymbol{t}) - \mathbf{B}\boldsymbol{U}(\boldsymbol{t}) - \mathbf{L}(\boldsymbol{Y}(\boldsymbol{t}) - \hat{\boldsymbol{Y}}(\boldsymbol{t})) \\ &= (\mathbf{A} - \mathbf{LC})\boldsymbol{X}(\boldsymbol{t}) - (\mathbf{A} - \mathbf{LC})\hat{\boldsymbol{X}}(\boldsymbol{t}) + \boldsymbol{f_i}\boldsymbol{\mu_i} \\ &= (\mathbf{A} - \mathbf{LC})\varepsilon(\boldsymbol{t}) + \boldsymbol{f_i}\boldsymbol{\mu_i} \end{aligned} \tag{4.6}$$

$$\hat{\varepsilon}(\boldsymbol{t}) = \boldsymbol{Y}(\boldsymbol{t}) - \hat{\boldsymbol{Y}}(\boldsymbol{t})$$
$$= \mathbf{C}\varepsilon(\boldsymbol{t}) \tag{4.7}$$

When considering the actuator fault situation, the design of the detection gain **L** needs to meet the condition that the output residual $\hat{\varepsilon}(\boldsymbol{t})$ be proportional to $\mathbf{C}\boldsymbol{f_i}$. This means that the direction of $\hat{\varepsilon}(\boldsymbol{t})$ is unique and $\hat{\varepsilon}(\boldsymbol{t})$ is only associated with the designed fault $\boldsymbol{f_i}$ during the system transient [49, 50 and 51]. The block diagram of the structure of the actuator failure system is presented in Figure 4.2.

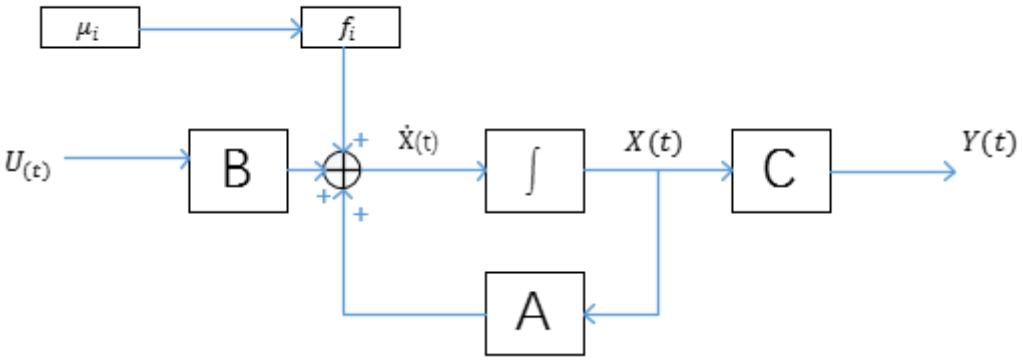

Figure 4.2 The structure of the actuator failure system

The system of (4.1) with sensor faults can commonly be modelled by adding a single fault component to the output equation of (4.1) to form:

$$\begin{cases} \dot{\boldsymbol{X}}(\boldsymbol{t}) = \mathbf{A}\boldsymbol{X}(\boldsymbol{t}) + \mathbf{B}\boldsymbol{U}(\boldsymbol{t}) \\ \boldsymbol{Y}(\boldsymbol{t}) = \mathbf{C}\boldsymbol{X}(\boldsymbol{t}) + \boldsymbol{e_i}\boldsymbol{\mu_i} \end{cases} \tag{4.8}$$

where $\boldsymbol{e_i}$ is a m×1 failure unit vector which is associated with the i^{th} sensor fault and $\boldsymbol{\mu_i}$ represents a time-varying scalar which normally is a function of $\boldsymbol{X}(\boldsymbol{t})$. Similar to the actuator failure, the selection of $\boldsymbol{\mu_i}$ is also arbitrary [48]. Based on (4.2) and (4.8), the state error and the output error can be derived from the difference between the failure system model and the reference model when there exists the i^{th} sensor fault in the system.

$$\dot{\varepsilon}(\boldsymbol{t}) = \dot{\boldsymbol{X}}(\boldsymbol{t}) - \dot{\hat{\boldsymbol{X}}}(\boldsymbol{t})$$
$$= \mathbf{A}\boldsymbol{X}(\boldsymbol{t}) + \mathbf{B}\boldsymbol{U}(\boldsymbol{t}) - \mathbf{A}\hat{\boldsymbol{X}}(\boldsymbol{t}) - \mathbf{B}\boldsymbol{U}(\boldsymbol{t}) - \mathbf{L}(\boldsymbol{Y}(\boldsymbol{t}) - \hat{\boldsymbol{Y}}(\boldsymbol{t}))$$
$$= \mathbf{A}\left(\boldsymbol{X}(\boldsymbol{t}) - \hat{\boldsymbol{X}}(\boldsymbol{t})\right) - \mathbf{LC}(\boldsymbol{X}(\boldsymbol{t}) - \hat{\boldsymbol{X}}(\boldsymbol{t})) + \mathbf{L}\boldsymbol{e_i}\boldsymbol{\mu_i}$$
$$= (\mathbf{A} - \mathbf{LC})\varepsilon(\boldsymbol{t}) + \boldsymbol{l_i}\boldsymbol{\mu_i} \tag{4.9}$$
$$\hat{\varepsilon}(\boldsymbol{t}) = \boldsymbol{Y}(\boldsymbol{t}) - \hat{\boldsymbol{Y}}(\boldsymbol{t})$$

$$= \mathbf{C}\boldsymbol{X}(\boldsymbol{t}) + \boldsymbol{e_i}\boldsymbol{\mu_i} - \mathbf{C}\hat{\boldsymbol{X}}(\boldsymbol{t})$$

$$= \mathbf{C}\varepsilon(\boldsymbol{t}) + \boldsymbol{e_i}\boldsymbol{\mu_i} \quad (4.10)$$

where $\boldsymbol{l_i}$ represents the i^{th} column of the detection gain **L**. When considering the sensor fault situation, the design of the detection gain **L** needs to meet the condition that the output residual $\hat{\varepsilon}(\boldsymbol{t})$ lies in the plane which is formed by the $\mathbf{C}\boldsymbol{l_i}$and $\boldsymbol{e_i}$ [48]. The block diagram of the structure of the sensor failure system is presented in Figure 4.3.

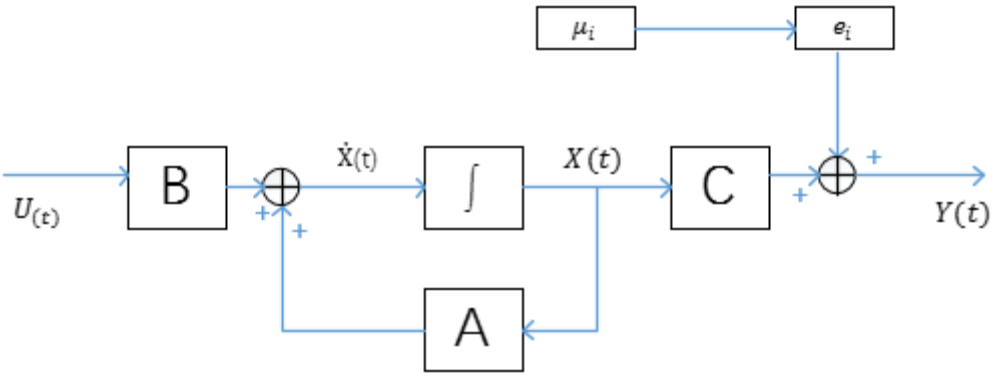

Figure 4.3 The structure of the sensor failure system

In this project, the actuator failure system will be mainly studied and analysed in the remaining sections because the theory and steps which are used to generate the detection gain **L** for the sensor failure system follow the same principle illustrated here.

4.2 BJ Filter Fault Detection Theory

In this section, the BJ filter fault detection theory which aims to generate the detection gain **L** will be fully described, and this section will mainly follow the Beard's thesis [25] to highlight the procedure of constructing the BJ filter. The BJ filter has the ability to utilize only one filter to detect multiple faults, so the methods for generating the detection gain for one-fault and multiple-fault situations are basically the same. Therefore, the first part will mainly focus on the detection theory for one-fault situation and the second part of this section explains the restrictions and conditions when extending the detection theory from one-fault situation to multiple-fault situation.

4.2.1 Detection Theory for One-Fault Situation

The development of the fault detection theory starts by a definition which states the basic goal of a detection filter. This definition is firstly proposed by Beard [25], and defines the fault detectability and requirement for the detection gain **L**.

Definition 1 (Definition 4.2 of [25]): A failure associated with a fault vector $\boldsymbol{f_i}$ is detectable if the detection gain **L** exists and meets two conditions such that:

1) The direction of the output residual $\hat{\varepsilon}(\boldsymbol{t})$ is fixed in the output space
2) All eigenvalues of **(A-LC)** can be chosen arbitrarily.

The first condition indicates the property of the BJ filter, which states that the output residual should follow the direction of the designed fault vector $\boldsymbol{f_i}$. The second condition provides the BJ filter with three advantages. The selection of proper eigenvalues enables the BJ filter to keep stable and allows the response time of the BJ filter to be adjusted. Based on these two advantages, the BJ filter can act as a state estimation observer. The last advantage enables detection gain **L** to be easily calculated mathematically due to the freedom in designing the BJ filter.

To meet the two conditions which are defined by Definition 1, the following theorems and lemmas are developed such that the detection gain **L** can be constructed properly to enable BJ filter to possess the fault detection capability.

Theorem 1 (Theorem 4.1 of [25]): If a vector in the state space is detectable, (**A**, **C**) must be an observable pair such that:

$$\mathbf{M} = \begin{bmatrix} \mathbf{C} \\ \mathbf{CA} \\ \vdots \\ \mathbf{CA}^{n-2} \\ \mathbf{CA}^{n-1} \end{bmatrix} \qquad \text{rank}(\mathbf{M}) = n \tag{4.11}$$

where matrices **A** and **C** are the system matrix and output matrix which have been stated in (4.5). *n* is the dimension of the state vector and matrix **M** is the observability matrix for (**A**, **C**). This observability limitation comes from the normal state estimation requirement [48]. In addition, through the next lemma, the relation between the state space concept and the condition of detectability is established [25].

Lemma 1 (Lemma 4.1 of [25]): The first condition of Definition 1 can be satisfied with the designed fault vector $\boldsymbol{f_i}$ if and only if

$$\text{rank } \mathbf{CW_f} = 1 \tag{4.12}$$

where $\mathbf{W_f}$ defined by (4.13) represents the controllable space of $\boldsymbol{f_i}$ related to (**A-LC**).

$$\mathbf{W_f} = [\boldsymbol{f_i}, (\mathbf{A} - \mathbf{LC})\boldsymbol{f_i}, \cdots, (\mathbf{A} - \mathbf{LC})^{n-1}\boldsymbol{f_i}] \tag{4.13}$$

The proof of this lemma can be briefly explained that the state error $\mathcal{E}(\boldsymbol{t})$ is in the controllable space of $\boldsymbol{f_i}$ due to (4.6), so the condition for output residual $\mathbf{C}\mathcal{E}(\boldsymbol{t})$ having a fixed direction must follow that the rank of $\mathbf{CW_f}$ is equal to 1. The detail proof is given in [25].

Based on the concept of Theorem 1 and Lemma 1, the following lemma introduces a specific vector which plays an important role in the design of the detection gain.

Lemma 2 (Lemma 4.2 of [25]): If the system meets the following three conditions:

1) ($\mathbf{A}$, $\mathbf{C}$) is an observable pair,
2) The rank of $\mathbf{W_f}$ is equal to k,
3) The rank of $\mathbf{CW_f}$ is equal to 1,

where $\mathbf{W_f}$ is defined in (4.13), there should exist a $n\times1$ vector $\mathbf{g}$ that is in the controllable space of $\boldsymbol{f_i}$ and meet the following equation:

$$\begin{bmatrix} \mathbf{C} \\ \mathbf{CA} \\ \vdots \\ \mathbf{CA}^{k-2} \end{bmatrix} \times \mathbf{g} = 0 \quad \text{and} \quad \mathbf{CA}^{k-1} \times \mathbf{g} \neq 0 \tag{4.14}$$

where k is the order of vector $\mathbf{g}$.

The proof of this lemma can be found in [25] in detail.

According to Lemma 2, it shows that this specific vector $\mathbf{g}$ is in the controllable space of vector $\mathbf{g}$ as well as the controllable space of fault vector $\boldsymbol{f_i}$, so this result yields (4.15) shown as:

$$[\mathbf{g},\ (\mathbf{A}-\mathbf{LC})\mathbf{g},\ \cdots,\ (\mathbf{A}-\mathbf{LC})^{k-1}\mathbf{g}] = [\mathbf{g},\ \mathbf{Ag}, \cdots, \mathbf{A}^{k-1}\mathbf{g}] \tag{4.15}$$

Therefore, the set of vectors $[\mathbf{g} \quad \mathbf{Ag} \quad \cdots \quad \mathbf{A}^{k-2}\mathbf{g} \quad \mathbf{A}^{k-1}\mathbf{g}]$ constructs the basis of controllable space for $\boldsymbol{f_i}$ such that the fault vector $\boldsymbol{f_i}$ can be expressed as:

$$\boldsymbol{f_i} = a_1\mathbf{g} + a_2\mathbf{Ag} + \cdots + a_k\mathbf{A}^{k-1}\mathbf{g} \tag{4.16}$$

where a_j is an arbitrary scalar and j=1, 2, $\cdots$, k. Equations (4.14) and (4.16) yield a solution which implies the relation between $\mathbf{C}\boldsymbol{f_i}$ and the specific vector $\mathbf{g}$.

$$\mathbf{C}\boldsymbol{f_i} = a_1\mathbf{Cg} + a_2\mathbf{CAg} + \cdots + a_k\mathbf{CA}^{k-1}\mathbf{g}$$

$$\because \mathbf{Cg} = \mathbf{CAg} = \cdots = \mathbf{CA}^{k-2}\mathbf{g} = 0 \qquad \therefore \mathbf{C}\boldsymbol{f_i} = a_k\mathbf{CA}^{k-1}\mathbf{g}$$

In addition, to simplify the problem, $\mathbf{g}$ is always chosen such that a_k is equal to 1.

$$\mathbf{C}\boldsymbol{f_i} = \mathbf{C}\mathbf{A}^{k-1}\mathbf{g} \tag{4.17}$$

Due to the property of this specific vector **g** as explained in Lemma 2, a definition about **g** is shown below.

Definition 2 (Definition 4.4 of [25]): The n×1 designed vector **g** is the k^{th} order detection generator for fault vector $\boldsymbol{f_i}$ if (4.14) and (4.16) are satisfied.

The order *k* represents the number of components in (4.16) which is used to represent the fault vector $\boldsymbol{f_i}$, and the value of *k* can be determined in the later explanations. The introduction of detection generator **g** is specialized for the development of the detection gain **L**. Although Lemma 2 shows that the construction of the detection generator is based on the information of the detection gain (due to the relation between $\mathbf{W_f}$ and **L**), the design of the detection generator only relies on the knowledge of **A**, **C** and the fault vector $\boldsymbol{f_i}$ according to (4.14) and (4.16). Therefore, the next theorem proposes an equation which can yield a solution for detection gain **L** based on the detection generator **g**. In addition, *k* eigenvalues of (**A**-**LC**) can also be selected arbitrarily, where the value *k* is exactly the order of the detection generator.

Theorem 2 (Theorem 4.2 of [25]): Under the case that the condition in Lemma 2 is satisfied, and *k* eigenvalues of (**A**-**LC**) can be obtained by the roots of (4.18).

$$s^k + p_k s^{k-1} + \cdots + p_2 s + p_1 = 0 \tag{4.18}$$

where p_j is an arbitrary scalar (j=1, 2, ⋯ , k). *s* is the complex variable which can be used to represent the poles of system. The solution of the detection gain **L** can be obtained as:

$$\mathbf{L}\mathbf{C}\mathbf{A}^{k-1}\mathbf{g} = p_1\mathbf{g} + p_2\mathbf{A}\mathbf{g} + \cdots + p_k\mathbf{A}^{k-1}\mathbf{g} + \mathbf{A}^k\mathbf{g} \tag{4.19}$$

where **g** is the k^{th} order detection generator for fault vector $\boldsymbol{f_i}$.

The proof of this theorem can be found in [25] in detail.

Based on the relation described in (4.17), (4.19) can be rewritten as:

$$\mathbf{L}\mathbf{C}\boldsymbol{f_i} = p_1\mathbf{g} + p_2\mathbf{A}\mathbf{g} + \cdots + p_k\mathbf{A}^{k-1}\mathbf{g} + \mathbf{A}^k\mathbf{g} \tag{4.20}$$

To calculate the detection gain **L** by solving (4.20), the following lemma provides a general solution directly.

Lemma 3 (Lemma 4.3 of [25]): Assume that there exist three matrices **L**, **P** and **Q**, which have the dimension *n*×*m*, *m*×*r* and *n*×*r*, respectively. Then the solution of **L** in

$$\mathbf{L} * \mathbf{P} = \mathbf{Q} \tag{4.21}$$

can be calculated as:

$$\mathbf{L} = \mathbf{Q}(\mathbf{P}^{\mathrm{T}}\mathbf{P})^{-1}\mathbf{P}^{\mathrm{T}} + \mathbf{L}'[\mathbf{I} - \mathbf{P}(\mathbf{P}^{\mathrm{T}}\mathbf{P})^{-1}\mathbf{P}^{\mathrm{T}}] \tag{4.22}$$

where matrix $\mathbf{L}'$ can be chosen arbitrarily and its dimension is $n \times m$, and it can be regarded as the freedom in matrix $\mathbf{L}$. $\mathbf{P}^{\mathrm{T}}$ means the transpose of matrix $\mathbf{P}$.

The proof of this lemma can be found in [52] in detail.

Based on (4.20) and (4.22), the solution of detection gain $\mathbf{L}$ can be calculated as:

$$\begin{aligned}\mathbf{L} = [p_1\mathbf{g} + p_2\mathbf{A}\mathbf{g} + \cdots + p_k\mathbf{A}^{k-1}\mathbf{g} + \mathbf{A}^k\mathbf{g}][(\mathbf{C}\boldsymbol{f_i})^T(\mathbf{C}\boldsymbol{f_i})]^{-1}(\mathbf{C}\boldsymbol{f_i})^T \\ +\mathbf{L}'[\mathbf{I} - (\mathbf{C}\boldsymbol{f_i})[(\mathbf{C}\boldsymbol{f_i})^T(\mathbf{C}\boldsymbol{f_i})]^{-1}(\mathbf{C}\boldsymbol{f_i})^T]\end{aligned} \tag{4.23}$$

However, the detection gain $\mathbf{L}$ cannot be solved directly from (4.23) due to an unknown detection generator $\mathbf{g}$. A new system can be constructed with a filter detection gain $\mathbf{L}'$ based on (4.23), and the form of this new system is the same as the original system. This new system can be used to determine the number of eigenvalues that can be chosen arbitrarily by the selection of $\mathbf{L}'$ [48].

According to (4.23), the new system can be constructed as:

$$\mathbf{A} - \mathbf{L}\mathbf{C} = \mathbf{A}' - \mathbf{L}'\mathbf{C}' \tag{4.24}$$

$$\mathbf{A}' = \mathbf{A} - [p_1\mathbf{g} + p_2\mathbf{A}\mathbf{g} + \cdots + p_k\mathbf{A}^{k-1}\mathbf{g} + \mathbf{A}^k\mathbf{g}][(\mathbf{C}\boldsymbol{f_i})^T(\mathbf{C}\boldsymbol{f_i})]^{-1}(\mathbf{C}\boldsymbol{f_i})^T\mathbf{C} \tag{4.25}$$

$$\mathbf{C}' = [\mathbf{I} - (\mathbf{C}\boldsymbol{f_i})[(\mathbf{C}\boldsymbol{f_i})^T(\mathbf{C}\boldsymbol{f_i})]^{-1}(\mathbf{C}\boldsymbol{f_i})^T]\mathbf{C} \tag{4.26}$$

So far, the above part can achieve some goals. In order to detect the fault vector $\boldsymbol{f_i}$, as explained in Definition 1, the condition that the output residual $\mathbf{C}\varepsilon(\boldsymbol{t})$ has fixed direction can be achieved by selecting proper parameter values in (4.23) so that the rank of $\mathbf{CW_f}$ is equal to 1. Besides, according to (4.18), k eigenvalues of (**A-LC**) can be set based on $[p_1, p_2, \cdots p_k]$. The second condition in Definition 1 can be met if the left n-k eigenvalues of (**A-LC**) can be designed arbitrarily due to the remaining freedom in detection gain $\mathbf{L}$ (which lies in the selection of $\mathbf{L}'$) and the number of these eigenvalues can be determined by the following lemma.

Lemma 4 (Lemma 4.4 of [25]): If three matrices $\mathbf{A}', \mathbf{C}'$ and $\mathbf{L}'$ have the dimensions $n \times n$, $m \times n$ and $n \times m$, respectively, there are q eigenvalues of $(\mathbf{A}' - \mathbf{L}'\mathbf{C}')$ that can be arbitrarily selected

based on the freedom in $\mathbf{L}'$, and according to the Theorem 1, q can be determined by the observable pair of $(\mathbf{A}', \mathbf{C}')$ such that:

$$q = \text{rank}\begin{bmatrix} \mathbf{C}' \\ \mathbf{C}'\mathbf{A}' \\ \vdots \\ \mathbf{C}'\mathbf{A}'^{n-1} \end{bmatrix} \tag{4.27}$$

where $\mathbf{A}'$ and $\mathbf{C}'$ have been defined by (4.25) and (4.26).

The proof of Lemma 4 is given in [48].

Because the eigenvalues of (**A**-**LC**) are equal to the eigenvalues of $(\mathbf{A}' - \mathbf{L}'\mathbf{C}')$, the total number of eigenvalues can be obtained as $k + q$ based on the above result. In order to satisfy the second condition in Definition 1, the equation $k + q = n$ needs to be met.

Now the problem has been transferred to identify the numbers of k and q. Although Lemma 4 implies that the number of q depends on $\mathbf{g}$ and k (due to the definition of $\mathbf{A}'$), the following theorem proves the irrelevance between them.

***Theorem 3 (Theorem 4.3 of [25])*:** Under the condition that detection gain $\mathbf{L}$ can be constructed by (4.20), the number of eigenvalues q that is specified randomly can be obtained by:

$$q = \text{rank}\begin{bmatrix} \mathbf{C}' \\ \mathbf{C}'\mathbf{A}' \\ \vdots \\ \mathbf{C}'\mathbf{A}'^{n-1} \end{bmatrix} = \text{rank}[\mathbf{M}'] = rank\begin{bmatrix} \mathbf{C}' \\ \mathbf{C}'\mathbf{K} \\ \vdots \\ \mathbf{C}'\mathbf{K}^{n-1} \end{bmatrix} \tag{4.28}$$

where $\mathbf{M}'$ is the observability matrix for $(\mathbf{A}', \mathbf{C}')$ and $\mathbf{K}$ is defined as:

$$\mathbf{K} = \mathbf{A} - \mathbf{A}\boldsymbol{f}_i[(\mathbf{C}\boldsymbol{f}_i)^{\mathrm{T}}(\mathbf{C}\boldsymbol{f}_i)]^{-1}(\mathbf{C}\boldsymbol{f}_i)^{\mathrm{T}}\mathbf{C} \tag{4.29}$$

The proof of this theorem is given in [25] in detail.

Because $\mathbf{K}$ and $\mathbf{C}'$ are not related to $\mathbf{g}$ and k, it is clearly shows that the number of eigenvalue q of (**A**-**LC**), which represents the left freedom in $\mathbf{L}$, only depends on $\mathbf{A}$, $\boldsymbol{f}$ and $\mathbf{C}$. In addition, this result also implies that the degree of freedom in $\mathbf{L}$ which determines the eigenvalue q is always the same once the system is fixed. Therefore, the focus now is to find the desired detection generator $\mathbf{g}$ which order is definitely equal to $n - q$, and this purpose leads to the following definitions.

Definition 3 (Definition 4.5 of [25]): The detection space of fault vector $\boldsymbol{f}_i$ can be defined by the null space of $\mathbf{M}'$.

Definition 4 (Definition 4.6 of [25]): The detection order (normally represented by v) of fault vector $\boldsymbol{f_i}$ can be defined by the dimension of the detection space of fault vector $\boldsymbol{f_i}$.

Definition 5 (Definition 4.7 of [25]): When the order of detection generator $\mathbf{g}$ is equal to the detection order of fault vector $\boldsymbol{f_i}$, this detection generator is regard as the maximal detection generator.

According to a series of definitions as shown above, the number of detection order meets the following condition:

$$v = n - \text{rank}\,[\mathbf{M}'] = n - q \tag{4.30}$$

Therefore, based on (4.30) and the condition for desired detection generator, the key to achieve detectability of fault vector $\boldsymbol{f_i}$ lies in the searching of maximal detection generator.

Finally, due to the knowledge of the order of the maximal detection generator ($k = v = n - q$), the detection generator can be obtained based on (4.14) in Lemma 2. The detection gain can then be designed through (4.20) based on Theorem 2 or (4.23) based on Lemma 3.

Throughout the whole theory in designing BJ filter for one-fault situation, there are two points needed to be reemphasized and highlighted [25].

1) The property of the detection space, detection order and maximal generator.

- Under the condition that ($\mathbf{A}$, $\mathbf{C}$) is observable, the detection space, detection order and maximal generator for every fault is unique. In addition, the transformation for matrix $\mathbf{A}$, such as $\mathbf{A}'' = \mathbf{A} - \mathbf{L}''\mathbf{C}$ (where $\mathbf{L}''$ can be chosen randomly with proper dimension) and the coordinate transformation for the system's state space representation will not influence the uniqueness of those three items. By taking advantage of this property, some complex calculations can be simplified.
- One fault vector $\boldsymbol{f_i}$ can produce many detection gain $\mathbf{g}$, but all of them must lie in the detection space of fault vector $\boldsymbol{f_i}$.
- Any n×1 vectors which lie in the detection space of fault vector $\boldsymbol{f_i}$ will have the identical detection order and space when compared with fault vector $\boldsymbol{f_i}$.

2) The construction of eigenvalues

Based on Theorem 2 and Lemma 3, the solution of detection gain $\mathbf{L}$ guarantees that v (or k by selecting the maximal detection generator) eigenvalues of ($\mathbf{A}$-$\mathbf{LC}$) are absolutely fixed and each eigenvalue is equal to the corresponding pole in the set of $[p_1, p_2, \cdots, p_k]$. The left q eigenvalues can be selected arbitrarily according to $\mathbf{L}'$ (the freedom in detection gain $\mathbf{L}$).

4.2.2 Detection Theory for Multiple-Fault Situation

As mentioned in the beginning, the methods and theory to generate detection gain for one-fault situation and multiple-fault situation are basically the same. Therefore, this section mainly illustrates the restrictions and conditions when dealing with multiple-fault detection.

In order to explain the restrictions for multiple-fault detection, the following definitions are developed.

Definition 6 (Definition 4.9 of [25]): Multiple-fault vectors $\{\boldsymbol{f_1}, \boldsymbol{f_2}, \cdots, \boldsymbol{f_r}\}$ are output separable if

$$\text{rank}\,(\mathbf{CF}) = r \tag{4.31}$$

where r is the number of fault vectors. $\mathbf{F}$ represents a $n \times r$ fault matrix and is defined by:

$$\mathbf{F} = [\boldsymbol{f_1} \quad \boldsymbol{f_2} \quad \cdots \quad \boldsymbol{f_r}] \tag{4.32}$$

This definition is intended to check the direction of different fault vectors. If the output error for two fault vectors have the same direction, the deigned BJ filter will fail to distinguish these two faults.

Definition 7 (Definition 4.10 of [25]): The dimension of state vector n can be defined to be the group detection order for the multiple-fault vectors $\{\boldsymbol{f_1}, \boldsymbol{f_2}, \cdots, \boldsymbol{f_r}\}$.

Based on Definition 6 and Definition 7, the most important criterion for multiple-fault detectability is explained in Theorem 4.

***Theorem 4 (Theorem 4.5 of [25])*:** Under the condition that multiple-fault vectors $\{\boldsymbol{f_1}, \boldsymbol{f_2}, \cdots, \boldsymbol{f_r}\}$ are output separable, these fault vectors are mutually detectable if and only if the sum of detection order for each $\boldsymbol{f_i}$ (i = 1, 2, ⋯, r) is equal to the group detection order such that:

$$\sum_1^r v_i = n \tag{4.33}$$

where v_i represents the detection order for each $\boldsymbol{f_i}$, and it can be obtained according to (4.30). The proof of this theorem is given in [48] in detail.

So far, if the multiple-fault vectors meet the criteria in Theorem 4, the rest work only needs to follow the method and theory as explained in one-fault situation in order to obtain each detection generator $\mathbf{g_i}$ for each fault vector $\boldsymbol{f_i}$. Finally, through (4.20) based on Theorem 2 or

(4.23) based on Lemma 3, the detection gain **L** can be designed based on the information provided by each detection generator $\mathbf{g}_i$.

4.3 Design Procedures and Example

In order to apply the theory previously discussed to practical problems, a random system with pre-defined fault vectors is used to better explain the construction process of the BJ filter.

Assume that there exists a system with 1 input and 2 outputs:

$$\begin{cases} \dot{\boldsymbol{X}}(\boldsymbol{t})_{3\times1} = \mathbf{A}_{3\times3}\boldsymbol{X}(\boldsymbol{t})_{3\times1} + \mathbf{B}_{3\times1}\boldsymbol{U}(\boldsymbol{t})_{1\times1} \\ \boldsymbol{Y}(\boldsymbol{t})_{2\times1} = \mathbf{C}_{2\times3}\boldsymbol{X}(\boldsymbol{t})_{3\times1} \end{cases} \tag{4.34}$$

where $\mathbf{A} = \begin{bmatrix} 0 & 3 & 4 \\ 1 & 2 & 3 \\ 0 & 2 & 5 \end{bmatrix}$ $\mathbf{B} = \begin{bmatrix} 1 \\ 1 \\ 1 \end{bmatrix}$ $\mathbf{C} = \begin{bmatrix} 0 & 1 & 0 \\ 0 & 0 & 1 \end{bmatrix}$ $\boldsymbol{f_1} = \begin{bmatrix} 3 \\ 1 \\ 0 \end{bmatrix}$

Step 1: Check the observability of (**A, C**).

According to Theorem 1, check whether the system (**A, C**) is an observable pair.

$$\operatorname{rank}(\mathbf{M}) = \operatorname{rank}\begin{bmatrix} \mathbf{C} \\ \mathbf{CA} \\ \mathbf{CA}^2 \end{bmatrix} = 3 = n \tag{4.35}$$

Therefore, the fault vector $\boldsymbol{f_1}$ in the state space is detectable.

Step 2: Simplify the matrix **A** (this step is only for the convenience of the calculations and thus can be omitted).

According to the theory explained above, without changing the maximal generator, detection order and detection space of fault vector $\boldsymbol{f_1}$, the system matrix **A** can be simplified by $\mathbf{A}'' = \mathbf{A} - \mathbf{L}''\mathbf{C}$. For this example,

$$\mathbf{L}'' = \begin{bmatrix} 3 & 4 \\ 2 & 3 \\ 2 & 5 \end{bmatrix}$$

Then A can be simplified to

$$\mathbf{A}'' = \begin{bmatrix} 0 & 0 & 0 \\ 1 & 0 & 0 \\ 0 & 0 & 0 \end{bmatrix}$$

Step 3: Compute the detection order *v*.

According to Theorem 3, the number of eigenvalues q can be obtained. Firstly, $\mathbf{C}'$ and **K** need to be calculated based on (4.26) and (4.29), respectively.

$$\mathbf{C}' = [\mathbf{I} - (\mathbf{C}\boldsymbol{f_1})[(\mathbf{C}\boldsymbol{f_1})^T(\mathbf{C}\boldsymbol{f_1})]^{-1}(\mathbf{C}\boldsymbol{f_1})^T]\mathbf{C} = \begin{bmatrix}0 & 0 & 0\\ 0 & 0 & 1\end{bmatrix} \tag{4.36}$$

$$\mathbf{K} = \mathbf{A}'' - \mathbf{A}''\boldsymbol{f_1}[(\mathbf{C}\boldsymbol{f_1})^{\mathrm{T}}(\mathbf{C}\boldsymbol{f_1})]^{-1}(\mathbf{C}\boldsymbol{f_1})^{\mathbf{T}}\mathbf{C} = \begin{bmatrix}0 & 0 & 0\\ 1 & -3 & 0\\ 0 & 0 & 0\end{bmatrix} \tag{4.37}$$

Then according to (4.28).

$$q = \mathrm{rank}(\mathbf{M}') = \mathrm{rank}\begin{bmatrix}\mathbf{C}'\\ \mathbf{C}'\mathbf{K}\\ \mathbf{C}'\mathbf{K}^2\end{bmatrix} = 1 \tag{4.38}$$

Finally, based on (4.30), the detection order can be obtained, and this order is equal to the order of desired maximal detection generator **g**.

$$k = v = n - q = 3 - 1 = 2 \tag{4.39}$$

Step 4: Find the maximal detection generator **g**.

Based on Lemma 2, the detection generator **g** can be calculated according to its definition in (4.14).

$$\mathbf{C} \times \mathbf{g} = 0 \quad \text{and} \quad \mathbf{C}\mathbf{A}'' \times \mathbf{g} = \mathbf{C}\boldsymbol{f_1} \tag{4.40}$$

$$\begin{cases}\begin{bmatrix}0 & 1 & 0\\ 0 & 0 & 1\end{bmatrix} \times \mathbf{g} = 0\\ \begin{bmatrix}1 & 0 & 0\\ 0 & 0 & 0\end{bmatrix} \times \mathbf{g} = \begin{bmatrix}1\\ 0\end{bmatrix}\end{cases} \tag{4.41}$$

From (4.41), the detection generator **g** can be calculated.

$$\mathbf{g} = \begin{bmatrix}1\\ 0\\ 0\end{bmatrix}$$

Step 5: Determine detection gain **L**

Assume detection gain **L** is a 3*2 matrix as shown below.

$$\mathbf{L} = \begin{bmatrix}l_{11} & l_{12}\\ l_{21} & l_{22}\\ l_{31} & l_{32}\end{bmatrix}$$

According to Theorem 2, the detection gain **L** can be solved through (4.20).

$$\mathbf{L}\mathbf{C}\boldsymbol{f_1} = p_1\mathbf{g} + p_2\mathbf{A}\mathbf{g} + A^2\mathbf{g} \tag{4.41}$$

$$\rightarrow \mathbf{L}\begin{bmatrix}1\\0\end{bmatrix} = \begin{bmatrix}l_{11}\\l_{21}\\l_{31}\end{bmatrix} = p_1\mathbf{g} + p_2\mathbf{Ag} + A^2\mathbf{g} \tag{4.42}$$

At this stage, because of the freedom in designing the BJ filter, the eigenvalues (or the system poles) can be designed randomly. To maintain the stability of the system, the eigenvalues can be places at s = -2 and s = -3, respectively. From the (4.18), the values of p_1 and p_2 can be determined.

$$(s+2)\times(s+3) = s^2 + 5s + 6 = s^2 + p_2 s + p_1 \tag{4.43}$$

$$\rightarrow \begin{cases} p_1 = 6 \\ p_2 = 5 \end{cases}$$

Therefore,

$$\begin{bmatrix}l_{11}\\l_{21}\\l_{31}\end{bmatrix} = 6\begin{bmatrix}1\\0\\0\end{bmatrix} + 5\begin{bmatrix}0\\1\\0\end{bmatrix} + \begin{bmatrix}3\\2\\2\end{bmatrix} = \begin{bmatrix}9\\7\\2\end{bmatrix} \tag{4.44}$$

Finally, the detection gain **L** can be determined and still has freedom in **L**.

$$\mathbf{L} = \begin{bmatrix}9 & l_{12}\\7 & l_{22}\\2 & l_{32}\end{bmatrix}$$

These five steps form the basic design process for BJ filter for one-fault detection as well as multiple-fault detection. Due to the freedom left in **L**, it is possible to allow this BJ filter to be able to detect another fault vector $\boldsymbol{f_2}$ for this system. However, the restriction of the BJ detection filter in detecting multiple faults will be examined first.

Assumed that there exists another fault

$$\boldsymbol{f_2} = \begin{bmatrix}1\\-0.5\\0.5\end{bmatrix}$$

Firstly, check if these two fault vectors are output separable using (4.31).

$$\text{rank}\,(\mathbf{CF}) = \text{rank}\left(\left[\begin{bmatrix}0 & 1 & 0\\0 & 0 & 1\end{bmatrix}\times\begin{bmatrix}-3 & 1\\1 & -0.5\\0 & 0.5\end{bmatrix}\right]\right) = 2 \tag{4.45}$$

Therefore, these two fault vectors are output separable. Then, follow Step 3 as explained before, the detection order for $\boldsymbol{f_2}$ can be calculated.

$$\mathbf{C'_2} = [\mathbf{I} - (\mathbf{C}\boldsymbol{f_2})[(\mathbf{C}\boldsymbol{f_2})^{\mathrm{T}}(\mathbf{C}\boldsymbol{f_2})]^{-1}(\mathbf{C}\boldsymbol{f_2})^{\mathrm{T}}]\mathbf{C} = \begin{bmatrix} 0 & 0.5 & 0.5 \\ 0 & 0.5 & 0.5 \end{bmatrix} \tag{4.46}$$

$$\mathbf{K_2} = \mathbf{A''} - \mathbf{A''}\boldsymbol{f_2}[(\mathbf{C}\boldsymbol{f_2})^{\mathrm{T}}(\mathbf{C}\boldsymbol{f_2})]^{-1}(\mathbf{C}\boldsymbol{f_2})^{\mathrm{T}}\mathbf{C} = \begin{bmatrix} 0 & 3.5 & 3.5 \\ 1 & 3.5 & 1.5 \\ 0 & 3.5 & 3.5 \end{bmatrix} \tag{4.47}$$

Then according to (4.28).

$$q_2 = \mathrm{rank}(\mathbf{M'_2}) = \mathrm{rank}\begin{bmatrix} \mathbf{C'_2} \\ \mathbf{C'_2}\mathbf{K_2} \\ \mathbf{C'_2}\mathbf{K_2}^2 \end{bmatrix} = 2 \tag{4.48}$$

Finally, based on (4.30), the detection order can be calculated, and this order is equal to the order of desired detection generator $\mathbf{g_2}$.

$$k_2 = v_2 = n - q_2 = 3 - 2 = 1 \tag{4.49}$$

Now, the mutually detectability can be checked based on Theorem 4.

$$\sum_1^2 v_i = 2 + 1 = 3 = n \tag{4.50}$$

Therefore, these two fault vectors are mutual detectable. Because the detection order for $\boldsymbol{f_2}$ is 1, the maximal detection generator $\mathbf{g_2}$ is equal to $\boldsymbol{f_2}$. Following Step 5, the detection gain $\mathbf{L}$ will meet:

$$\mathbf{L}\mathbf{C}\boldsymbol{f_2} = \begin{bmatrix} 9 & d_{12} \\ 7 & d_{22} \\ 2 & d_{32} \end{bmatrix} \times \begin{bmatrix} -0.5 \\ 0.5 \end{bmatrix} = p_3\boldsymbol{f_2} + \mathbf{A}\boldsymbol{f_2} \tag{4.51}$$

Similar to the former design method, the eigenvalue can be placed at s = -4, and p_3 is directly equal to -4 due to only one pole.

$$\begin{bmatrix} 9 & l_{12} \\ 7 & l_{22} \\ 2 & l_{32} \end{bmatrix} \times \begin{bmatrix} -0.5 \\ 0.5 \end{bmatrix} = -4\begin{bmatrix} 1 \\ -0.5 \\ 0.5 \end{bmatrix} + \begin{bmatrix} 0 & 3 & 4 \\ 1 & 2 & 3 \\ 0 & 2 & 5 \end{bmatrix} \times \begin{bmatrix} 1 \\ -0.5 \\ 0.5 \end{bmatrix} \tag{4.52}$$

Finally, all the parameters in the detection gain $\mathbf{L}$ can be obtained, and based on the design of the detection gain, the BJ filter is able to detect these two fault vectors.

$$\mathbf{L} = \begin{bmatrix} 9 & 18 \\ 7 & 6 \\ 2 & 9 \end{bmatrix}$$

Figure 4.4 shows the whole block diagram for the design of the detection gain $\mathbf{L}$.

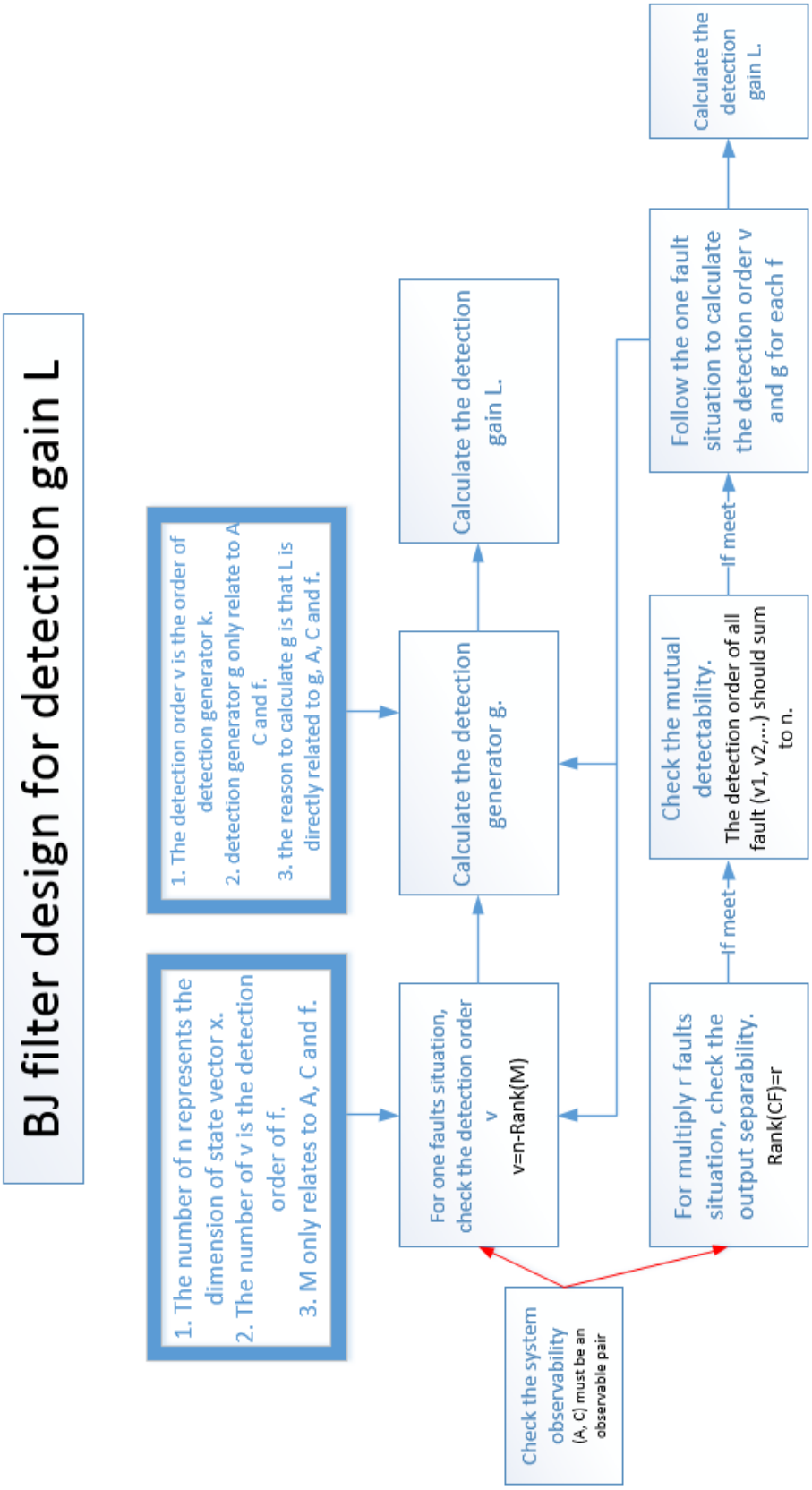

Figure 4.4 Design procedure for the detection gain of BJ filter

4.4 Simulation Construction and Explanation

In this section, the random system and its corresponding BJ filter are constructed using MATLAB SIMULINK in order to validate the feature of the BJ filter in fault detection problem.

The SIMULINK model of the whole structure is shown below. Figure 4.5 shows the whole fault detection system, Figure 4.6 shows the subsystem of the plate structure and Figure 4.7 shows the subsystem of the BJ filter structure.

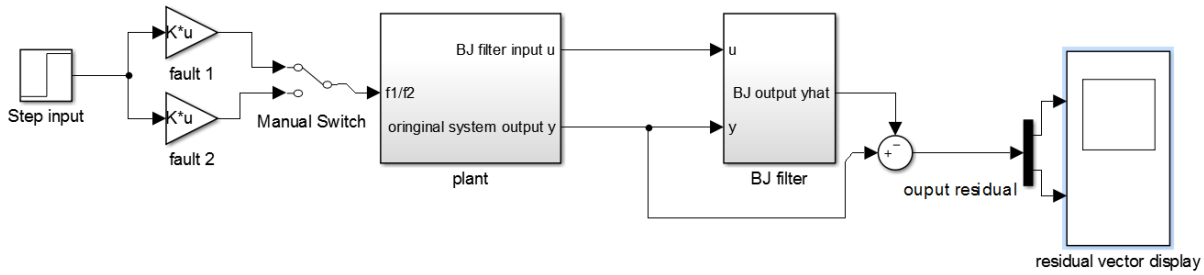

Figure 4.5 Fault detection system for example system

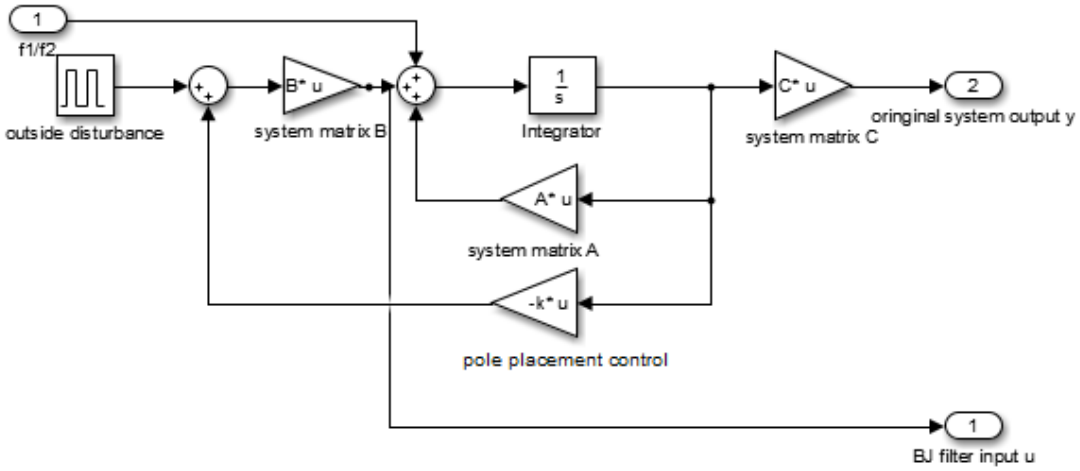

Figure 4.6 Subsystem of plate structure for example system

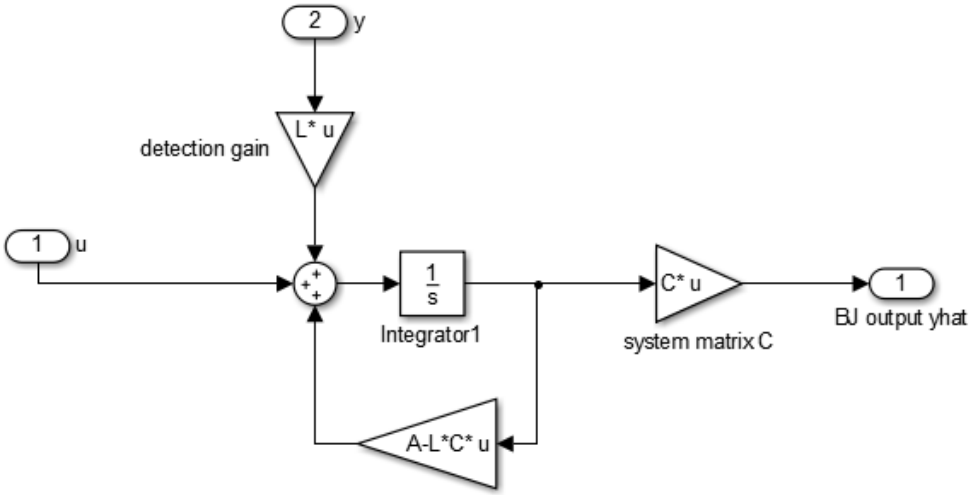

Figure 4.7 Subsystem of BJ filter structure for example system

In the fault detection system (Figure 4.5), two fault vectors are activated by the step input signal and then inserted into the plant. The original system output signal and the BJ filter output signal are compared to produce the output residual which can be displayed in the scope. In the plate structure (Figure 4.6), the square wave is used as the external disturbance which can keep this control system in operation, and the pole placement control gain is used for keeping the system stable (i.e., placing the system poles at negative values). In the BJ filter structure (Figure 4.7), the input and output signals of the original system are introduced to the BJ filter in order to produce an estimated fault-free output signal.

According to the theory explained before, the output residual $\hat{\varepsilon}(\boldsymbol{t})$ should be proportional to $\mathbf{C}\boldsymbol{f_i}$ with respect to the corresponding fault vector $\boldsymbol{f_i}$. Firstly, the value of $\mathbf{C}\boldsymbol{f_i}$ for two fault vectors are presented as:

$$\mathbf{C}\boldsymbol{f_1} = \begin{bmatrix}1\\0\end{bmatrix} \quad \mathbf{C}\boldsymbol{f_2} = \begin{bmatrix}-0.5\\0.5\end{bmatrix} \tag{4.53}$$

Then the value of the output residual for fault vector $\boldsymbol{f_1}$ is examined by simulation result shown in Figure 4.8.

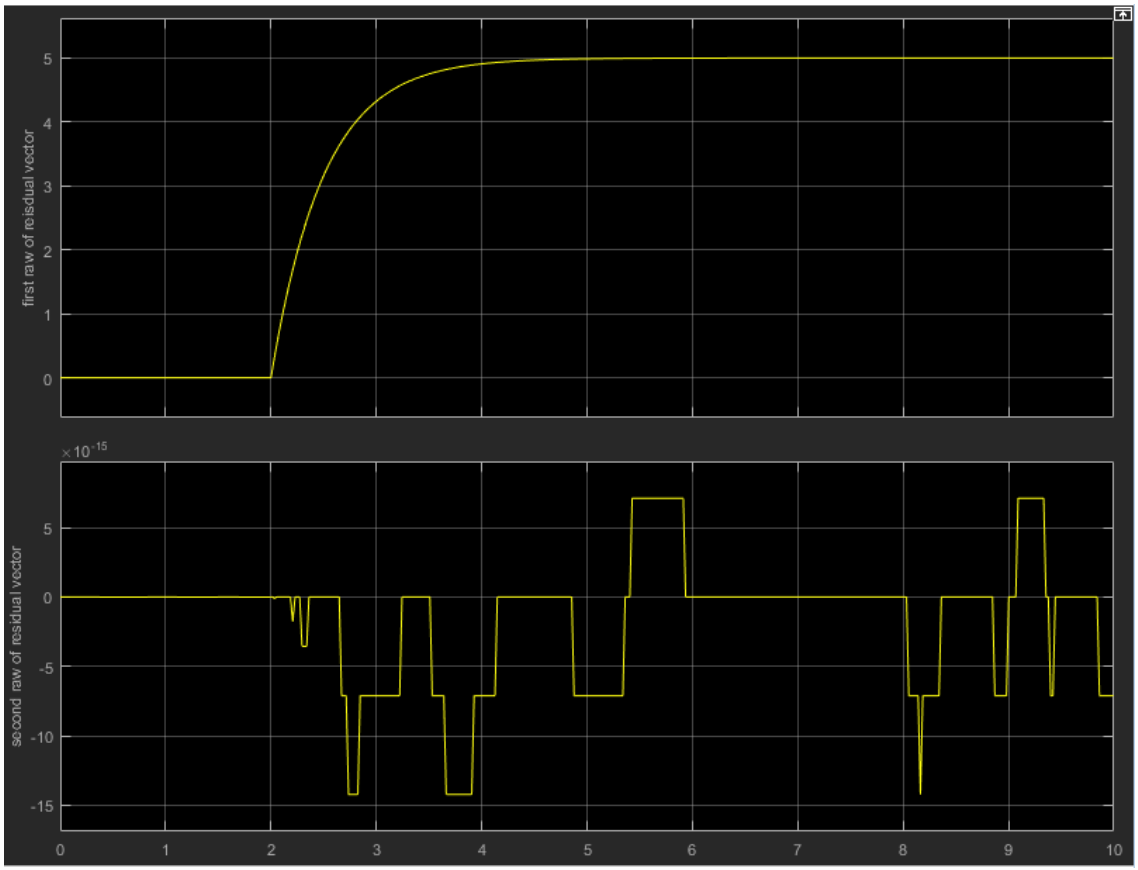

(a)

(b)

Figure 4.8 Simulation result for $\boldsymbol{f_1}$ of the example system
(a) 1st row of the residual vector; (b) 2nd row of the residual vector

From Figure 4.8, it shows that the output residual for $\boldsymbol{f_1}$ is stable at value of [5; 0], which is proportional to $\boldsymbol{Cf_1}$, so the BJ filter can be used to detect the fault vector $\boldsymbol{f_1}$ successfully.

Finally, the value of the output residual for fault vector $\boldsymbol{f_2}$ is examined by simulation result shown in Figure 4.9.

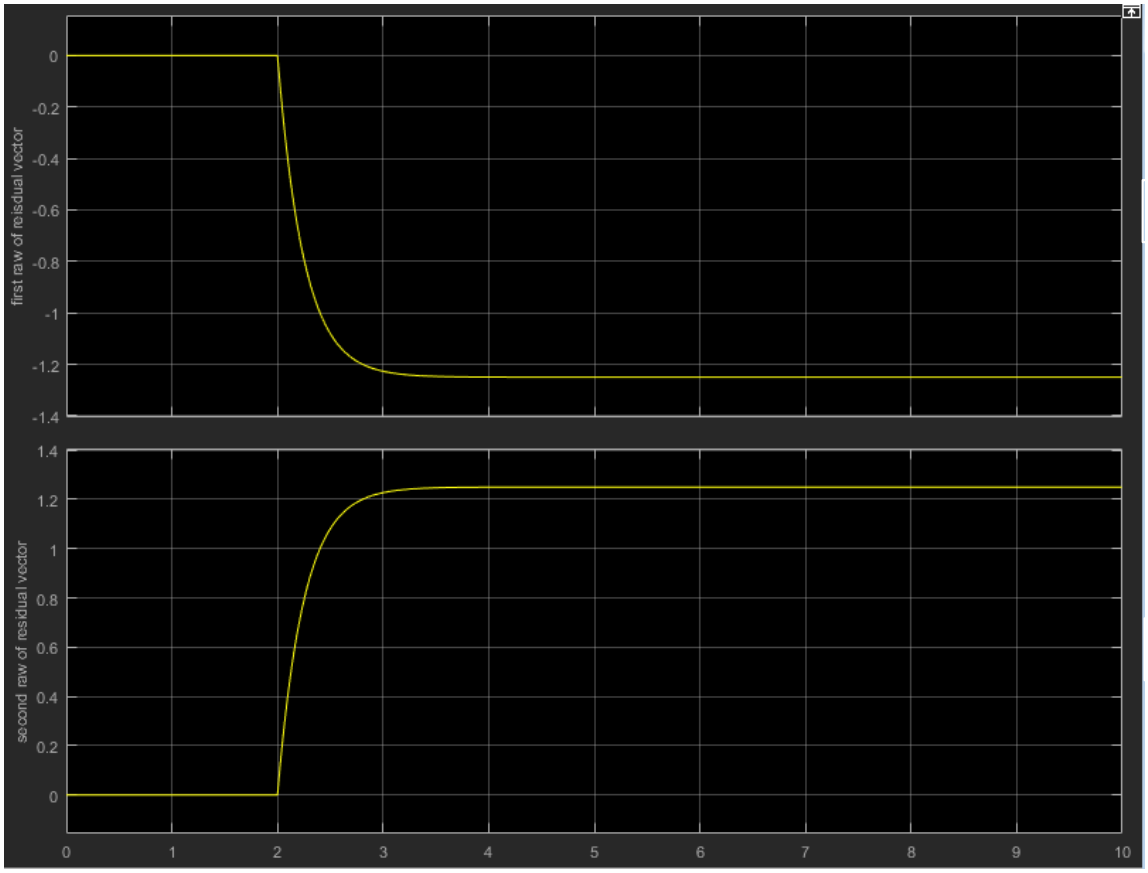

Figure 4.9 Simulation result for $\boldsymbol{f_2}$ of the example system
(a) 1st row of the residual vector; (b) 2nd row of the residual vector

From Figure 4.9, it shows that the output residual for $\boldsymbol{f_2}$ is stable at value of [-1.4; 1.4], which is proportional to $\mathbf{C}\boldsymbol{f_2}$, so the BJ filter can be used to detect the fault vector $\boldsymbol{f_2}$ successfully as well.

In conclusion, the designed BJ filter is a useful and practical fault detection method for one-fault as well as multiple-fault situations.

Chapter 5 : Conceptual BJ Filter Validation

Based on the knowledge of the BJ filter theory and the developed state space representation of the plate control system, a conceptual BJ filter structure for implementing fault detection with pre-defined faults is designed and tested in MATLAB SIMULINK from simple case to complex case following the design procedure and restriction of the BJ filter. In this chapter, three configurations (namely, SISO configuration – considering one pair of the inputs and outputs of the real system only, 2I2O configuration – considering two pairs of the inputs and outputs of the real system only, and MIMO configuration – considering all three pairs of the inputs and outputs of the real system, respectively) are constructed for validation.

5.1 BJ Filter Design for SISO Configuration

In this section, only one pair of the inputs and outputs of the real system is taken into consideration for fault detection and this system only considers the first mode of the real system. A pre-defined fault vector is introduced to this system for validation. The block diagram of this new simplified system is shown in Figure 5.1.

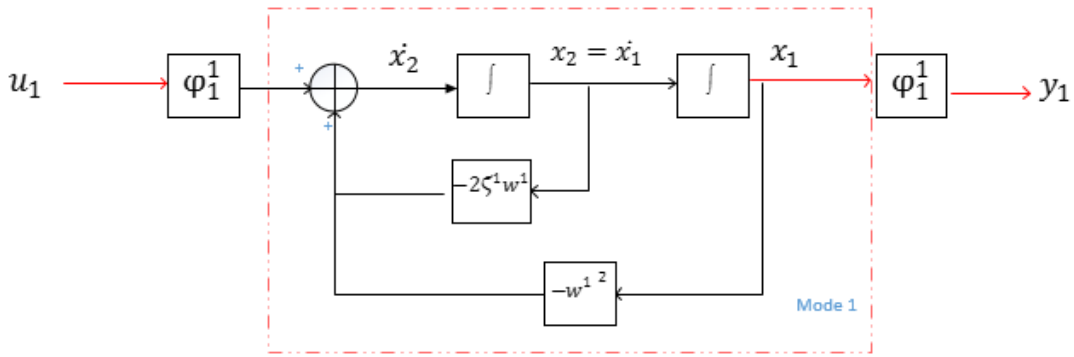

Figure 5.1 The block diagram of new simplified SISO system for BJ filter design

According to Figure 5.1, the state space representation of this SISO system is shown in (5.1) and the setting of the pre-defined fault vector $\boldsymbol{f}$ is shown below.

$$\begin{cases} \dot{\boldsymbol{X}}(\boldsymbol{t})_{2\times1} = \mathbf{A}_{2\times2}\boldsymbol{X}(\boldsymbol{t})_{2\times1} + \mathbf{B}_{2\times1}\boldsymbol{U}(\boldsymbol{t})_{1\times1} \\ \boldsymbol{Y}(\boldsymbol{t})_{1\times1} = \mathbf{C}_{1\times2}\boldsymbol{X}(\boldsymbol{t})_{2\times1} \end{cases} \tag{5.1}$$

where $\mathbf{A} = \begin{bmatrix} 0 & 1 \\ -w^{1\,2} & -2\zeta^1 w^1 \end{bmatrix}$ $\mathbf{B} = \begin{bmatrix} 0 \\ \varphi_1^1 \end{bmatrix}$ $\mathbf{C} = [\varphi_1^1 \quad 0]$ $\boldsymbol{f} = \begin{bmatrix} 1 \\ 0 \end{bmatrix}$

The parameters in this SISO system can be obtained from the real system data that has been developed in Chapter 3. Based on the BJ filter design procedure developed in Chapter 4, the detection gain **L** can be calculated using the algorithm designed in MATLAB and the result is shown in (5.2). The MATLAB script can refer to Appendix A.

$$\mathbf{L} = \begin{bmatrix} -7.1304 \\ -55642 \end{bmatrix} \tag{5.2}$$

The SIMULINK model of this SISO fault detection system is shown as follows. Figure 5.2 shows the whole fault detection system, Figure 5.3 shows the subsystem of the plate structure and Figure 5.4 shows the subsystem of the BJ filter structure.

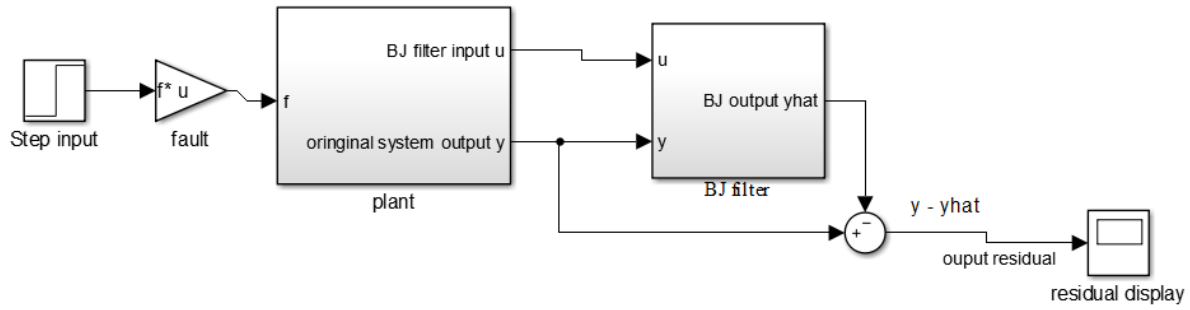

Figure 5.2 Fault detection system for the SISO system

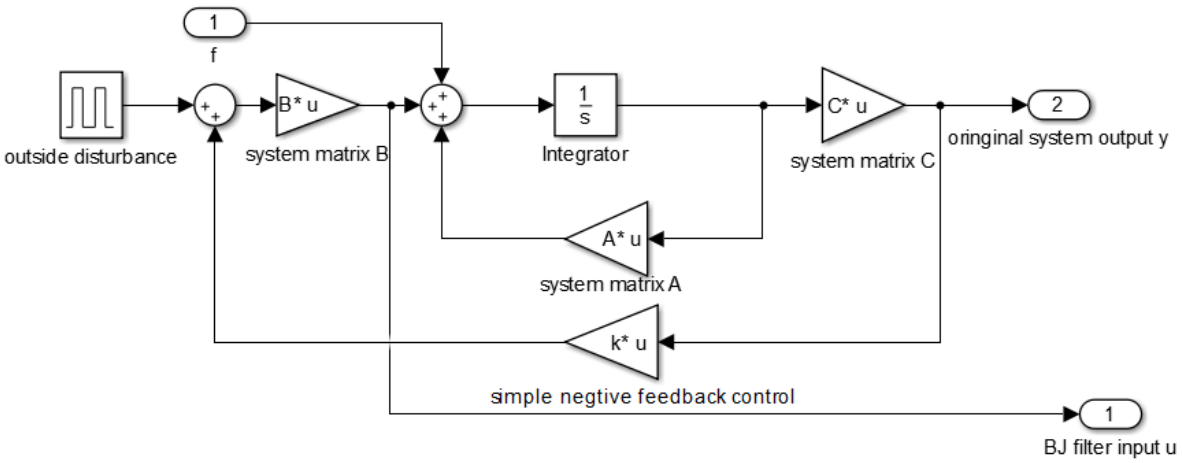

Figure 5.3 Subsystem of the plate structure for the SISO system

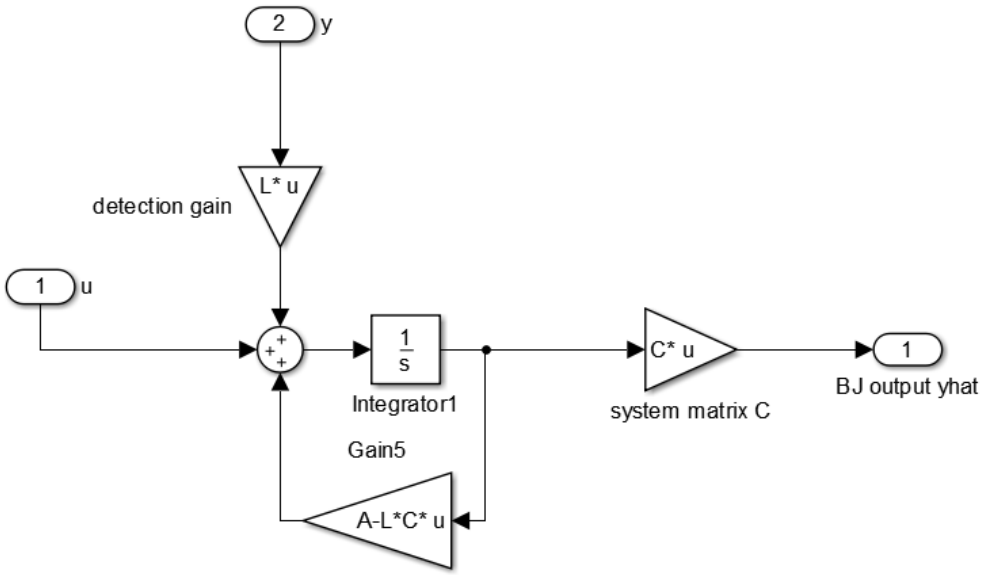

Figure 5.4 Subsystem of the BJ filter structure for the SISO system

In the fault detection system (Figure 5.2), the fault vector $\boldsymbol{f}$ is activated by the step input signal and then inserted into the plant. The output signals of the SISO system and the BJ filter are compared to produce the output residual which can be displayed in the scope. In the plate structure (Figure 5.3), the square wave (where frequency is set to be the same as the first mode of the system) is used as the external disturbance which keeps this control system in operation, and the negative control gain is used for suppressing the system vibration. In the BJ filter structure (Figure 5.4), the input and output signals of the SISO system are introduced to the BJ filter in order to produce an estimated fault-free output signal.

According to the fault detection theory explained in Chapter 4, the output residual $\hat{\varepsilon}(\boldsymbol{t})$ should be proportional to $\boldsymbol{Cf}$ with respect to the corresponding pre-defined fault vector $\boldsymbol{f}$. Firstly, the value of $\boldsymbol{Cf}$ for the pre-defined fault vector $\boldsymbol{f}$ is presented as:

$$\boldsymbol{Cf} = 0.3639 \tag{5.3}$$

After running the simulation, the output residual shown in Figure 5.5 for the pre-defined fault vector $\boldsymbol{f}$ can be examined.

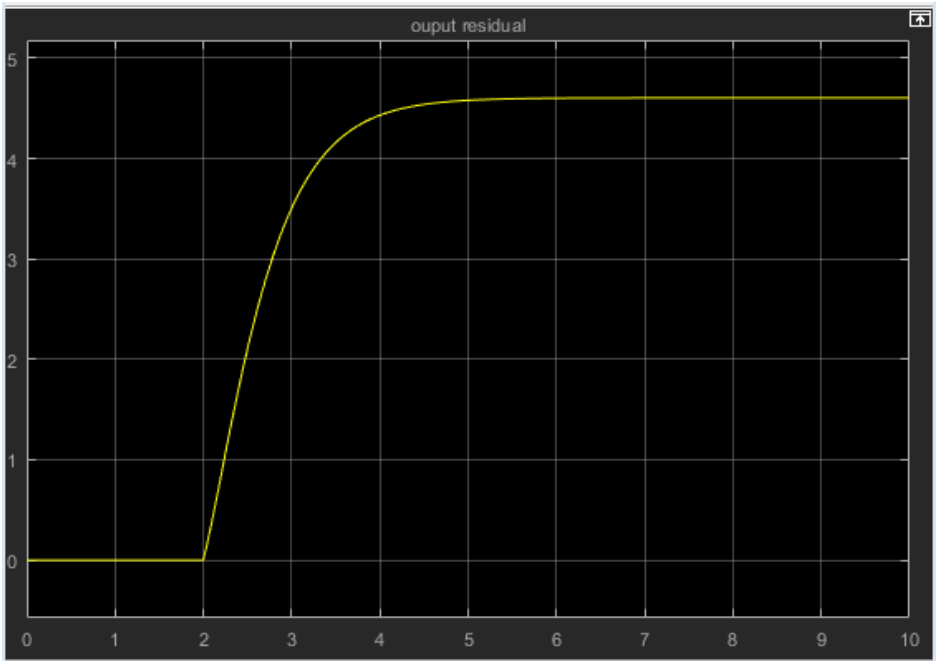

Figure 5.5 Simulation result for $\boldsymbol{f}$ of the SISO system

From Figure 5.5, it shows that after the fault detection system becomes stable, the output residual for $\boldsymbol{f}$ is stable at the value of 4.7, which is obviously proportional to $\mathbf{C}\boldsymbol{f}$. Therefore, the designed conceptual BJ filter is able to detect the pre-defined fault vector $\boldsymbol{f}$ in this SISO system successfully.

5.2 BJ Filter Design for 2I2O Configuration

In this section, two pairs of the inputs and outputs of the real system are taken into consideration for fault detection and this 2I2O system considers the first and second modes of the real system. Two pre-defined fault vectors are introduced to this system for validation. The block diagram of this 2I2O system is shown in Figure 5.6.

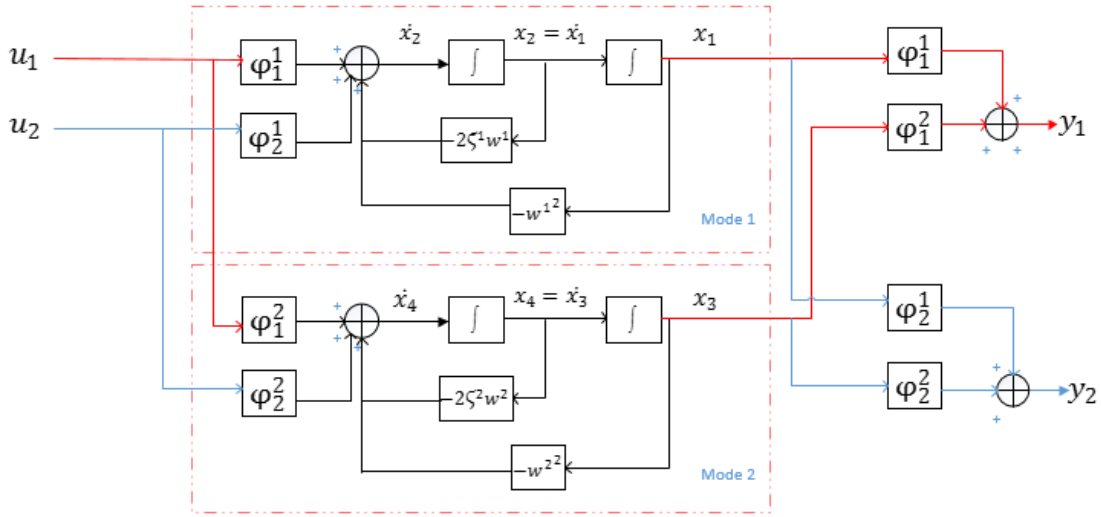

Figure 5.6 The block diagram of the new simplified 2I2O system for BJ filter design

According to Figure 5.6, the state space representation for this 2I2O system is shown in (5.4) and the settings of the pre-defined fault vectors $\boldsymbol{f_1}$ and $\boldsymbol{f_2}$ are shown below.

$$\begin{cases} \dot{\boldsymbol{X}}(\boldsymbol{t})_{4\times1} = \mathbf{A}_{4\times4}\boldsymbol{X}(\boldsymbol{t})_{4\times1} + \mathbf{B}_{4\times2}\boldsymbol{U}(\boldsymbol{t})_{2\times1} \\ \boldsymbol{Y}(\boldsymbol{t})_{2\times1} = \mathbf{C}_{2\times4}\boldsymbol{X}(\boldsymbol{t})_{4\times1} \end{cases} \tag{5.4}$$

where $\mathbf{A} = \begin{bmatrix} 0 & 1 & 0 & 0 \\ -w^{1^2} & -2\zeta^1 w^1 & 0 & 0 \\ 0 & 0 & 0 & 1 \\ 0 & 0 & -w^{2^2} & -2\zeta^2 w^2 \end{bmatrix}$ $\mathbf{B} = \begin{bmatrix} 0 & 0 \\ \varphi_1^1 & \varphi_2^1 \\ 0 & 0 \\ \varphi_1^2 & \varphi_2^2 \end{bmatrix}$

$$\mathbf{C} = \begin{bmatrix} \varphi_1^1 & 0 & \varphi_1^2 & 0 \\ \varphi_2^1 & 0 & \varphi_2^2 & 0 \end{bmatrix} \quad \boldsymbol{f_1} = \begin{bmatrix} 10 \\ 0 \\ 0 \\ 0 \end{bmatrix} \quad \boldsymbol{f_2} = \begin{bmatrix} 0 \\ 0 \\ 1 \\ 0 \end{bmatrix}$$

The parameters of this 2I2O system can be obtained from the real system data that has been developed in Chapter 3. Based on the BJ filter design procedure developed in Chapter 4, the detection gain **L** can be calculated using the algorithm designed in MATLAB and the result is shown in (5.5). The MATLAB script can refer to Appendix A.

$$\mathbf{L} = \begin{bmatrix} 42.6399 & -64.1898 \\ 332740 & -500910 \\ -2.3826 & 3.0730 \\ -321430 & 414550 \end{bmatrix} \tag{5.5}$$

The SIMULINK model of this 2I2O fault detection system is shown as follows. Figure 5.7 shows the whole fault detection system, Figure 5.8 shows the subsystem of the plate structure and Figure 5.9 shows the subsystem of the BJ filter structure.

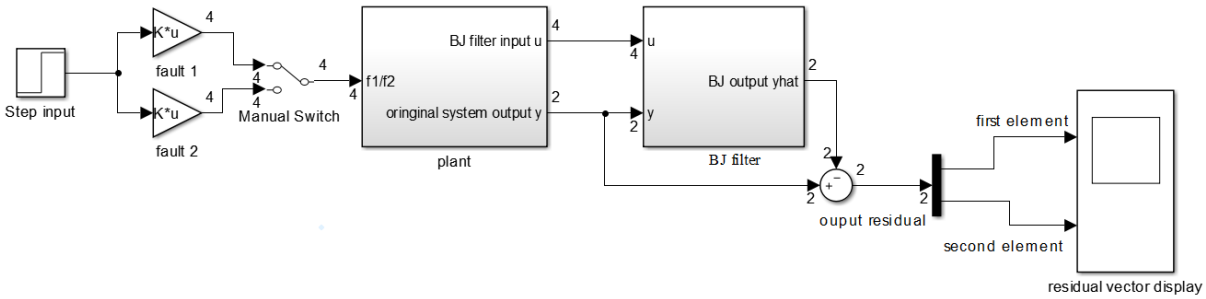

Figure 5.7 Fault detection system for the 2I2O system

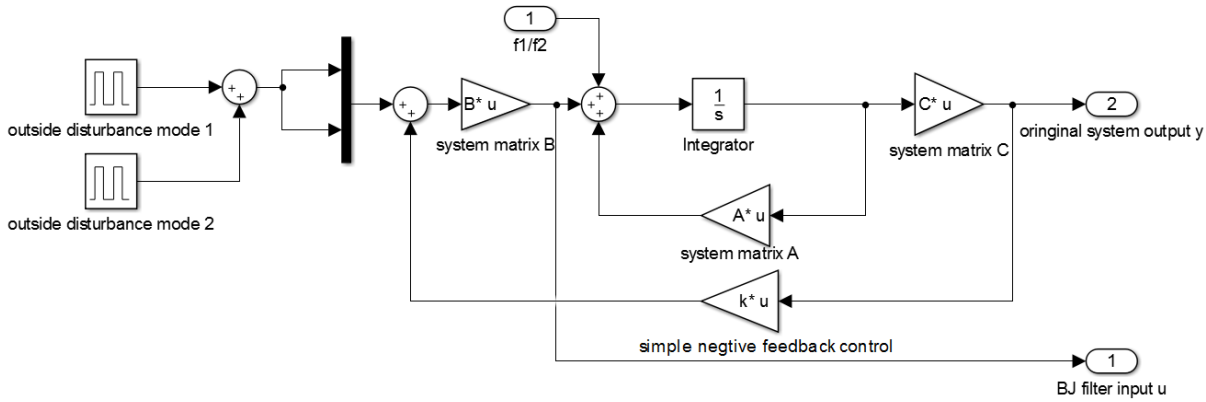

Figure 5.8 Subsystem of the plate structure for the 2I2O system

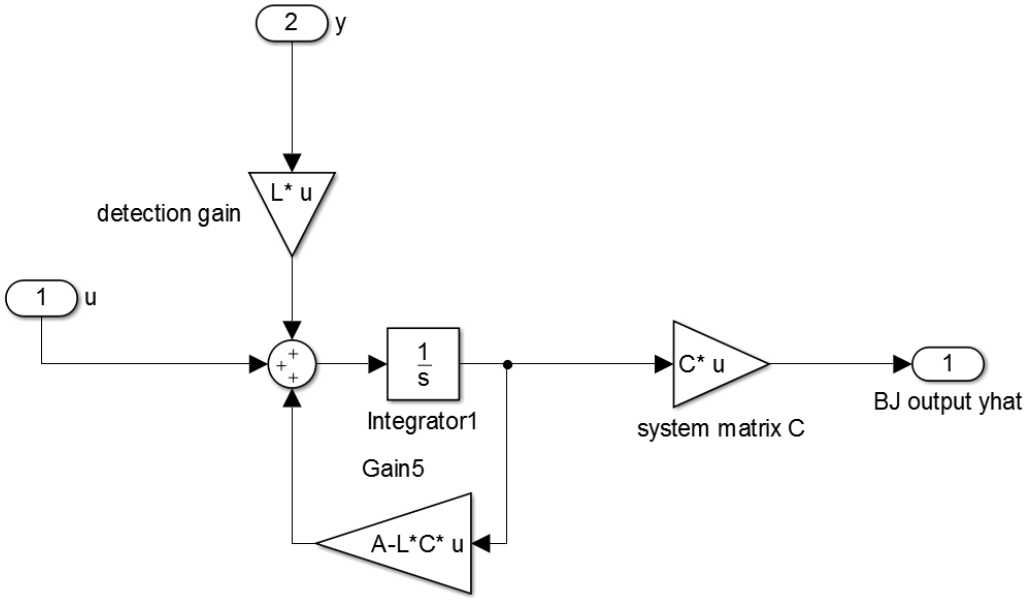

Figure 5.9 Subsystem of the BJ filter structure for the 2I2O system

Similar to the SISO system, in the fault detection system (Figure 5.7), the fault vectors $\boldsymbol{f_1}$ and $\boldsymbol{f_2}$ are activated by the step input signal and then inserted into the plant. The output signals of this 2I2O system and the BJ filter are compared to produce the output residual (2-dimensional) which can be displayed in the scope. In the plate structure (Figure 5.8), two square waves

(where frequencies are set to be the same as those of the first and second modes of the system, respectively) are used as the external disturbances which keep this control system in operation, and the negative control gain is used for suppressing the system vibration. In the BJ filter structure (Figure 5.9), the input and output signals of the 2I2O system are introduced to the BJ filter in order to produce an estimated fault-free output signal.

According to the fault detection theory explained in Chapter 4, the output residual $\hat{\varepsilon}(\boldsymbol{t})$ should be proportional to $\mathbf{C}\boldsymbol{f_i}$ with respect to corresponding fault vector $\boldsymbol{f_i}$. Firstly, the value of $\mathbf{C}\boldsymbol{f_i}$ for two pre-defined fault vectors are presented as:

$$\mathbf{C}\boldsymbol{f_1} = \begin{bmatrix} 3.6385 \\ 2.8212 \end{bmatrix} \quad \mathbf{C}\boldsymbol{f_2} = \begin{bmatrix} 0.723 \\ 0.4803 \end{bmatrix} \tag{5.6}$$

When the fault vector $\boldsymbol{f_1}$ is introduced to the system, the value of the output residual shown in Figure 5.10 for fault vector $\boldsymbol{f_1}$ can be examined.

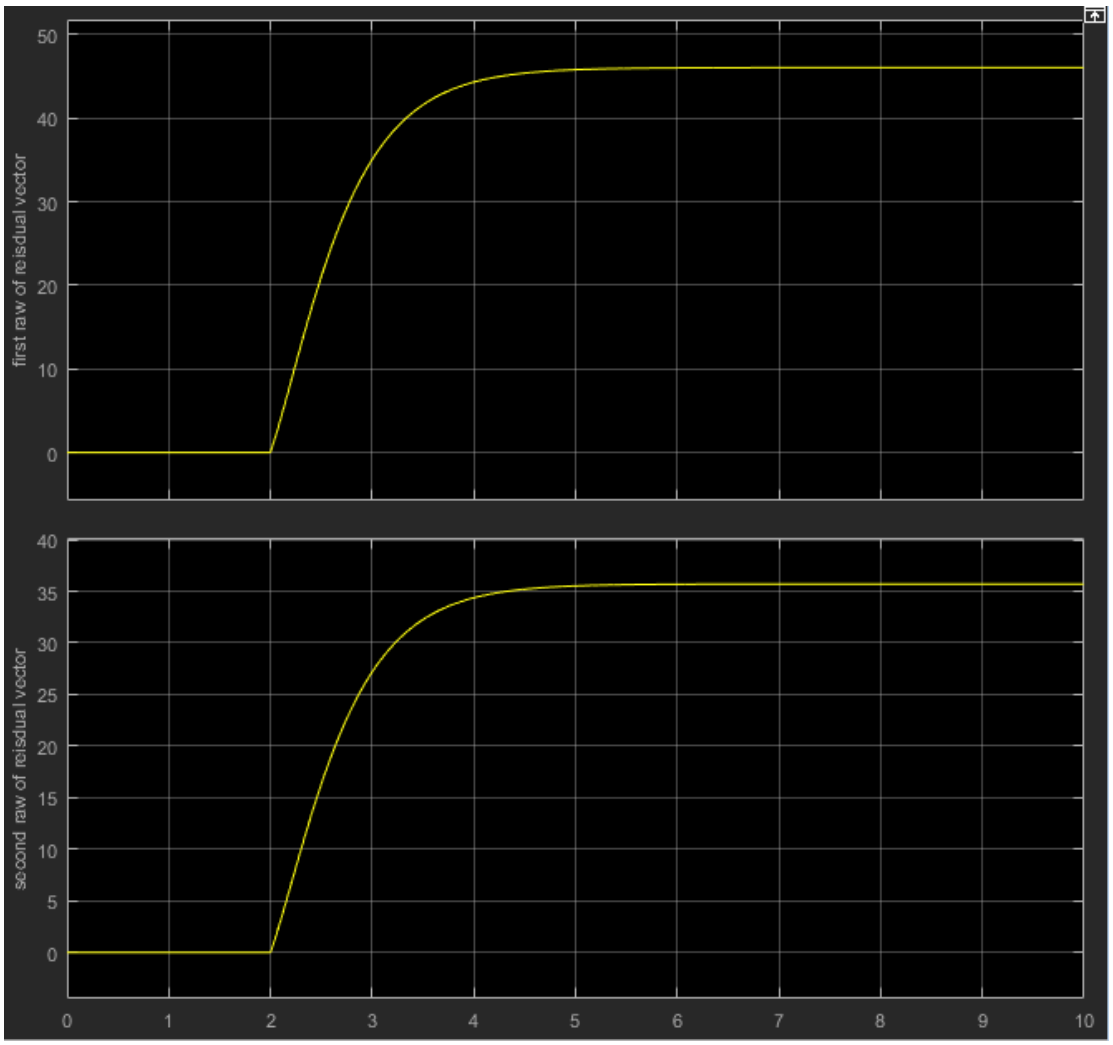

(a)

(b)

Figure 5.10 Simulation result for $\boldsymbol{f_1}$ of the 2I2O system
(a) 1st row of the residual vector; (b) 2nd row of the residual vector

From Figure 5.10, it shows that after the fault detection system becomes stable, the output residual for $\boldsymbol{f_1}$ is stable at value of [46.05; 35.71], which is proportional to $\mathbf{C}\boldsymbol{f_1}$ as calculated in (5.7). Therefore, the designed conceptual BJ filter is able to detect the pre-defined fault vector $\boldsymbol{f_1}$ in this 2I2O system successfully.

$$\text{Output residual for } \boldsymbol{f_1} = \begin{bmatrix} 46.05 \\ 35.71 \end{bmatrix} = 12.66 \times \mathbf{C}\boldsymbol{f_1} = 12.66 * \begin{bmatrix} 3.6385 \\ 2.8212 \end{bmatrix} \tag{5.7}$$

When the fault vector $\boldsymbol{f_2}$ is introduced to the system, the value of the output residual shown in Figure 5.11 for fault vector $\boldsymbol{f_2}$ can be examined.

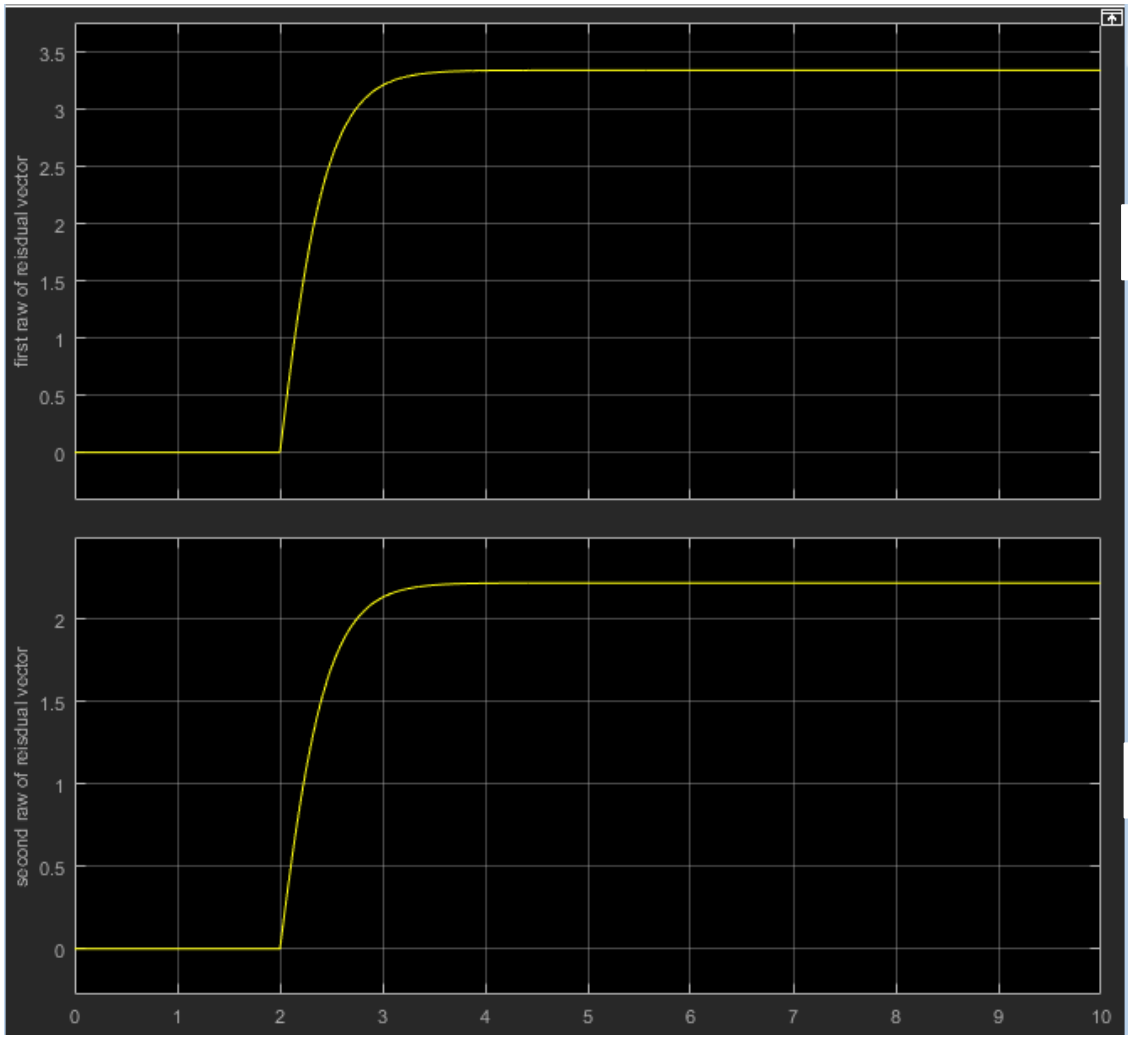

Figure 5.11 Simulation result for $\boldsymbol{f_2}$ of the new 2I2O system
(a) 1st row of the residual vector; (b) 2nd row of the residual vector

From Figure 5.11, it shows that after the fault detection system becomes stable, the output residual for $\boldsymbol{f_2}$ is stable at value of [3.343; 2.22], which is proportional to $\mathbf{C}\boldsymbol{f_2}$ as calculated in (5.8). Therefore, the designed conceptual BJ filter is able to detect the pre-defined fault vector $\boldsymbol{f_2}$ in this 2I2O system successfully.

$$\text{Output residual for } \boldsymbol{f_2} = \begin{bmatrix} 3.343 \\ 2.22 \end{bmatrix} = 4.62 \times \mathbf{C}\boldsymbol{f_2} = 4.62 \times \begin{bmatrix} 0.723 \\ 0.4803 \end{bmatrix} \tag{5.8}$$

5.3 BJ Filter Design for MIMO Configuration

In this section, the entire real system (three pairs of inputs and outputs) is taken into consideration for fault detection and the first three modes of the real system are all considered in the design. Three pre-defined fault vectors are introduced to this system for validation. In addition, the verification of three fault detection capabilities can provide a guarantee for the implementation of experiments to detect three actuator faults in the real system. The block diagram of the MIMO system has been established in Figure 3.7.

The state space representation for the MIMO system is shown in (5.9) and the settings of the pre-defined fault vectors $\boldsymbol{f_1}$, $\boldsymbol{f_2}$ and $\boldsymbol{f_3}$ are shown below.

$$\begin{cases} \dot{\boldsymbol{X}}(\boldsymbol{t})_{6\times1} = \mathbf{A}_{6\times6}\boldsymbol{X}(\boldsymbol{t})_{6\times1} + \mathbf{B}_{6\times3}\boldsymbol{U}(\boldsymbol{t})_{3\times1} \\ \boldsymbol{Y}(\boldsymbol{t})_{3\times1} = \mathbf{C}_{3\times6}\boldsymbol{X}(\boldsymbol{t})_{6\times1} \end{cases} \tag{5.9}$$

where $\mathbf{A} = \begin{bmatrix} 0 & 1 & & & & \\ -{w^1}^2 & -2\zeta^1 w^1 & & & & \\ & & 0 & 1 & & \\ & & -{w^2}^2 & -2\zeta^2 w^2 & & \\ & & & & 0 & 1 \\ & & & & -{w^3}^2 & -2\zeta^3 w^3 \end{bmatrix}$ $\mathbf{B} = \begin{bmatrix} 0 & 0 & 0 \\ \varphi_1^1 & \varphi_2^1 & \varphi_3^1 \\ 0 & 0 & 0 \\ \varphi_1^2 & \varphi_2^2 & \varphi_3^2 \\ 0 & 0 & 0 \\ \varphi_1^3 & \varphi_2^3 & \varphi_3^3 \end{bmatrix}$

$$\mathbf{C} = \begin{bmatrix} \varphi_1^1 & 0 & \varphi_1^2 & 0 & \varphi_1^3 & 0 \\ \varphi_2^1 & 0 & \varphi_2^2 & 0 & \varphi_2^3 & 0 \\ \varphi_3^1 & 0 & \varphi_3^2 & 0 & \varphi_3^3 & 0 \end{bmatrix} \quad \boldsymbol{f_1} = \begin{bmatrix} 50 \\ 0 \\ 0 \\ 0 \\ 0 \\ 0 \end{bmatrix} \quad \boldsymbol{f_2} = \begin{bmatrix} 0 \\ 0 \\ 10 \\ 0 \\ 0 \\ 0 \end{bmatrix} \quad \boldsymbol{f_3} = \begin{bmatrix} 0 \\ 0 \\ 0 \\ 0 \\ 1 \\ 0 \end{bmatrix}$$

The parameters of the MIMO system can be obtained from the real system data that has been developed in Chapter 3. Based on the BJ filter design procedure developed in Chapter 4, the detection gain **L** can be calculated using the algorithm designed in MATLAB and the result is shown in (5.10). The MATLAB script can refer to Appendix A.

$$\mathbf{L} = \begin{bmatrix} -3.3348 & -106.6227 & 120.3395 \\ -26023.5 & -832040 & 939080 \\ -3.5341 & 44.7344 & -47.527 \\ -52353 & 662680 & -704050 \\ 2.1219 & 1.9584 & -5.5541 \\ 63704 & 58796 & -166750 \end{bmatrix} \tag{5.10}$$

The SIMULINK model of the MIMO fault detection system is shown as follows. Figure 5.12 shows the whole fault detection system, Figure 5.13 shows the subsystem of the plate structure and Figure 5.14 shows the subsystem of the BJ filter structure.

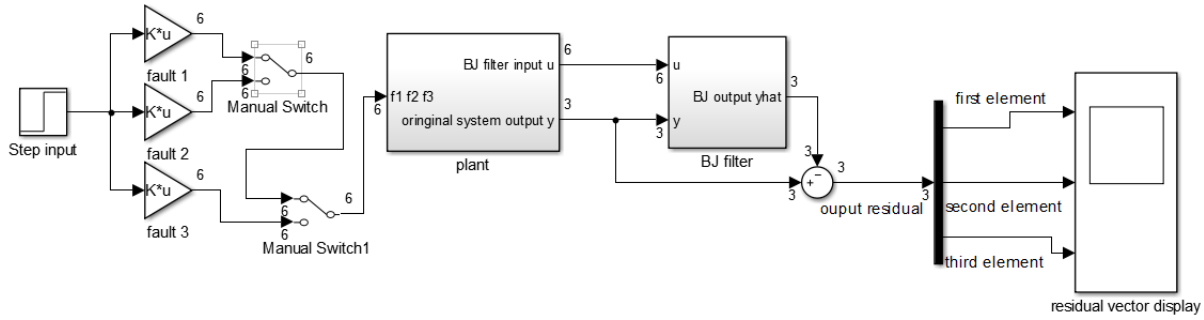

Figure 5.12 Fault detection system for the MIMO system

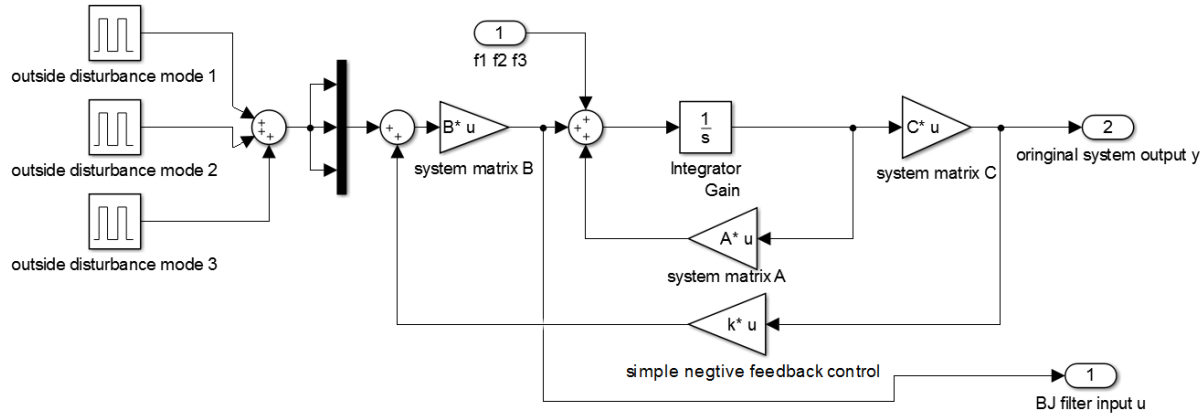

Figure 5.13 Subsystem of the plate structure for the MIMO system

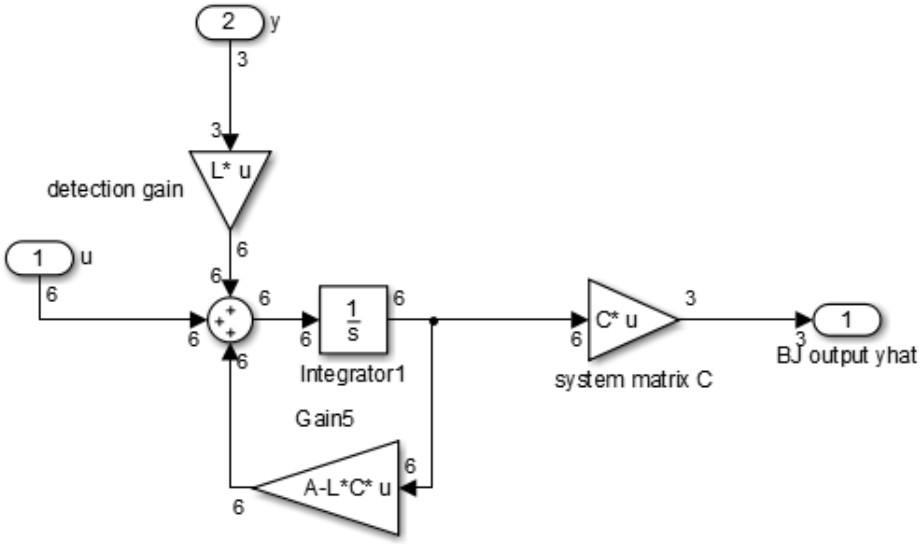

Figure 5.14 Subsystem of the BJ filter structure for the MIMO system

In the fault detection system (Figure 5.12), the fault vectors $\boldsymbol{f_1}$, $\boldsymbol{f_2}$ and $\boldsymbol{f_3}$ are activated by the step input signal and then inserted into the plant. The output signals of the MIMO system and the BJ filter are compared to produce the output residual (3-dimensional) which can be displayed in the scope. In the plate structure (Figure 5.13), three square waves (where frequencies are set to be the same as those of the first, second and third modes of the system, respectively) are used as the external disturbances which can keep this control system in operation and the negative control gain is used for suppressing the system vibration. In the BJ filter structure (Figure 5.14), the input and output signals of the original system are introduced to the BJ filter in order to produce an estimated fault-free output signal.

According to the fault detection theory explained in Chapter 4, the output residual $\hat{\varepsilon}(\boldsymbol{t})$ should be proportional to $\mathbf{C}\boldsymbol{f_i}$ with respect to corresponding fault vector $\boldsymbol{f_i}$. Firstly, the value of $\mathbf{C}\boldsymbol{f_i}$ for three pre-defined fault vectors are presented as:

$$\mathbf{C}\boldsymbol{f_1} = \begin{bmatrix} 18.1925 \\ 14.1058 \\ 11.9241 \end{bmatrix} \quad \mathbf{C}\boldsymbol{f_2} = \begin{bmatrix} 7.2299 \\ 4.8027 \\ 4.4556 \end{bmatrix} \quad \mathbf{C}\boldsymbol{f_3} = \begin{bmatrix} 0.4552 \\ 0.8414 \\ 0.7581 \end{bmatrix} \tag{5.11}$$

When the fault vector $\boldsymbol{f_1}$ is introduced to the system, the value of output residual shown in Figure 5.15 for fault vector $\boldsymbol{f_1}$ can be examined.

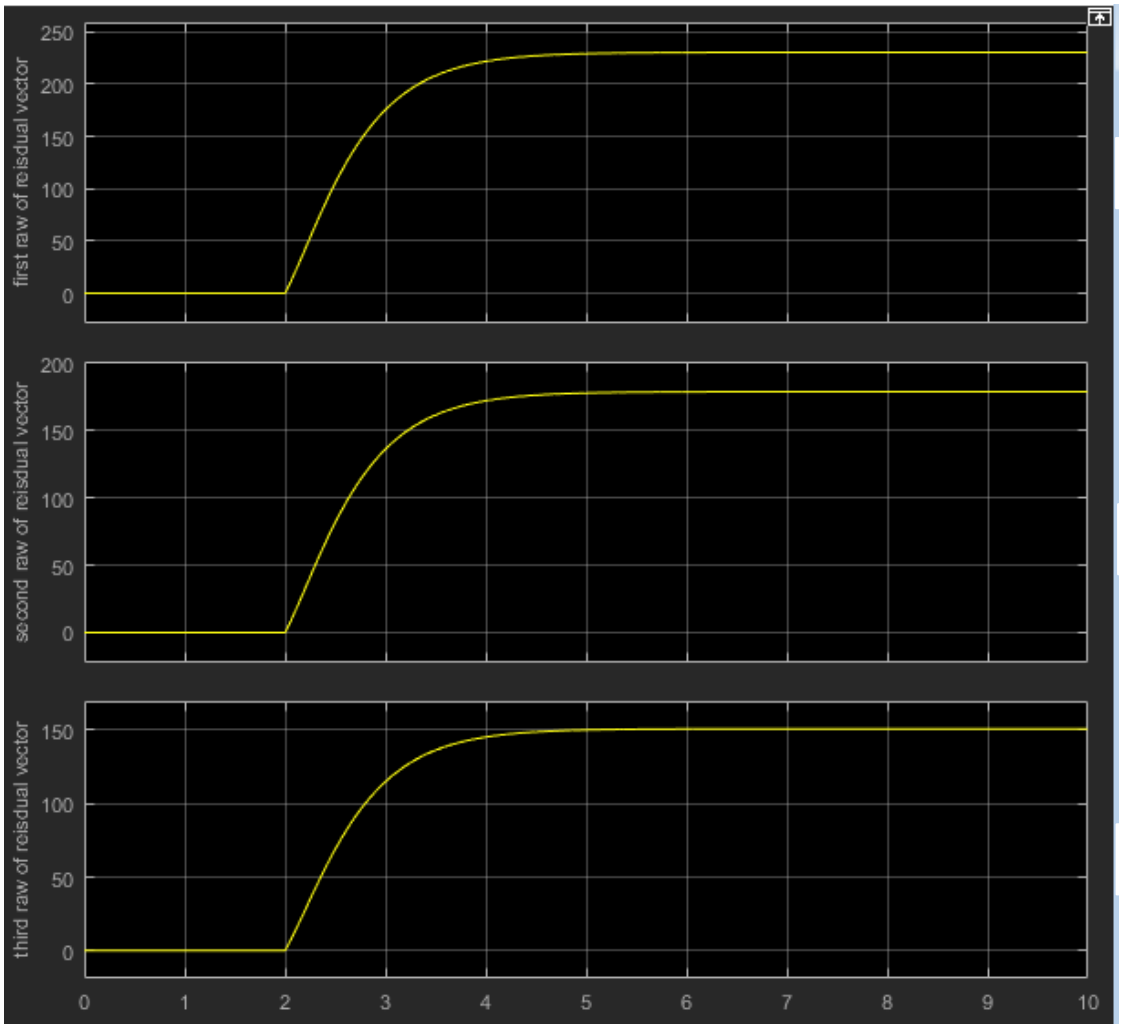

Figure 5.15 Simulation result for $\boldsymbol{f_1}$ of the MIMO system
(a) 1st row of the residual vector; (b) 2nd row of the residual vector; (c) 3rd row of the residual vector

From Figure 5.15, it shows that after the fault detection system becomes stable, the output residual for $\boldsymbol{f_1}$ is stable at value of [230.3; 178.5; 150.9], which is proportional to $\mathbf{C}\boldsymbol{f_1}$ as calculated in (5.12). Therefore, the designed conceptual BJ filter is able to detect the pre-defined fault vector $\boldsymbol{f_1}$ in the MIMO system successfully.

$$\text{Output residual for } \boldsymbol{f_1} = \begin{bmatrix} 230.3 \\ 178.5 \\ 150.9 \end{bmatrix} = 12.6 \times \mathbf{C}\boldsymbol{f_1} = 12.6 \times \begin{bmatrix} 18.1925 \\ 14.1058 \\ 11.9241 \end{bmatrix} \tag{5.12}$$

When the fault vector $\boldsymbol{f_2}$ is introduced to the system, the value of the output residual shown in Figure 5.16 for fault vector $\boldsymbol{f_2}$ can be examined.

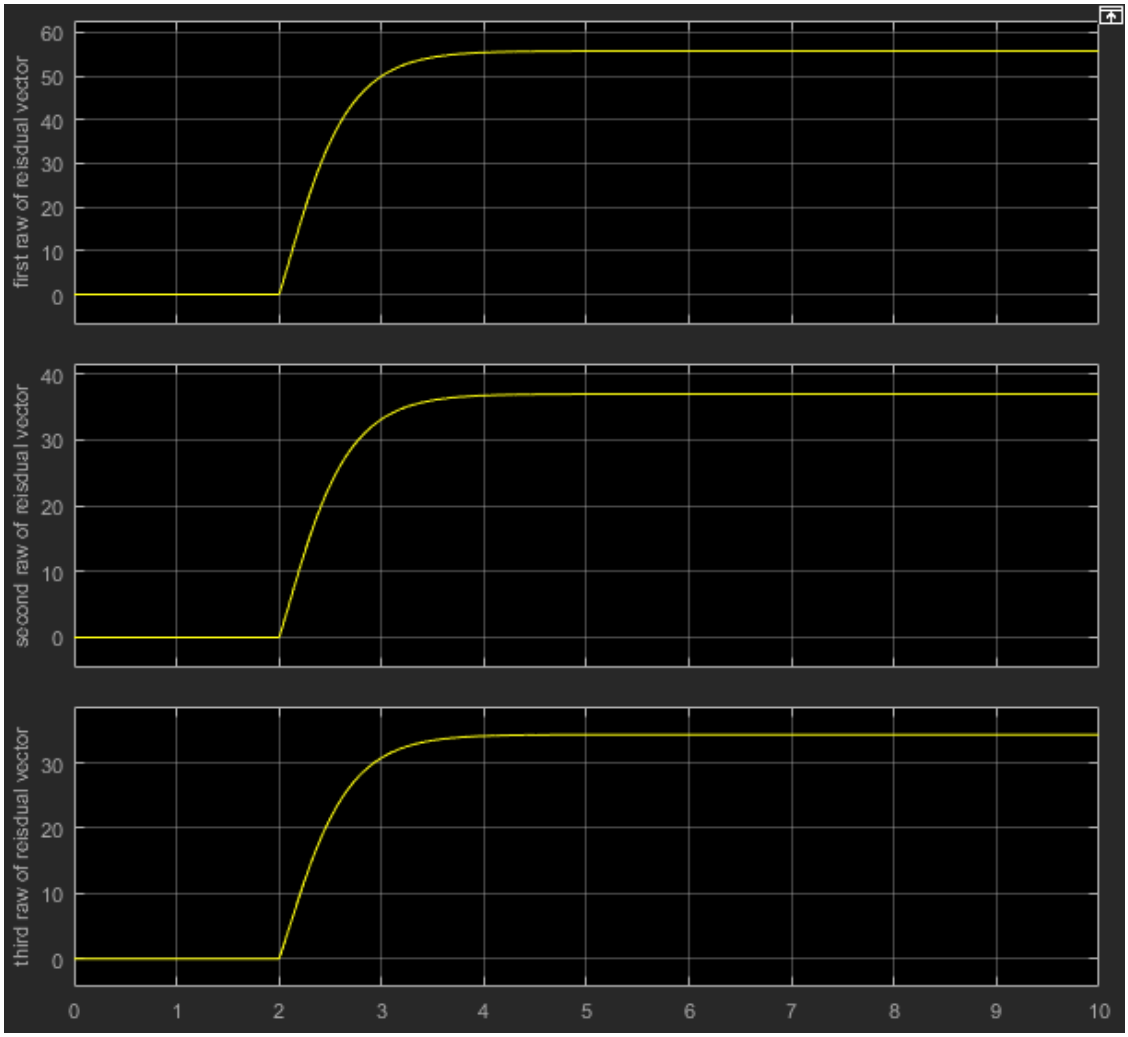

Figure 5.16 Simulation result for $\boldsymbol{f_2}$ of the MIMO system
(a) 1st row of the residual vector; (b) 2nd row of the residual vector; (c) 3rd row of the residual vector

From Figure 5.16, it shows that after the fault detection system becomes stable, the output residual for $\boldsymbol{f_2}$ is stable at value of [55.71; 37.01; 34.33], which is proportional to $\mathbf{C}\boldsymbol{f_2}$ as calculated in (5.13). Therefore, the designed conceptual BJ filter is able to detect the pre-defined fault vector $\boldsymbol{f_2}$ in the MIMO system successfully.

$$\text{Output residual for } \boldsymbol{f_2} = \begin{bmatrix} 55.71 \\ 37.01 \\ 34.33 \end{bmatrix} = 7.7 \times \mathbf{C}\boldsymbol{f_2} = 7.7 \times \begin{bmatrix} 7.2299 \\ 4.8027 \\ 4.4556 \end{bmatrix} \tag{5.13}$$

When the fault vector $\boldsymbol{f_3}$ is introduced to the system, the value of the output residual shown in Figure 5.17 for fault vector $\boldsymbol{f_3}$ can be examined.

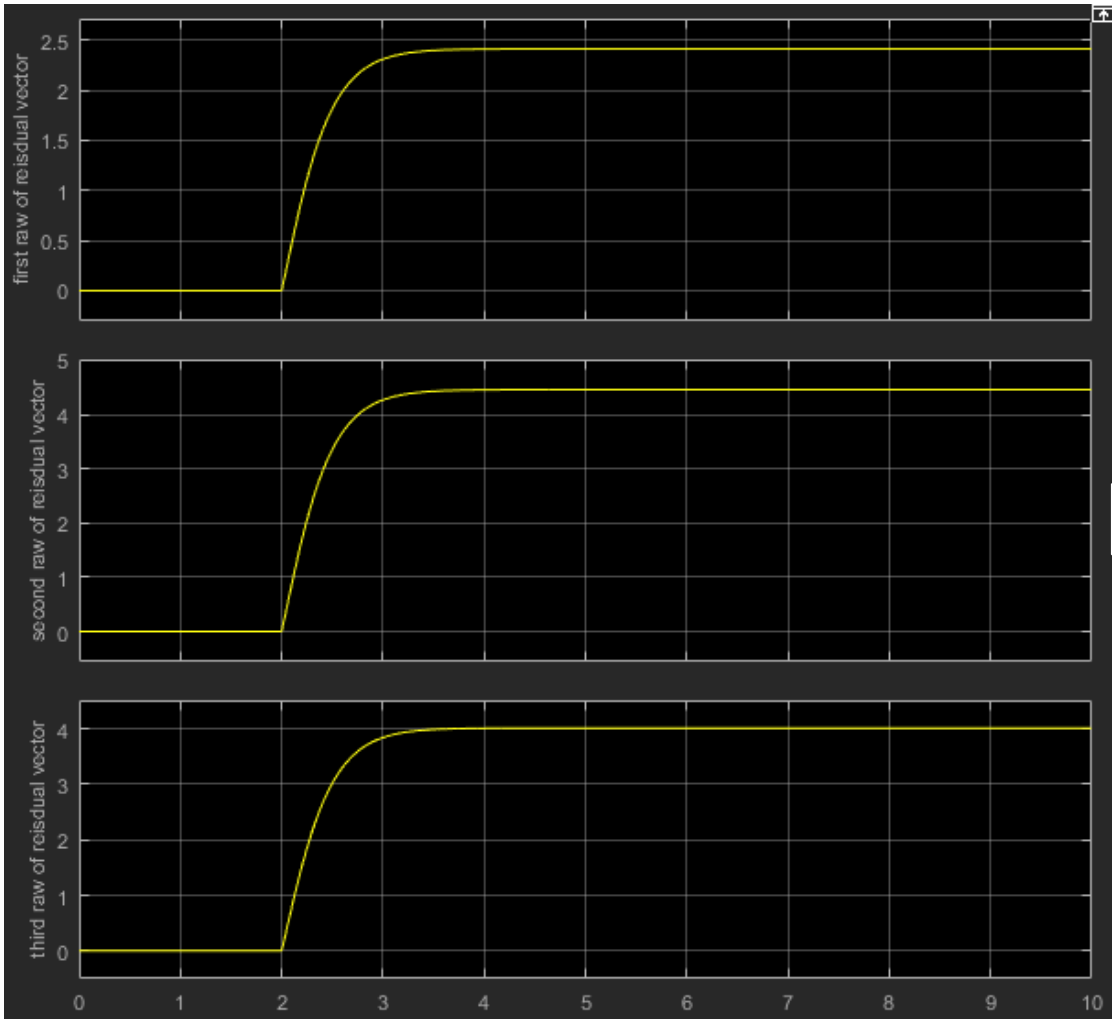

Figure 5.17 Simulation result for $\boldsymbol{f_3}$ of the MIMO system
(a) 1st row of the residual vector; (b) 2nd row of the residual vector; (c) 3rd row of the residual vector

From Figure 5.17, it shows that after the fault detection system becomes stable, the output residual for $\boldsymbol{f_3}$ is stable at value of [2.412; 4.458; 4.017], which is proportional to $\boldsymbol{Cf_3}$ as calculated in (5.13). Therefore, the designed conceptual BJ filter is able to detect the pre-defined fault vector $\boldsymbol{f_3}$ in the MIMO system successfully.

$$\text{Output residual for } \boldsymbol{f_3} = \begin{bmatrix} 2.412 \\ 4.458 \\ 4.017 \end{bmatrix} = 5.23 \times \boldsymbol{Cf_3} = 5.23 \times \begin{bmatrix} 0.4552 \\ 0.8414 \\ 0.7581 \end{bmatrix} \tag{5.13}$$

In conclusion, simulation results via three different configurations confirm that the designed conceptual BJ filters are able to detect the pre-defined faults in the real plate system successfully.

Chapter 6 : Operable BJ Filter Validation and Experiment

Upon the validation of the conceptual BJ filter design principle and procedure, an operable BJ filter is discussed in this chapter specifically for actuator fault detection of the given plate control system in real-time operations via simulation and experiment.

6.1 Construction of Fault Vectors

To design the operable BJ filter for detecting three actuator faults in real-time operations, the specific fault vectors $\boldsymbol{f_i}$ associated with corresponding actuator faults need to be constructed. The key in building the proper fault vectors is to analyse the state space representation of the given plate control system with actuator faults.

$$\begin{cases} \dot{\boldsymbol{X}}(\boldsymbol{t}) = \mathbf{A}\boldsymbol{X}(\boldsymbol{t}) + \mathbf{B}\boldsymbol{U}(\boldsymbol{t}) + \boldsymbol{f_i}\boldsymbol{\mu_i} \\ \boldsymbol{Y}(\boldsymbol{t}) = \mathbf{C}\boldsymbol{X}(\boldsymbol{t}) \end{cases} \tag{6.1}$$

According to (6.1), it shows that one completely failed actuator (for example $\boldsymbol{u_1}$ completely fault) can be simulated by making the first column of matrix **B** to zero, and this result can be achieved by setting $\boldsymbol{f_1}$ equal to the first column of matrix **B** and setting $\boldsymbol{\mu_1}$ equal to $-\boldsymbol{U}(\boldsymbol{t})$. In this way, the first actuator in the system is completely invalid. Similarly, the second and third actuator faults can be modelled by setting the fault vector equal to the second and third columns of matrix **B**, respectively. Therefore, this fault-vector construction method leads to the condition that the whole fault matrix **F** ($[\boldsymbol{f_1} \quad \boldsymbol{f_2} \quad \boldsymbol{f_3}]$) is equal to matrix **B**.

The reason why using this type of fault-vector construction method is that during the experimental verification, the actuator fault can be made artificially by disconnecting the corresponding actuator and the effect of this action is just corresponded with the effect of introduced fault vectors.

6.2 Construction of Operable BJ Filter in Extended MIMO (3I6O) System

Unfortunately, the fault-vector construction method explained above cannot be applied directly to the current mathematical model of the given plate control system. According to the detection theory for a multiple-fault situation, the first and critical restriction is the output separability. Based on (6.2) and the given system's matrices **B** and **C**, the output separability can be tested. Since:

$$\text{rank}\,(\mathbf{CF}) = \text{rank}\,(\mathbf{CB}) = 0 \tag{6.2}$$

This system cannot meet the restriction of output separability. Therefore, a modification of the original system needs to be made to fit this system into the BJ filter theory. From the configurations of the given matrices **B** and **C**:

$$\mathbf{B} = \begin{bmatrix} 0 & 0 & 0 \\ \varphi_1^1 & \varphi_2^1 & \varphi_3^1 \\ 0 & 0 & 0 \\ \varphi_1^2 & \varphi_2^2 & \varphi_3^2 \\ 0 & 0 & 0 \\ \varphi_1^3 & \varphi_2^3 & \varphi_3^3 \end{bmatrix} \quad \mathbf{C} = \begin{bmatrix} \varphi_1^1 & 0 & \varphi_1^2 & 0 & \varphi_1^3 & 0 \\ \varphi_2^1 & 0 & \varphi_2^2 & 0 & \varphi_2^3 & 0 \\ \varphi_3^1 & 0 & \varphi_3^2 & 0 & \varphi_3^3 & 0 \end{bmatrix} \tag{6.3}$$

it can be seen that the only way to address this issue is to modify the configuration of **B** or **C**. The system input (relating to matrix **B**) cannot be altered due to the physical system setup, while the system output (relating to matrix **C**) can be extended artificially. Based on the knowledge of the given physical system, this problem can be solved by extending the dimension of the output vector $\boldsymbol{Y}(\boldsymbol{t})$ to 6, which can be achieved by adding $\dot{\boldsymbol{Y}}(\boldsymbol{t})$ (the velocity of the system) to the system output vector.

The relation between $\dot{\boldsymbol{Y}}(\boldsymbol{t})$ and $\boldsymbol{X}(\boldsymbol{t})$ can be developed from (3.41).

$$\begin{cases} y_1 = \varphi_1^1 x_1 + \varphi_1^2 x_3 + \varphi_1^3 x_5 \\ y_2 = \varphi_2^1 x_1 + \varphi_2^2 x_3 + \varphi_2^3 x_5 \\ y_3 = \varphi_3^1 x_1 + \varphi_3^2 x_3 + \varphi_3^3 x_5 \end{cases} \text{ and } \begin{cases} \dot{x}_1 = x_2 \\ \dot{x}_3 = x_4 \\ \dot{x}_5 = x_6 \end{cases}$$

$$\rightarrow \begin{cases} \dot{y}_1 = \varphi_1^1 \dot{x}_1 + \varphi_1^2 \dot{x}_3 + \varphi_1^3 \dot{x}_5 \\ \dot{y}_2 = \varphi_2^1 \dot{x}_1 + \varphi_2^2 \dot{x}_3 + \varphi_2^3 \dot{x}_5 \\ \dot{y}_3 = \varphi_3^1 \dot{x}_1 + \varphi_3^2 \dot{x}_3 + \varphi_3^3 \dot{x}_5 \end{cases} \rightarrow \begin{cases} \dot{y}_1 = \varphi_1^1 x_2 + \varphi_1^2 x_4 + \varphi_1^3 x_6 \\ \dot{y}_2 = \varphi_2^1 x_2 + \varphi_2^2 x_4 + \varphi_2^3 x_6 \\ \dot{y}_3 = \varphi_3^1 x_2 + \varphi_3^2 x_4 + \varphi_3^3 x_6 \end{cases} \tag{6.4}$$

Therefore, based on (6.4) and the block diagram of the original MIMO system (Figure 3.13), the block diagram of the 3I6O system can be developed in Figure 6.1.

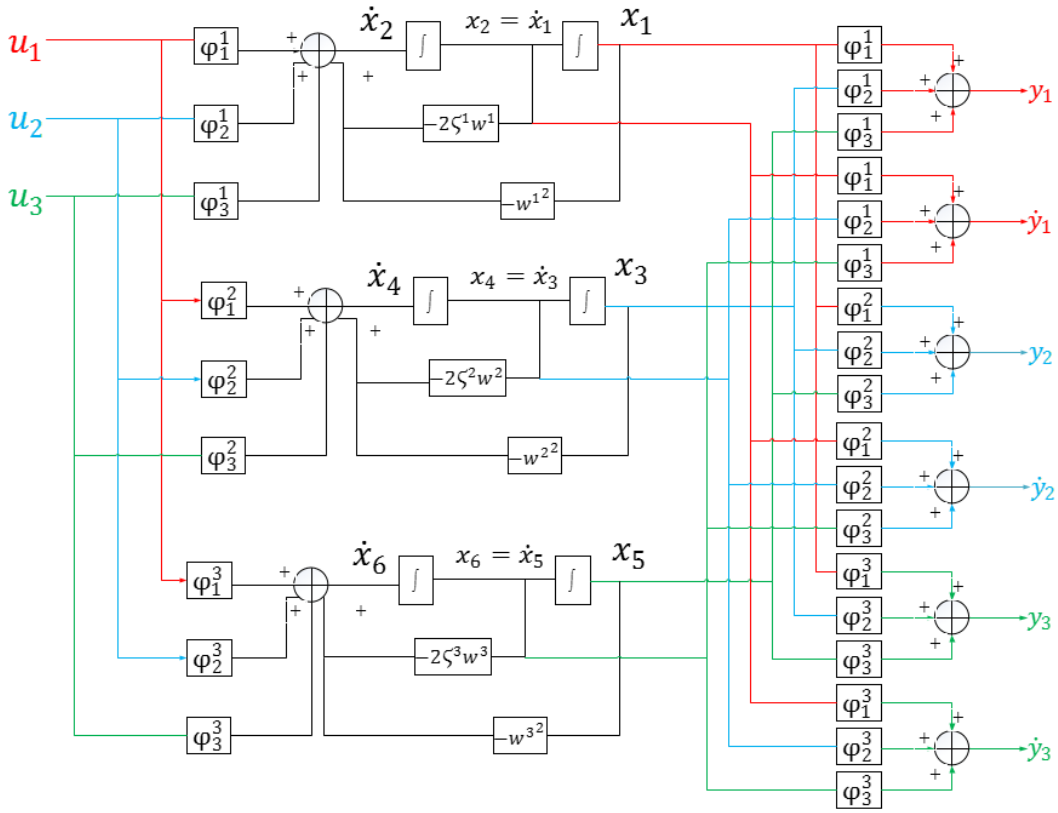

Figure 6.1 The block diagram of 3I6O system for the BJ filter design

According to Figure 6.1, the state space representation for this 3I6O system can be derived as shown in (6.5), together with the fault vectors associated with actuator faults.

$$\begin{cases} \dot{\boldsymbol{X}}(\boldsymbol{t})_{6\times1} = \mathbf{A}_{6\times6}\boldsymbol{X}(\boldsymbol{t})_{6\times1} + \mathbf{B}_{6\times3}\boldsymbol{U}(\boldsymbol{t})_{3\times1} \\ \boldsymbol{Y}(\boldsymbol{t})_{6\times1} = \mathbf{C}_{6\times6}\boldsymbol{X}(\boldsymbol{t})_{6\times1} \end{cases} \tag{6.5}$$

where $\mathbf{A} = \begin{bmatrix} 0 & 1 & & & & \\ -w^{1\,2} & -2\zeta^1 w^1 & & & & \\ & & 0 & 1 & & \\ & & -w^{2\,2} & -2\zeta^2 w^2 & & \\ & & & & 0 & 1 \\ & & & & -w^{3\,2} & -2\zeta^3 w^3 \end{bmatrix}$ $\mathbf{B} = \begin{bmatrix} 0 & 0 & 0 \\ \varphi_1^1 & \varphi_2^1 & \varphi_3^1 \\ 0 & 0 & 0 \\ \varphi_1^2 & \varphi_2^2 & \varphi_3^2 \\ 0 & 0 & 0 \\ \varphi_1^3 & \varphi_2^3 & \varphi_3^3 \end{bmatrix}$

$$\mathbf{C} = \begin{bmatrix} \varphi_1^1 & 0 & \varphi_1^2 & 0 & \varphi_1^3 & 0 \\ 0 & \varphi_1^1 & 0 & \varphi_1^2 & 0 & \varphi_1^3 \\ \varphi_2^1 & 0 & \varphi_2^2 & 0 & \varphi_2^3 & 0 \\ 0 & \varphi_2^1 & 0 & \varphi_2^2 & 0 & \varphi_2^3 \\ \varphi_3^1 & 0 & \varphi_3^2 & 0 & \varphi_3^3 & 0 \\ 0 & \varphi_3^1 & 0 & \varphi_3^2 & 0 & \varphi_3^3 \end{bmatrix} \qquad \mathbf{F} = [\boldsymbol{f_1} \quad \boldsymbol{f_2} \quad \boldsymbol{f_3}] = \mathbf{B}$$

Such an arrangement guarantees that this extended system, while keeping the features of the original plate control system, provides a revised form of the system output matrix **C** that satisfies the output separability requirement as:

$$\text{rank}\,(\mathbf{CF}) = \text{rank}\,(\mathbf{CB}) = 3 \tag{6.6}$$

The parameters of this 3I6O system can be obtained from the real system data that has been developed in Chapter 3. Based on the BJ filter design procedure developed in Chapter 4, the detection gain **L** can be calculated using the algorithm designed in MATLAB and the result is shown in (6.7). The MATLAB script can refer to Appendix A.

$$\mathbf{L} = \begin{bmatrix} 1 & 1.29 & 1.1 & 41.09 & 1.2 & -46.38 \\ 2 & -15.44 & 2.1 & -753.31 & 2.2 & 847.08 \\ 3 & 1.57 & 3.1 & -19.91 & 3.2 & 21.15 \\ 4 & -27.89 & 4.1 & -931.28 & 4.2 & 1053.6 \\ 5 & -1.33 & 5.1 & -1.23 & 5.2 & 3.48 \\ 6 & -16.07 & 6.1 & -1768.8 & 6.2 & 1967.1 \end{bmatrix} \tag{6.7}$$

6.3 Construction of Positive Position Feedback (PPF) Controller

To implement the fault detection using the operable BJ filter in real-time operations, PPF controller needs to be constructed to keep the given plate control system stable. PPF controller is extremely suitable for resonance system due to its advantages. PPF controller is insensitive to spill-over effects because it acts as a second-order compensator which rolls off quickly at high frequencies [46]. In addition, PPF controller is not only capable of controlling multiple modes by one pair of co-located sensor and actuator, but also able to introduce a high level of damping [53].

The overall MIMO-PPF controller system can be written as [46]:

$$\text{Structure: } \ddot{\boldsymbol{\xi}} + \mathbf{D}\dot{\boldsymbol{\xi}} + \boldsymbol{\Omega}\boldsymbol{\xi} = \boldsymbol{\Psi}^{\mathbf{T}}\mathbf{G}\boldsymbol{\eta} \tag{6.8}$$

$$\text{PPF controller: } \ddot{\boldsymbol{\eta}} + \mathbf{D_c}\dot{\boldsymbol{\eta}} + \boldsymbol{\Omega_c}\boldsymbol{\eta} = \boldsymbol{\Omega_c}\boldsymbol{\psi}\boldsymbol{\xi} \tag{6.9}$$

where $\boldsymbol{\xi}$ represents the plate structure coordinate, $\boldsymbol{\eta}$ represents the PPF controller coordinate, matrices **D**, **Ω**, and **ψ** include the system parameters which have been developed in Chapter 3.

$$\mathbf{D} = \begin{bmatrix} 2\varsigma^1 w^1 & 0 & 0 \\ 0 & 2\varsigma^2 w^2 & 0 \\ 0 & 0 & 2\varsigma^3 w^3 \end{bmatrix} \quad \boldsymbol{\Omega} = \begin{bmatrix} {w^1}^2 & 0 & 0 \\ 0 & {w^2}^2 & 0 \\ 0 & 0 & {w^3}^2 \end{bmatrix} \quad \boldsymbol{\psi} = \begin{bmatrix} \varphi_1^1 & \varphi_1^2 & \varphi_1^3 \\ \varphi_2^1 & \varphi_2^2 & \varphi_2^3 \\ \varphi_3^1 & \varphi_3^2 & \varphi_3^3 \end{bmatrix}$$

Matrices $\mathbf{D_c}$, $\mathbf{\Omega_c}$, and $\mathbf{G}$ include the gains g^k, natural frequencies w_c^k, and damping ratios ς_c^k (k= 1, 2, 3) of the PPF controller, which all need to be designed.

$$\mathbf{D_c} = \begin{bmatrix} 2\varsigma_c^1 w_c^1 & 0 & 0 \\ 0 & 2\varsigma_c^2 w_c^2 & 0 \\ 0 & 0 & 2\varsigma_c^3 w_c^3 \end{bmatrix} \quad \mathbf{\Omega_c} = \begin{bmatrix} {w_c^1}^2 & 0 & 0 \\ 0 & {w_c^2}^2 & 0 \\ 0 & 0 & {w_c^3}^2 \end{bmatrix} \quad \mathbf{G} = \begin{bmatrix} g^1 & 0 & 0 \\ 0 & g^2 & 0 \\ 0 & 0 & g^3 \end{bmatrix}$$

In order to effectively control the resonant behaviour of the given plate control system at the first three modes, w_c^k is designed to be equal to w^k (k= 1, 2, 3) of the plate structure. The selection of g^k and ς_c^k relies on H_∞ optimization technique. $H_{ij-cl}(s)$ (i, j=1,2, 3) is defined as the close-loop FRFs of the control system, and the H_∞ norm of $H_{ij-cl}(s)$ can be regarded as the maximum magnitude in the bode plot of $H_{ij-cl}(s)$. Therefore, through genetic algorithm, the minimum value of the H_∞ norm of $H_{ij-cl}(s)$ can be achieved by optimizing g^k and ς_c^k for three modes simultaneously [53].

The parameters of PPF controller for three modes are listed in Table 6.1.

Table 6.1 The parameters of PPF controller for three modes

$G_{ij}(s)$ (i, j=1,2, 3)	Mode 1 $w_c^1 = 142.3 rad/s$	Mode 2 $w_c^1 = 182.4 rad/s$	Mode 3 $w_c^1 = 218.9 rad/s$
Control gains g^k	$g^1 = 0.7$	$g^2 = 0.4267$	$g^3 = 0.3008$
damping ratios ς_c^k	$\varsigma_c^1 = 0.572$	$\varsigma_c^2 = 0.5656$	$\varsigma_c^3 = 0.6999$

Based on the designed PPF controller parameters, the MIMO-PPF controller can be established as shown in Figure 6.2.

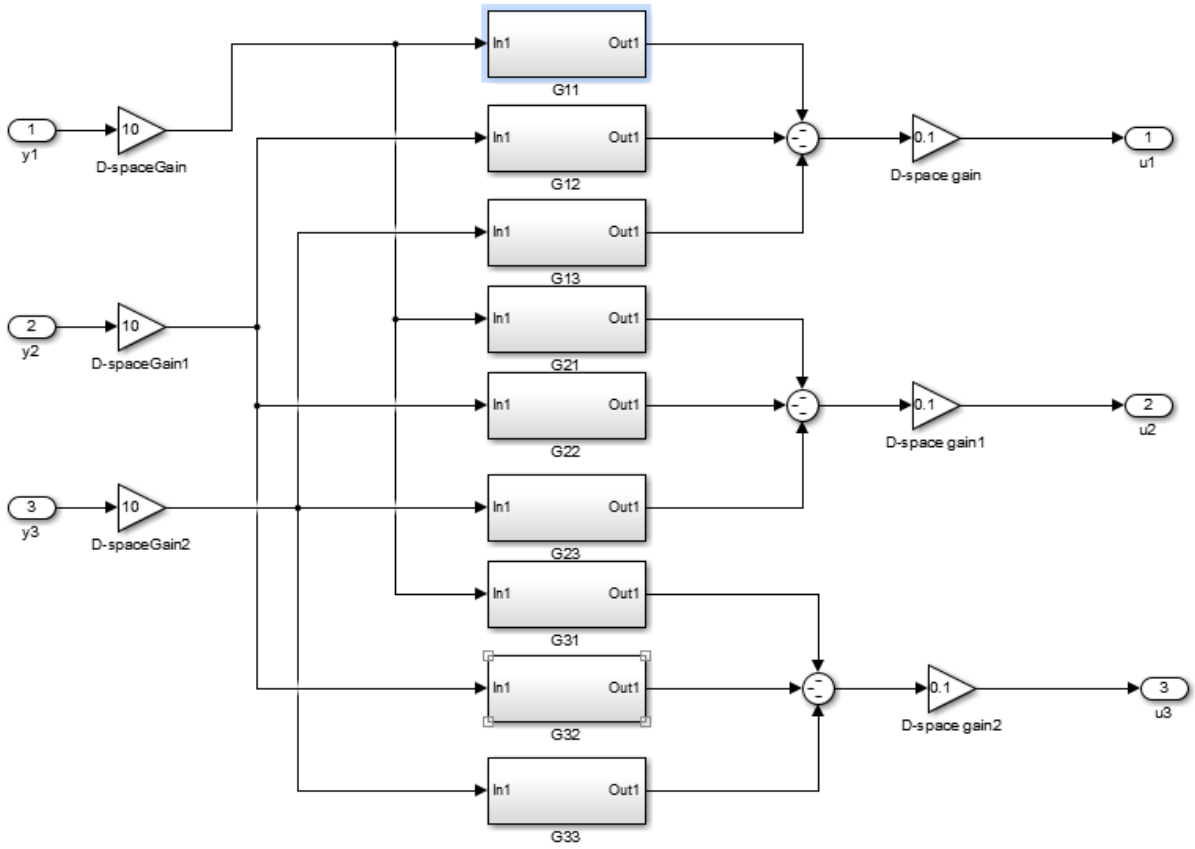

Figure 6.2 The structure of the MIMO-PPF controller

For each $G_{ij}(s)$ (i, j=1,2, 3) in the MIMO-PPF controller, they all have the same structure as shown in Figure 6.3.

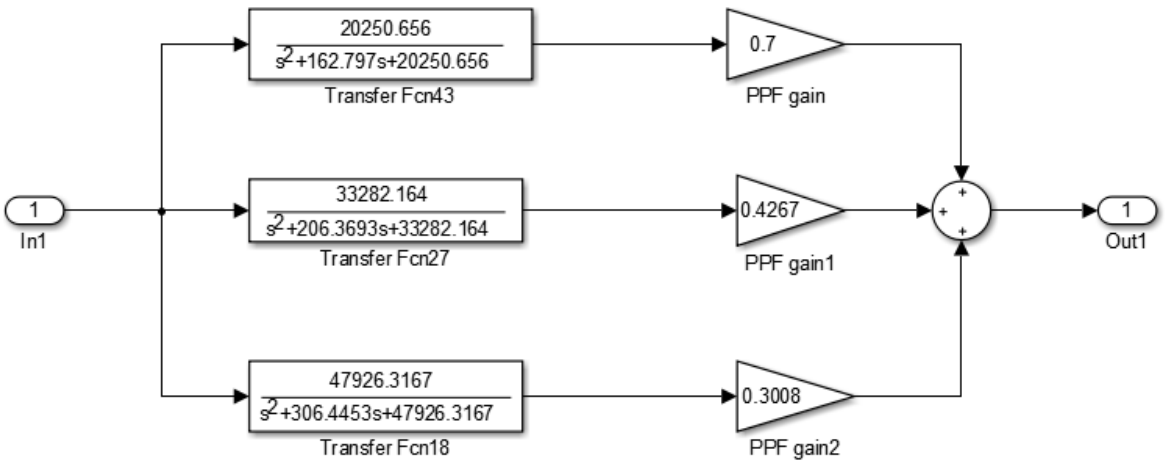

Figure 6.3 The structure of each $G_{ij}(s)$ in the MIMO-PPF controller

Finally, this MIMO-PPF controller can be integrated into the whole fault detection system using the operable BJ filter, and the validation of the operable BJ filter is discussed in the next section.

6.4 Operable BJ Filter Validation via Simulation

Based on the extended system (3I6O system), the designed operable BJ filter, capable of performing real-time actuator fault detection of the given plate control system, can be validated via two simulations in MATLAB SIMULINK.

6.4.1 Introduce Fault Vectors into System

The first simulation is to introduce fault vectors into the system, which aims to validate the fault detectability of the designed operable BJ filter. The SIMULINK model of the 3I6O fault detection system (introduced faults) is shown as follows. Figure 6.4 shows the whole fault detection system, Figure 6.5 shows the subsystem of the plate structure and Figure 6.6 shows the subsystem of the BJ filter structure.

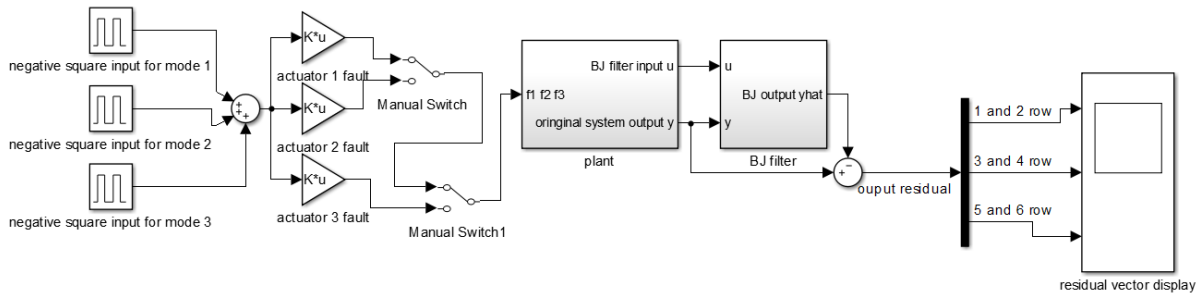

Figure 6.4 Fault detection system for the 3I6O system (introduced faults)

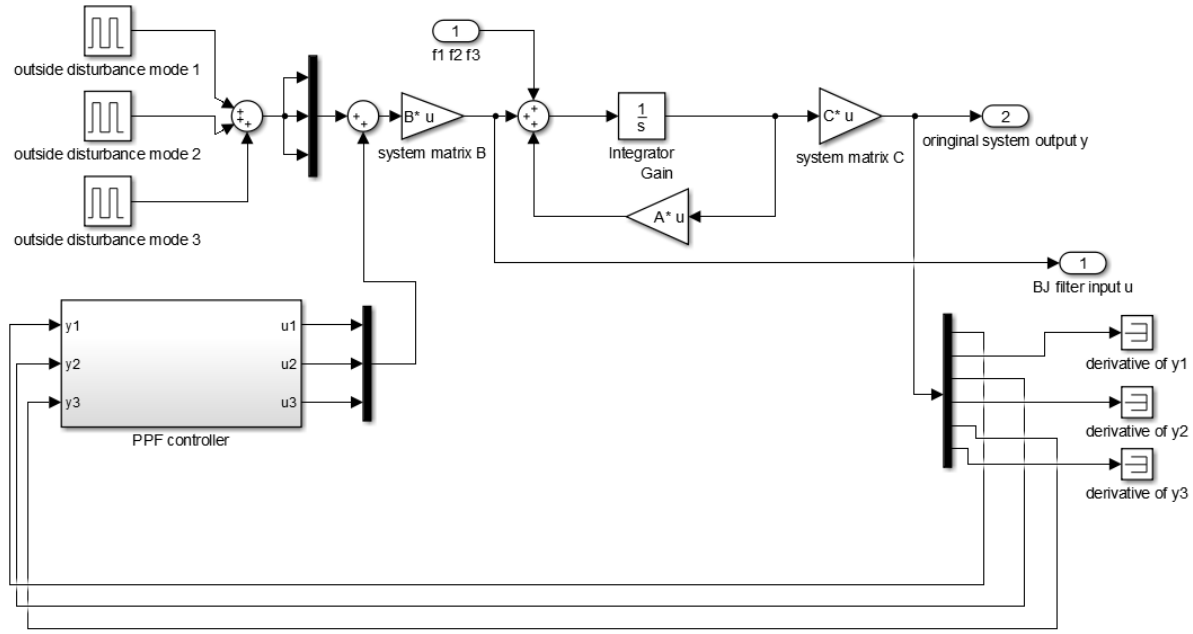

Figure 6.5 Subsystem of the plate structure for the 3I6O system (introduced faults)

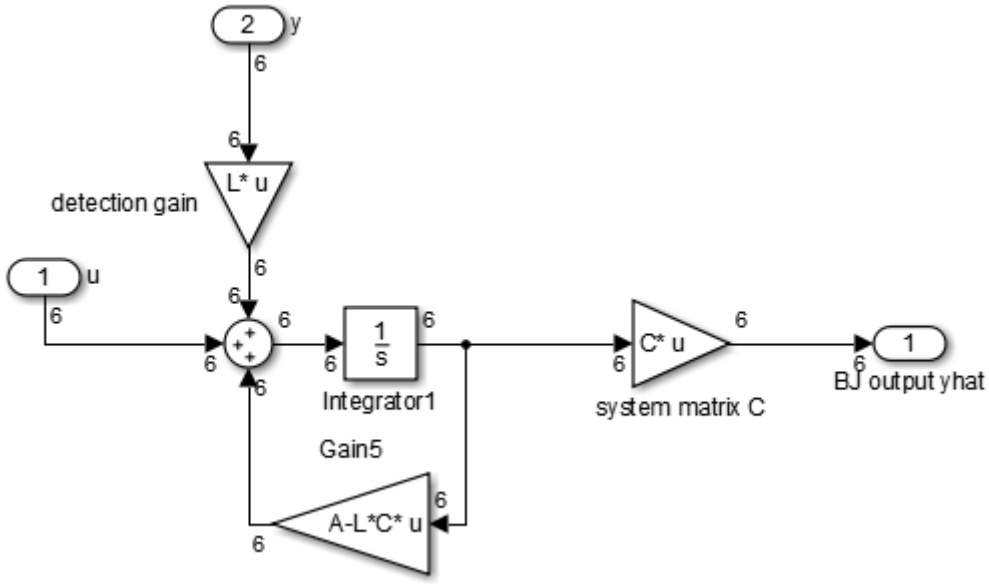

Figure 6.6 Subsystem of the BJ filter structure for the 3I6O system (introduced faults)

In the fault detection system (Figure 6.4), the fault vectors $\boldsymbol{f_1}$, $\boldsymbol{f_2}$ and $\boldsymbol{f_3}$ which are associated with each of the actuator faults are activated by the negative square input signal and then inserted into the plant in order to simulate each completely failed actuator. The output signals of the MIMO system and the BJ filter are compared to produce the output residual (6-dimensional) which can be displayed in the scope. In the plate structure (Figure 6.5), three square waves (where frequencies are set to be the same as those of the first, second and third modes of the system, respectively) are used as the external disturbance which can keep this

control system in operation, and the pre-designed PPF controller is used for suppressing the system vibration. In the BJ filter structure (Figure 6.6), the input and output signals of the original system is introduced to the BJ filter in order to produce an estimated fault-free output signal.

According to the fault detection theory explained in Chapter 4, the output residual $\hat{\varepsilon}(\boldsymbol{t})$ should be proportional to $\mathbf{C}\boldsymbol{f_i}$ with respect to corresponding fault vector $\boldsymbol{f_i}$. Firstly, the value of $\mathbf{C}\boldsymbol{f_i}$ for three fault vectors (associate with each actuator fault) are presented as:

$$\mathbf{C}\boldsymbol{f_1} = \begin{bmatrix} 0 \\ 0.8623 \\ 0 \\ 0.8329 \\ 0 \\ 0.754 \end{bmatrix} \quad \mathbf{C}\boldsymbol{f_2} = \begin{bmatrix} 0 \\ 0.8329 \\ 0 \\ 1.0181 \\ 0 \\ 0.9191 \end{bmatrix} \quad \mathbf{C}\boldsymbol{f_3} = \begin{bmatrix} 0 \\ 0.754 \\ 0 \\ 0.9191 \\ 0 \\ 0.8301 \end{bmatrix} \tag{6.10}$$

When the fault vector $\boldsymbol{f_1}$ is introduced to the system, the value of the output residual shown in Figure 6.7 for fault vector $\boldsymbol{f_1}$ can be examined.

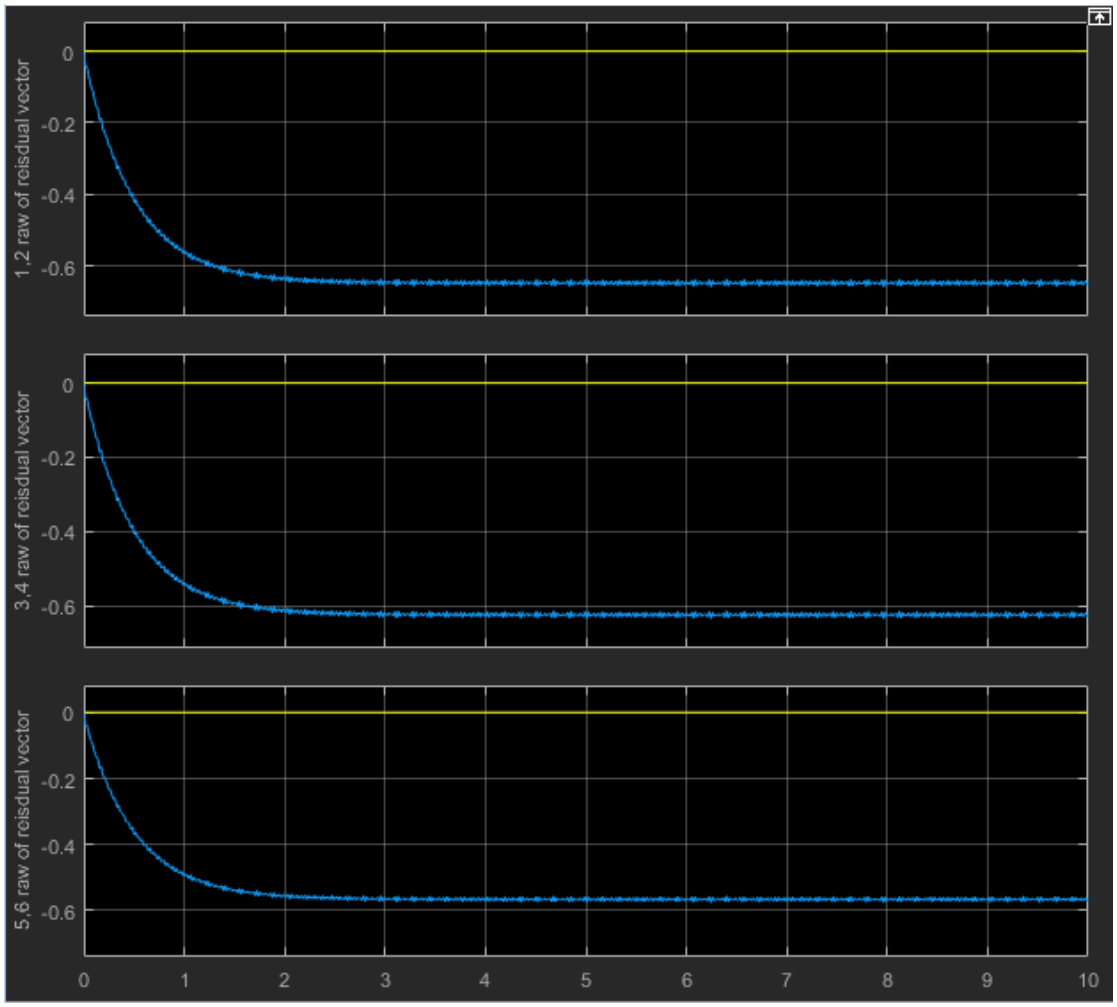

Figure 6.7 Simulation result for $\boldsymbol{f_1}$ of the 3I6O system (introduced faults)
(a) Yellow - 1st row of the residual vector; Blue - 2nd row of the residual vector; (b) Yellow – 3rd row of the residual vector; Blue – 4th row of the residual vector; (c) Yellow – 5th row of the residual vector; Blue – 6th row of the residual vector

From Figure 6.7, it shows that there exists slight fluctuation in the output residual, so the value of the output residual can be selected at a random time after the system becomes stable. The value of the output residual is therefore selected when system operates to 8th second, and the value is [0; 0.6488; 0; 0.6267; 0; 0.5673] (ignoring the negative sign), which is proportional to $\mathbf{C}\boldsymbol{f_1}$ as calculated in (6.11). Therefore, the designed operable BJ filter is able to detect the fault vector $\boldsymbol{f_1}$ associated with Actuator 1 fault successfully.

$$\text{output residual for } \boldsymbol{f_1} = \begin{bmatrix} 0 \\ 0.6488 \\ 0 \\ 0.6267 \\ 0 \\ 0.5673 \end{bmatrix} = 0.7524 \times \mathbf{C}\boldsymbol{f_1} = 0.7524 \times \begin{bmatrix} 0 \\ 0.8623 \\ 0 \\ 0.8329 \\ 0 \\ 0.754 \end{bmatrix} \tag{6.11}$$

When the fault vector $\boldsymbol{f_2}$ is introduced to the system, the value of output residual shown in Figure 6.8 for fault vector $\boldsymbol{f_2}$ can be examined.

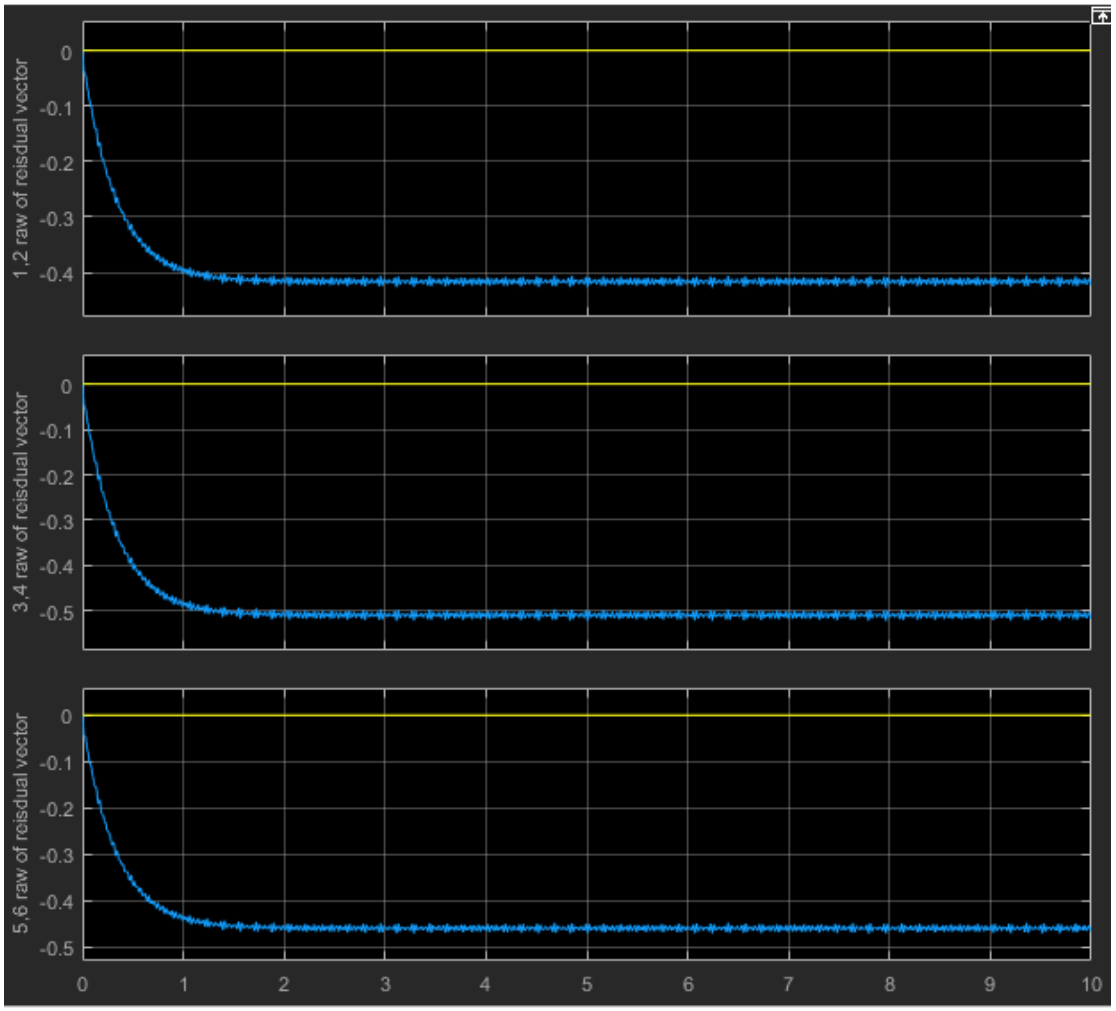

Figure 6.8 Simulation result for $\boldsymbol{f_2}$ of the 3I6O system (introduced faults)
(a) Yellow - 1st row of the residual vector; Blue - 2nd row of the residual vector; (b) Yellow – 3rd row of the residual vector; Blue – 4th row of the residual vector; (c) Yellow – 5th row of the residual vector; Blue – 6th row of the residual vector

From Figure 6.8, it shows that there exists slight fluctuation in the output residual, so the value of the output residual can be selected at a random time after the system becomes stable. The value of the output residual is therefore selected when system operates to 8th second, and the value is [0; 0.4185; 0; 0.5115; 0; 0.4618] (ignoring the negative sign), which is proportional to $\boldsymbol{Cf_2}$ as calculated in (6.12). Therefore, the designed operable BJ filter is able to detect the fault vector f_2 associated with Actuator 2 fault successfully.

$$\text{output residual for } \boldsymbol{f_2} = \begin{bmatrix} 0 \\ 0.4185 \\ 0 \\ 0.5115 \\ 0 \\ 0.4618 \end{bmatrix} = 0.5025 \times \mathbf{C}\boldsymbol{f_2} = 0.5025 \times \begin{bmatrix} 0 \\ 0.8329 \\ 0 \\ 1.0181 \\ 0 \\ 0.9191 \end{bmatrix} \tag{6.12}$$

When the fault vector $\boldsymbol{f_3}$ is introduced to the system, the value of output residual shown in Figure 6.9 for fault vector $\boldsymbol{f_3}$ can be examined.

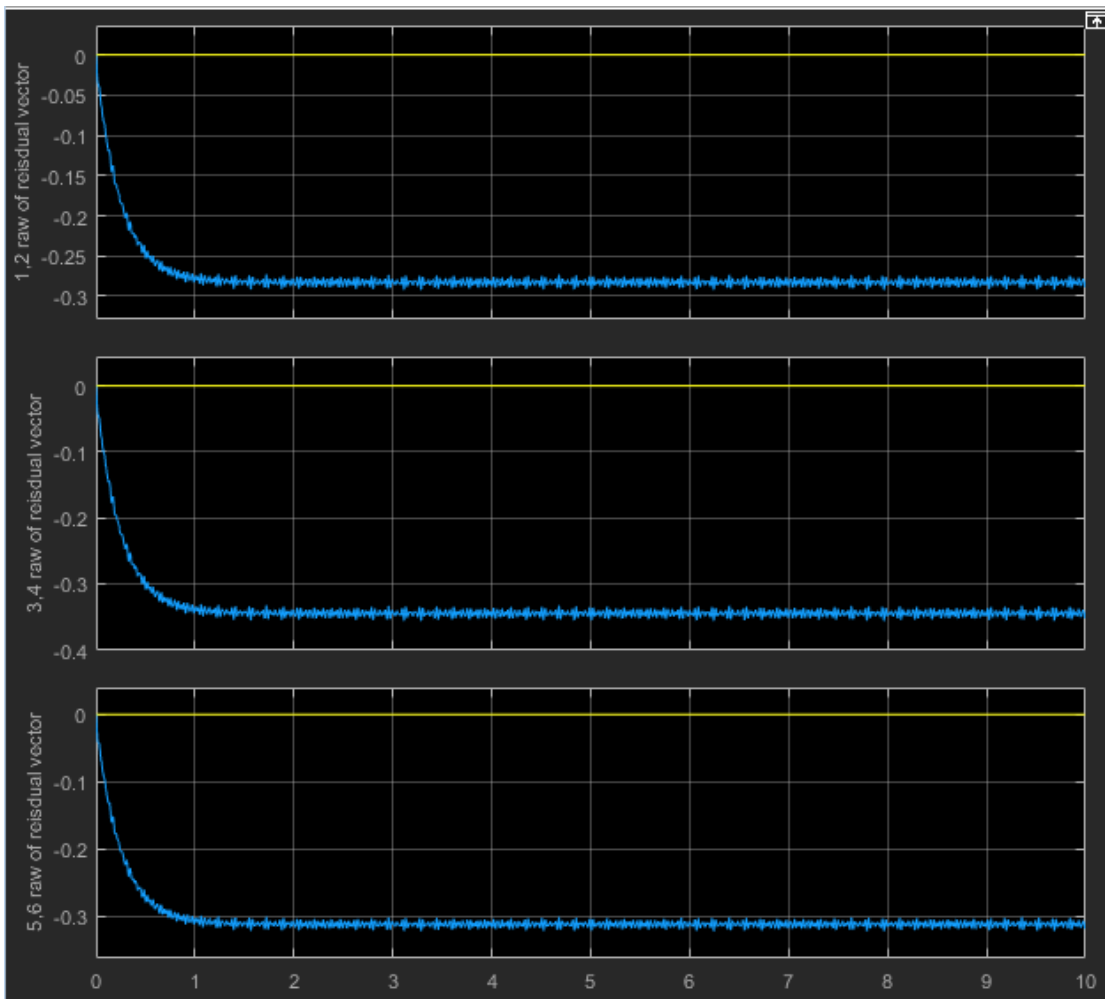

Figure 6.9 Simulation result for $\boldsymbol{f_3}$ of the 3I6O system (introduced faults)
(a) Yellow - 1st row of the residual vector; Blue - 2nd row of the residual vector; (b) Yellow – 3rd row of the residual vector; Blue – 4th row of the residual vector; (c) Yellow – 5th row of the residual vector; Blue – 6th row of the residual vector

From Figure 6.9, it shows that there exists slight fluctuation in the output residual, so the value of the output residual can be selected at a random time after the system becomes stable. The value of the output residual is therefore selected when system operates to 8th second, and the value is [0; 0.2846; 0; 0.3469; 0; 0.3133] (ignoring the negative sign), which is proportional to

$\boldsymbol{Cf_3}$ as calculated in (6.13). Therefore, the designed operable BJ filter is able to detect the fault vector f_3 associated with Actuator 3 fault successfully.

$$\text{output residual for } \boldsymbol{f_3} = \begin{bmatrix} 0 \\ 0.2846 \\ 0 \\ 0.3469 \\ 0 \\ 0.3133 \end{bmatrix} = 0.3774 \times \boldsymbol{Cf_3} = 0.3774 \times \begin{bmatrix} 0 \\ 0.754 \\ 0 \\ 0.9191 \\ 0 \\ 0.8301 \end{bmatrix} \tag{6.13}$$

So far, the above simulation results validate the fault detectability of the designed operable BJ filter when introducing fault vectors into the plate control system.

6.4.2 Disconnect Each Actuator to Simulate Real Actuator Faults

The second simulation is to artificially disconnect each actuator to simulate the real actuator faults, which aims to verify that the constructed fault vectors are indeed associated with the actuator faults, and to validate the fault detectability of the designed operable BJ filter. The SIMULINK model of the 3I6O fault detection system (disconnect actuators) is shown as follows. Figure 6.10 shows the whole fault detection system, Figure 6.11 shows the subsystem of the plate structure and Figure 6.12 shows the subsystem of the BJ filter structure.

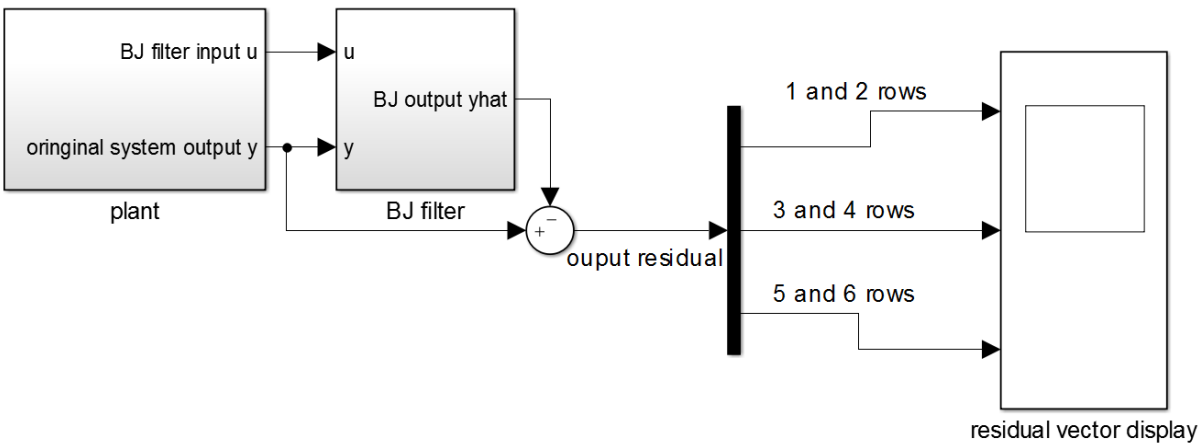

Figure 6.10 Fault detection system for the 3I6O system (disconnect actuators)

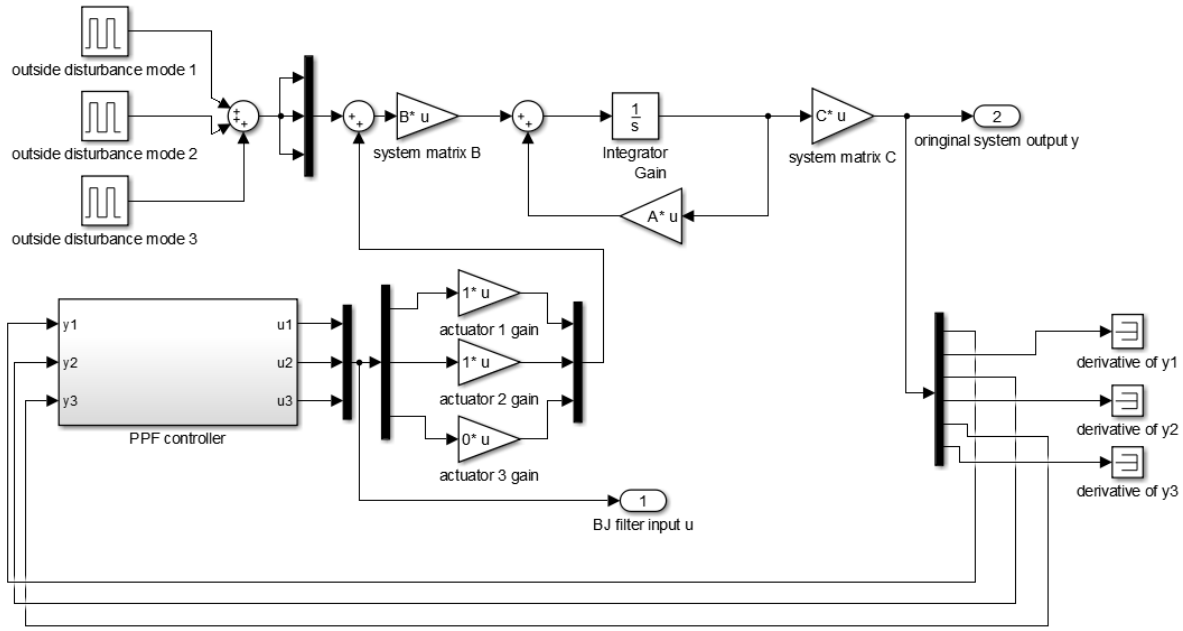

Figure 6.11 Subsystem of the plate structure for the 3I6O system (disconnect actuators)

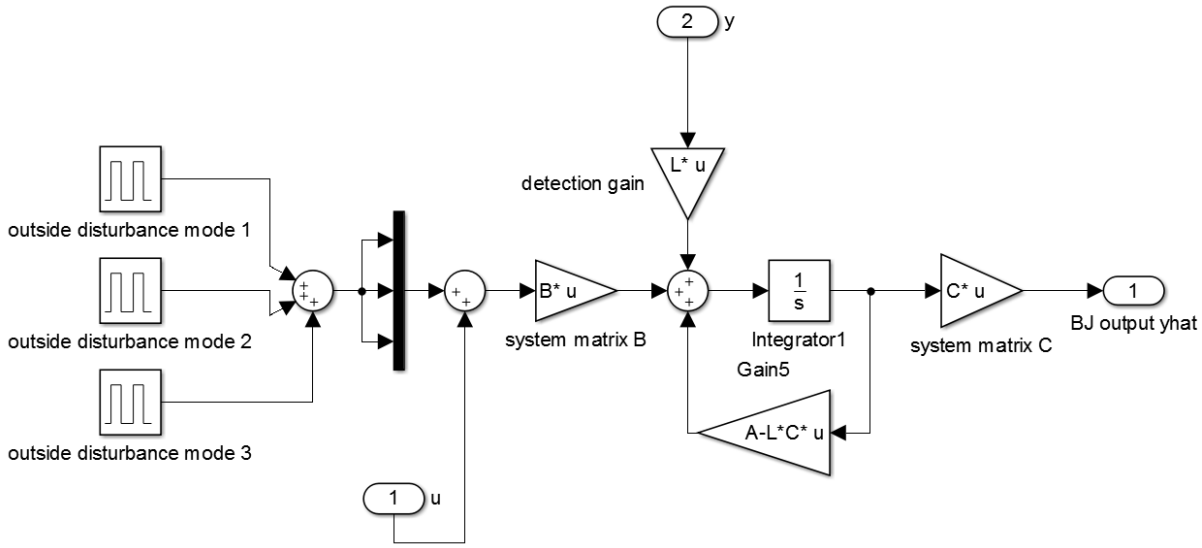

Figure 6.12 Subsystem of the BJ filter structure for the 3I6O system (disconnect actuators)

In the fault detection system (Figure 6.10), there is no need to introduce faults because each actuator will be directly disconnected in the plate structure to simulate each actuator fault. The output signals of the MIMO system and the BJ filter are compared to produce the output residual (6-dimension) which can be displayed in the scope. In the plate structure (Figure 6.11), three square waves (where frequencies are set to be the same as those of the first, second and third modes of the system, respectively) are used as the external disturbances which can keep this control system in operation, and the designed PPF controller is used for suppressing the system vibration. There are three actuator gains that can be set to 0 in order to artificially

disconnect each actuator. In the BJ filter structure (Figure 6.12), the input and output signals of the original system is introduced to the BJ filter in order to produce an estimated fault-free output signal.

As explained in the first section, the effect of disconnecting each actuator is corresponded with the effect of introduced fault vector $\boldsymbol{f_i}$ as before. Therefore, the output residual $\hat{\varepsilon}(\boldsymbol{t})$ should still be proportional to $\boldsymbol{Cf_i}$ (shown in (6.8)) with respect to each actuator fault.

When disconnecting Actuator 1 (setting Actuator 1 gain to zero) of the system, the value of output residual shown in Figure 6.13 can be examined.

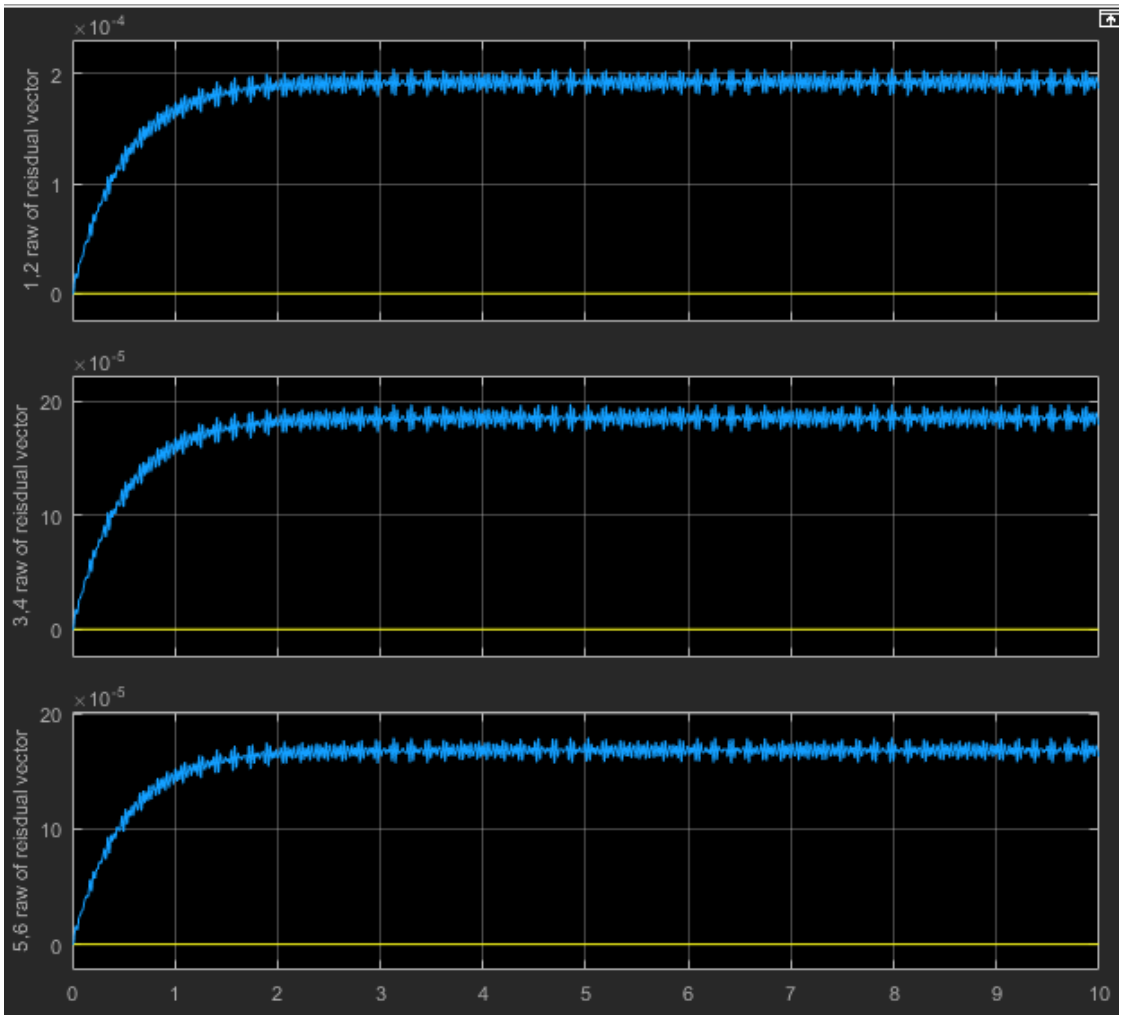

Figure 6.13 Simulation result for Actuator 1 fault of the 3I6O system (disconnect actuators) (a) Yellow - 1st row of the residual vector; Blue - 2nd row of the residual vector; (b) Yellow – 3rd row of the residual vector; Blue – 4th row of the residual vector; (c) Yellow – 5th row of the residual vector; Blue – 6th row of the residual vector

From Figure 6.13, it shows that there exists slight fluctuation in the output residual, so the value of the output residual can be selected at a random time after the system becomes stable. The

value of the output residual is therefore selected when system operates to 8th second, and the value is [0; 1.955; 0; 1.888; 0; 1.71] (ignoring the scalar 10^{-4}), which is proportional to $\mathbf{C}\boldsymbol{f_1}$ as calculated in (6.14). Therefore, the designed operable BJ filter is able to detect Actuator 1 fault successfully.

$$\text{output residual for Actuator 1 fault} = \begin{bmatrix} 0 \\ 1.955 \\ 0 \\ 1.888 \\ 0 \\ 1.71 \end{bmatrix} = 2.267 \times \mathbf{C}\boldsymbol{f_1} = 2.267 \times \begin{bmatrix} 0 \\ 0.8623 \\ 0 \\ 0.8329 \\ 0 \\ 0.754 \end{bmatrix} \tag{6.14}$$

When disconnecting Actuator 2 (setting Actuator 2 gain to zero) of the system, the value of the output residual shown in Figure 6.14 can be examined.

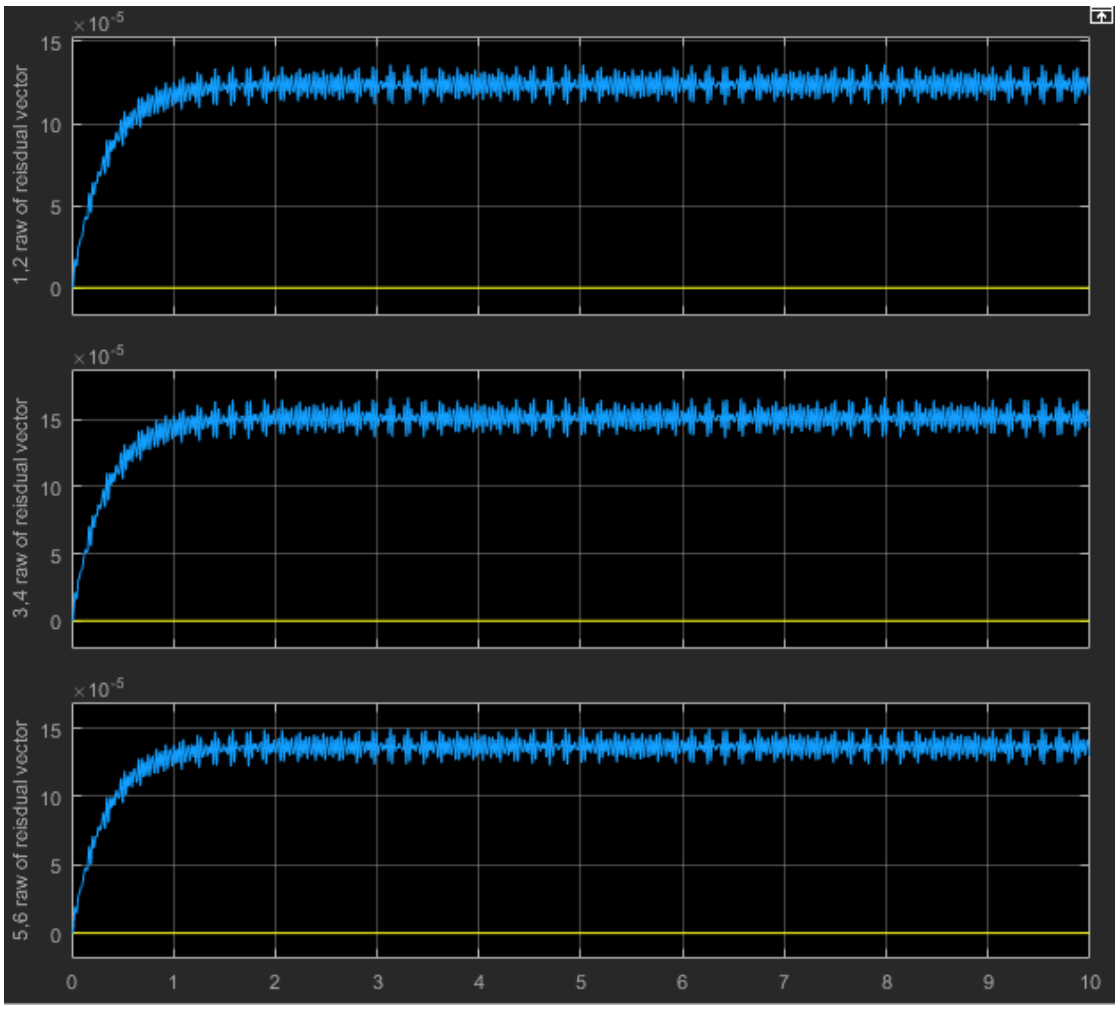

Figure 6.14 Simulation result for Actuator 2 fault of the 3I6O system (disconnect actuators) (a) Yellow - 1st row of the residual vector; Blue - 2nd row of the residual vector; (b) Yellow – 3rd row of the residual vector; Blue – 4th row of the residual vector; (c) Yellow – 5th row of the residual vector; Blue – 6th row of the residual vector

From Figure 6.14, it shows that there exists slight fluctuation in the output residual, so the value of the output residual can be selected at a random time after the system becomes stable. The value of the output residual is therefore selected when system operates to 8th second, and the value is [0; 1.268; 0; 1.55; 0; 1.399] (ignoring the scalar 10^{-4}), which is proportional to $\mathbf{C}\boldsymbol{f_2}$ as calculated in (6.15). Therefore, the designed operable BJ filter is able to detect Actuator 2 fault successfully.

$$\text{output residual for Actuator 2 fault} = \begin{bmatrix} 0 \\ 1.268 \\ 0 \\ 1.55 \\ 0 \\ 1.399 \end{bmatrix} = 1.522 \times \mathbf{C}\boldsymbol{f_2} = 1.522 \times \begin{bmatrix} 0 \\ 0.8329 \\ 0 \\ 1.0181 \\ 0 \\ 0.9191 \end{bmatrix} \tag{6.15}$$

When disconnecting Actuator 3 (setting Actuator 3 gain to zero) of the system, the value of output residual shown in Figure 6.15 can be examined.

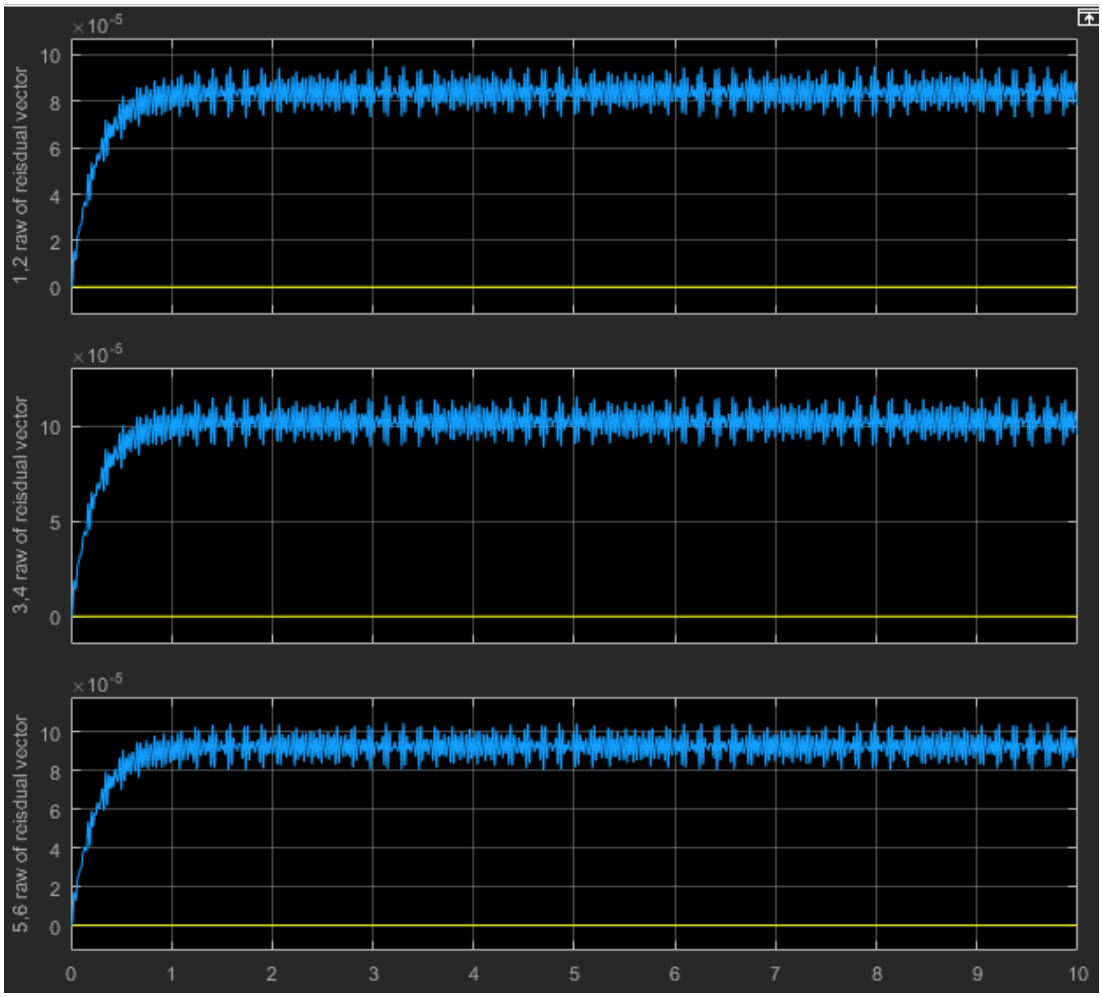

(a)

(b)

(c)

Figure 6.15 Simulation result for Actuator 3 fault of the 3I6O system (disconnect actuators)

(a) Yellow - 1st row of the residual vector; Blue - 2nd row of the residual vector; (b) Yellow – 3rd row of the residual vector; Blue – 4th row of the residual vector; (c) Yellow – 5th row of the residual vector; Blue – 6th row of the residual vector

From Figure 6.15, it shows that there exists slight fluctuation in the output residual, so the value of the output residual can be selected at a random time after the system becomes stable. The value of the output residual is therefore selected when system operates to 8th second, and the value is [0; 0.2846; 0; 0.3469; 0; 0.3133] (ignoring the scalar 10^{-4}), which is proportional to $\mathbf{Cf_3}$ as calculated in (6.16). Therefore, the designed operable BJ filter is able to detect Actuator 3 fault successfully.

$$\text{output residual for Actuator 3 fault} = \begin{bmatrix} 0 \\ 0.8702 \\ 0 \\ 1.061 \\ 0 \\ 0.9581 \end{bmatrix} = 1.154 \times \mathbf{Cf_3} = 1.154 \times \begin{bmatrix} 0 \\ 0.754 \\ 0 \\ 0.9191 \\ 0 \\ 0.8301 \end{bmatrix} \tag{6.16}$$

In conclusion, through these two simulations, it is seen that the operable BJ filter is capable of performing real-time actuator fault detection and diagnosis of the given plate control system.

6.5 The Improvement in Identifying Each Actuator Fault

Rather than comparing the proportional relationship between the output residual and $\mathbf{Cf_i}$ with respect to the corresponding actuator fault, this section illustrates an improvement in identifying each actuator fault.

Based on the understanding of the relationship between the output residual and $\mathbf{Cf_i}$ from several simulation results, it is seen that the actual values of these proportional relationships are varying depended on different configurations and different magnitudes of the disturbance signals. However, the inner relationships of the output residuals (the ratio between the second, fourth and sixth rows) remain unchanged and are equal to the inner relationships of the corresponding $\mathbf{Cf_i}$ (the ratio between the second, fourth and sixth rows). Instead of mathematically calculating the ever-changing proportional relationships, this property provides an effective approach to identify and indicate each actuator fault online. The procedure of this approach to identify each actuator fault is shown in Figure 6.16.

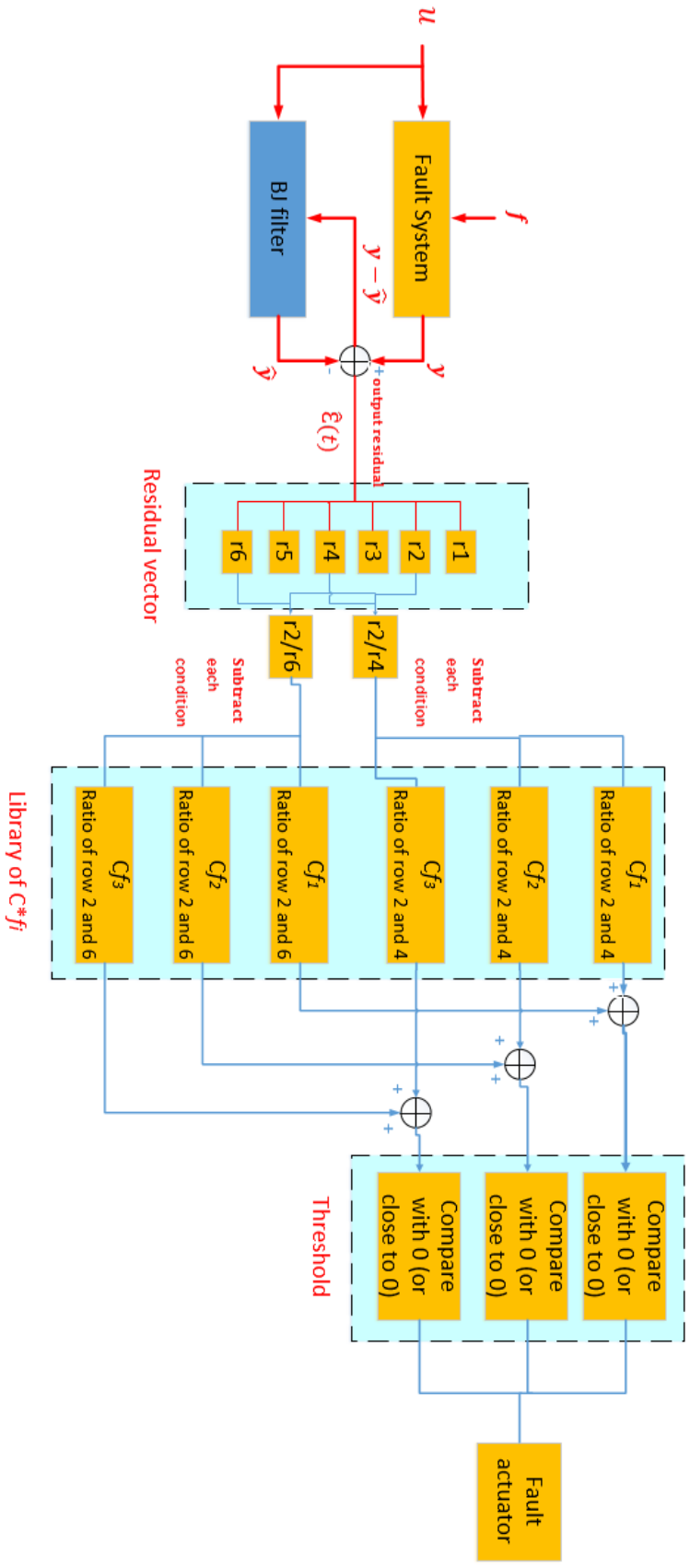

Figure 6.16 The block diagram of identifying each actuator fault

After the output residual ($[r1 \quad r2 \quad r3 \quad r4 \quad r5 \quad r6]^T$) is generated from the output difference between the fault system and the BJ filter, $r2$, $r4$ and $r6$ will be used for further analysis, as $r1$, $r3$ and $r5$ are constant zero. The inner relationships of output residuals ($\frac{r2}{r4}$ and $\frac{r2}{r6}$) are then calculated and compared with the library of pre-calculated inner relationships of $\mathbf{Cf_i}$. If the following condition (6.17) is met, the corresponding actuator fault will be identified successfully.

$$\left|\frac{r2}{r4} - \frac{\mathbf{Cf_i}[2]}{\mathbf{Cf_i}[4]}\right| + \left|\frac{r2}{r6} - \frac{\mathbf{Cf_i}[2]}{\mathbf{Cf_i}[6]}\right| \leq threshold \quad \rightarrow \quad Actuator\ i\ fault \tag{6.17}$$

where $\mathbf{Cf_i}[2]$, $\mathbf{Cf_i}[4]$ and $\mathbf{Cf_i}[6]$ are the second, fourth and sixth rows of $\mathbf{Cf_i}$, respectively, and the threshold can be set to 0.0001. Ideally, the threshold should be set to zero, but in practice, 0.0001 is small enough for this fault detection system to identify actuator fault successfully.

The library which contains the inner relationships of $\mathbf{Cf_i}$ with respect to each corresponding actuator fault is given in Table 6.2.

Table 6.2 The library of inner relationship of $\mathbf{Cf_i}$

$\mathbf{Cf_i}$ with respect to each corresponding actuator fault	$\frac{\mathbf{Cf_i}[2]}{\mathbf{Cf_i}[4]}$	$\frac{\mathbf{Cf_i}[2]}{\mathbf{Cf_i}[6]}$
$\mathbf{Cf_1}$	1.035298	1.143634
$\mathbf{Cf_2}$	0.818092	0.906212
$\mathbf{Cf_3}$	0.820368	0.908324

The SIMULINK model of this improved 3I6O fault detection system is shown as follows. Figure 6.17 shows the improved fault detection system. The subsystem of the plate structure and the subsystem of the BJ filter structure remain unchanged, as shown in Figure 6.11 and Figure 6.12, respectively.

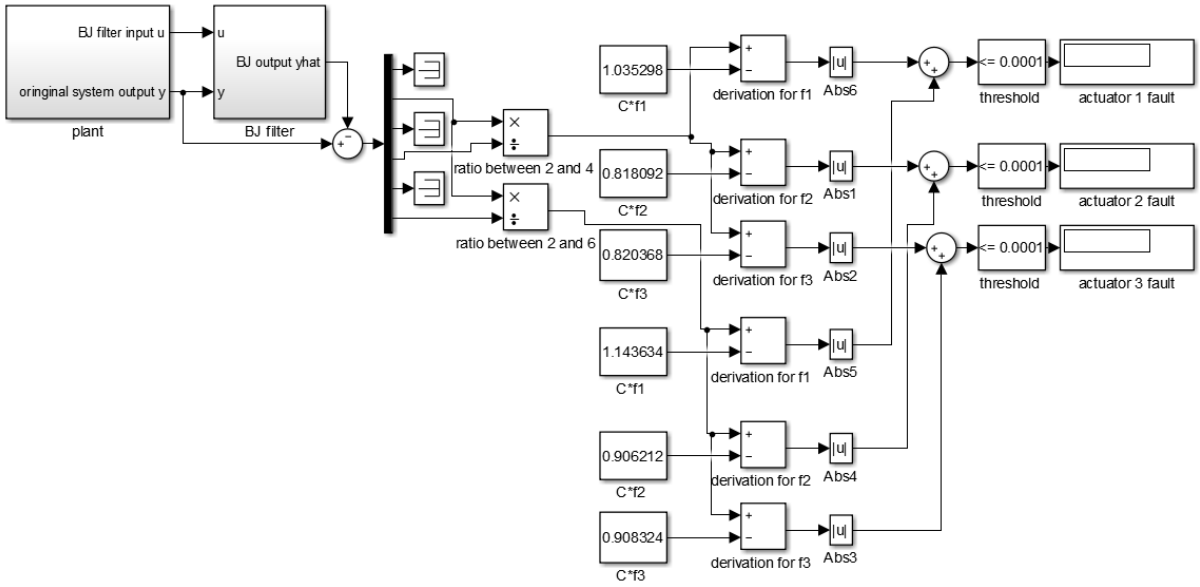

Figure 6.17 Improved Fault detection system for the 3I6O system

In the improved fault detection system (Figure 6.17), instead of displaying the output residual in the scope, using a series of mathematical processing based on the block diagram in Figure 6.16, the faulty actuators can be displayed directly on the screen ("1" representing fault and "0" representing no-fault).

When disconnecting Actuators 1, 2 and 3 of the system, respectively (by setting the corresponding actuator's gain to zero), the simulation results shown in Figure 6.18 validate the capability of faults identification in this improved fault detection system.

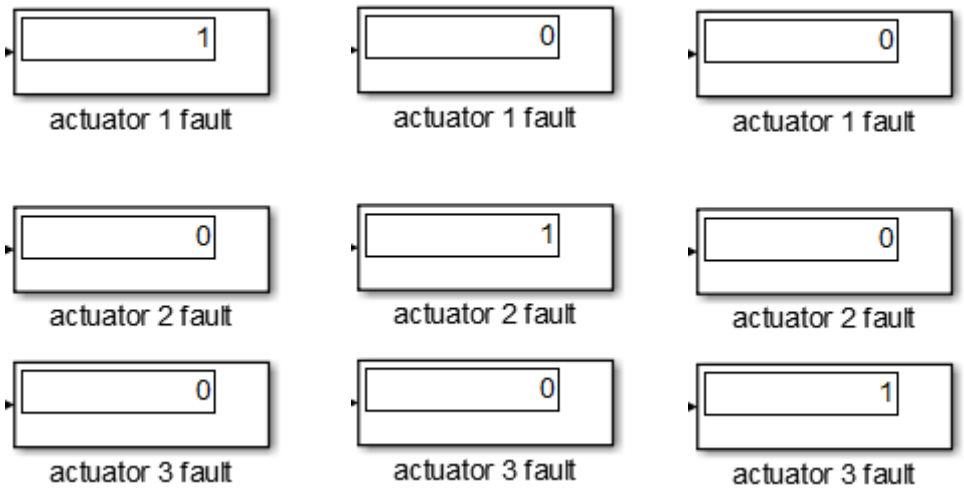

a. Disconnect Actuator 1 b. Disconnect Actuator 2 c. Disconnect Actuator 3

Figure 6.18 Simulation result of the improved 3I6O fault detection system

This improved 3I6O fault detection system thus can be applied into the experiment in the next section in order to achieve the online fault detection and diagnosis.

6.6 Operable BJ Filter Experiment

For effective actuator fault detection and diagnosis, a dual BJ filter configuration is implemented where one BJ filter acts as an online observer of the given plate system by producing the extended system output from the truncated model of the true plant, and another BJ filter acts as a fault detector and identifier to produce the required residual. This arrangement has three advantages:

- The online observer can produce three extra outputs for the extended system.
- This arrangement can eliminate inevitable modelling errors between the real plant and the modelled plant used for the BJ filter design purpose.
- This arrangement can increase the accuracy of the fault detection and diagnosis in practice.

The block diagram of the operable BJ filter experiment using the dual BJ filter configuration is shown in Figure 6.19. The physical system is controlled by the designed PPF controller such that the system can remain stationary despite the external disturbance excitation. Actuators can be disconnected from either the physical system or the online observer to simulate each actuator fault in the experiment. Using the input and output of the physical system as the inputs of the online observer and the operable BJ filter, the outputs of the online observer and the operable BJ filter are compared to generate the output residual which can be interpreted to indicate the failed actuator by the procedure explained in the last section.

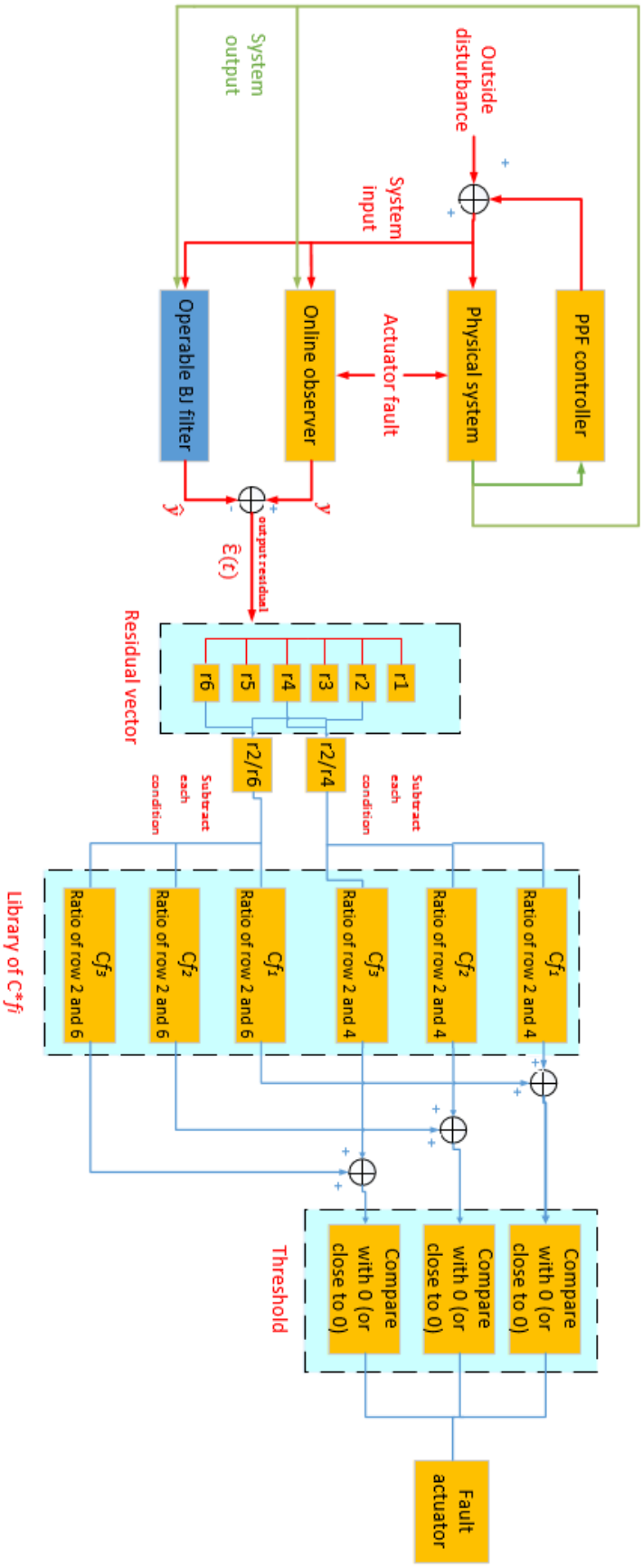

Figure 6.19 The block diagram of the operable BJ filter experiment

The arrangement of the physical system and the experiment setup have been explained in Chapter 3. The PPF controller, online observer and operable BJ filter are realized using dsPACE DS1103 in order to achieve the online fault detection and diagnosis. The SIMULINK model of the fault detection system (dual BJ filter configuration) used in the dsPACE environment is designed as shown in Figure 6.20, and the subsystem of each operable BJ filter structures is shown in Figure 6.21.

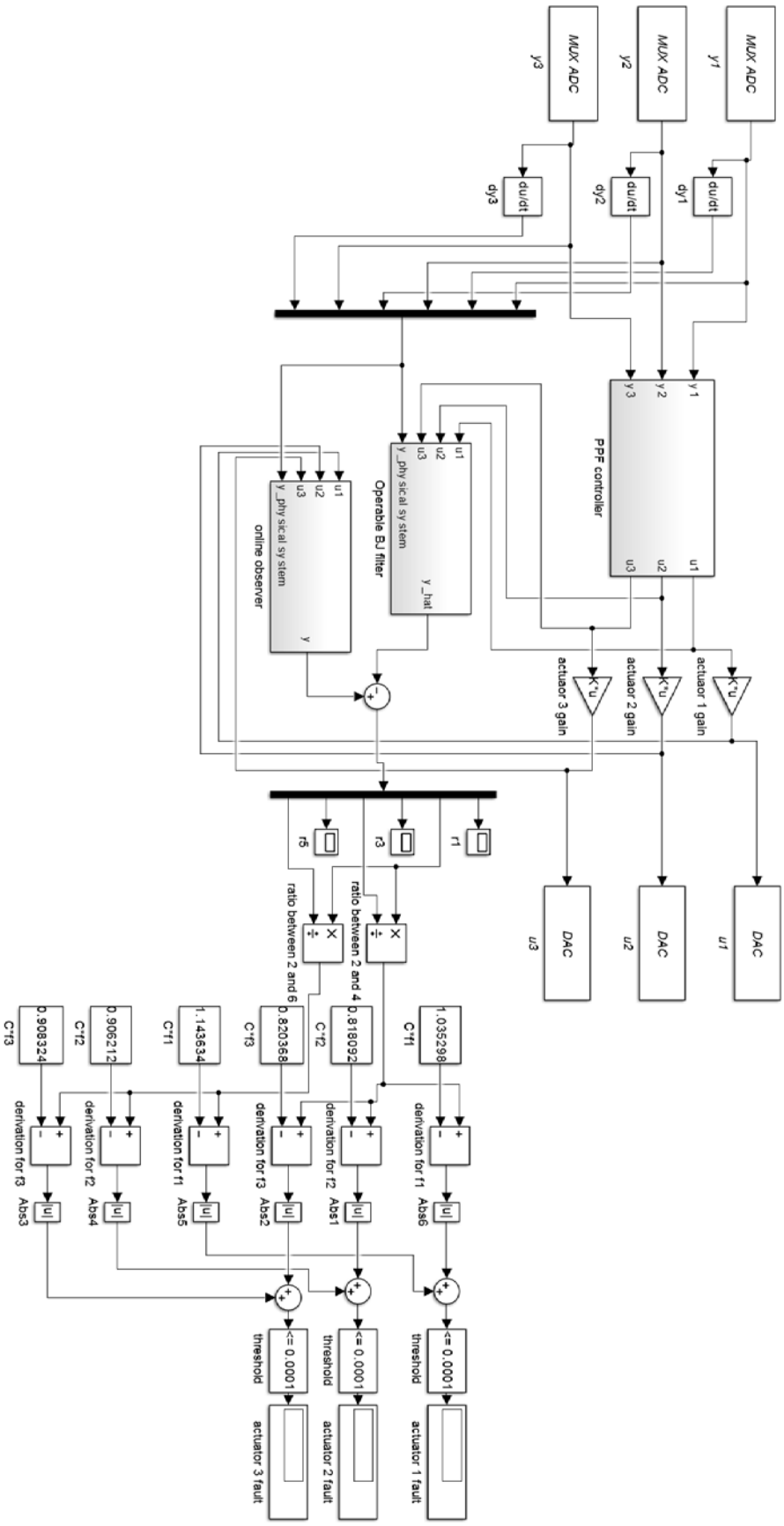

Figure 6.20 The fault detection system (dual BJ filter configuration) used in the dsPACE environment

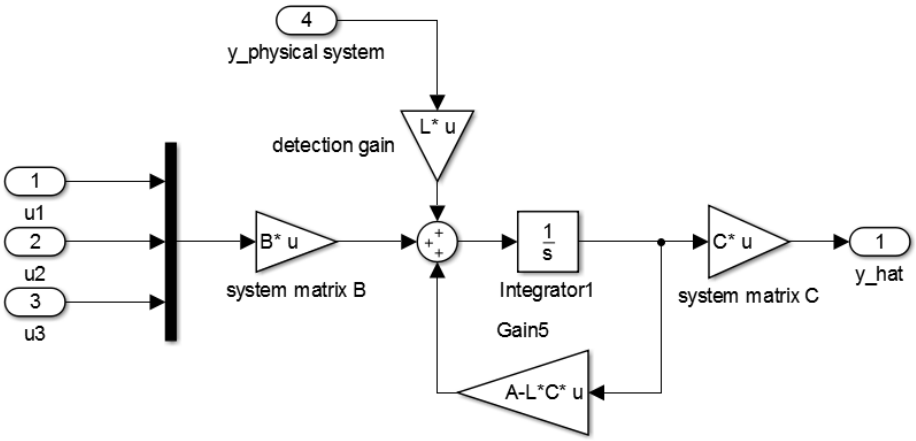

Figure 6.21 The subsystem of each operable BJ filter structures

In the fault detection system using the dual BJ filter configuration (Figure 6.20), three inputs and three outputs are introduced to the dsPACE in order to control and monitor the operation of the physical system. The designed PPF controller is used for suppressing the system vibration. There are three actuator gains that can be set to 0 in order to artificially disconnect each actuator to simulate each actuator fault. Using a series of mathematical processing, the output residual can be interpreted to indicate failed actuators, and the results can be displayed directly on the screen ("1" representing fault and "0" representing no-fault). In each operable BJ filter structures (Figure 6.21), one operable BJ filter, regarded as an online observer, is used to produce the output of the faulty actuator system and another operable BJ filter, regarded as a fault detector and identifier, is used to produce an estimated fault-free output signal.

When disconnecting Actuator 1 (setting Actuator 1 gain to zero) of the system, the experiment result shown in Figure 6.22 validates that the designed operable BJ filter is able to detect Actuator 1 fault successfully.

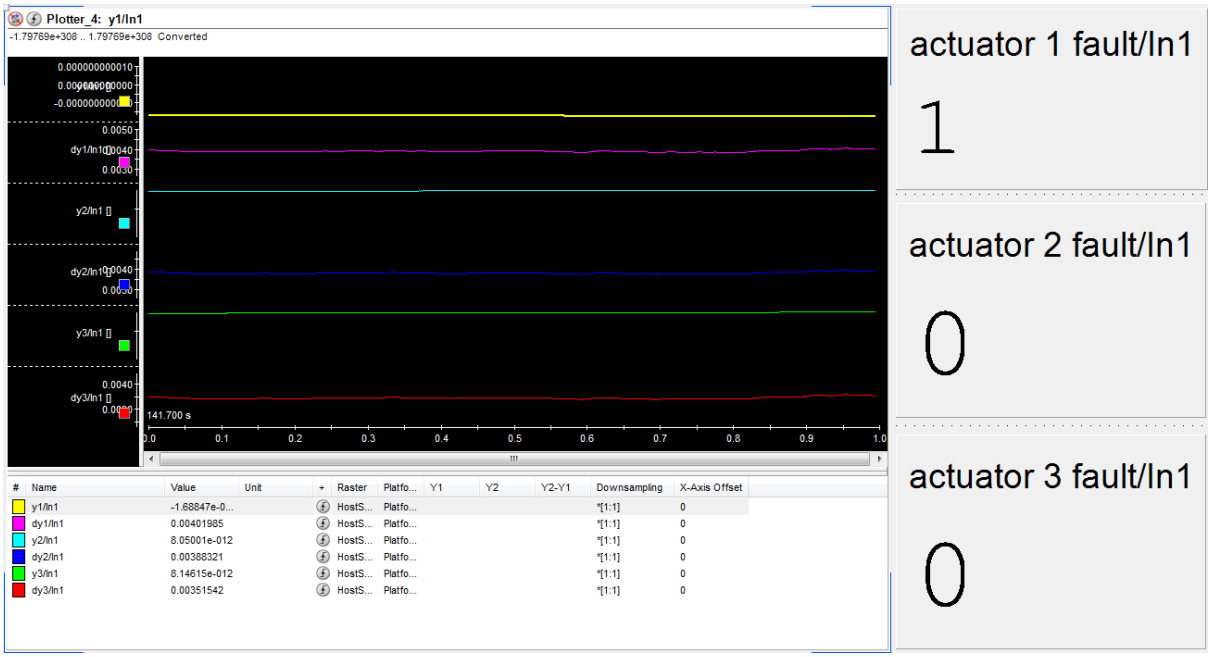

Figure 6.22 The experiment result for Actuator 1 fault of the physical system

In addition, the experiment data of the output residual for Actuator 1 fault can also be extracted to verify the result, which is shown in Figure 6.23.

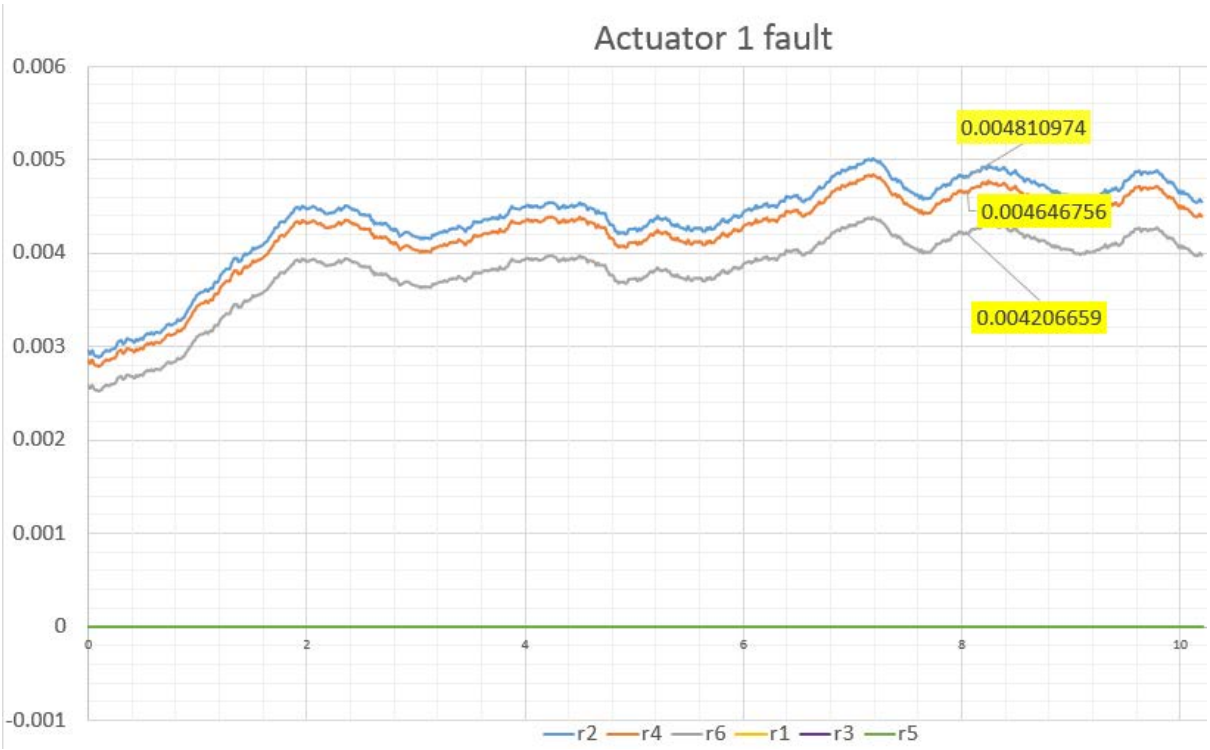

Figure 6.23 The experiment data of the output residual for Actuator 1 fault

From Figure 6.23, it shows that there exists fluctuation in the output residual, so the value of the output residual can be selected at a random time after the system becomes stable. The value

of the output residual is therefore selected when system operates to 8th second, and the value is [0; 0.004811; 0; 0.004647; 0; 0.004207], which is proportional to $\mathbf{Cf_1}$ as calculated in (6.18). This result also validates that the designed operable BJ filter is able to detect Actuator 1 fault successfully.

$$\text{output residual for Actuator 1 fault} = \begin{bmatrix} 0 \\ 0.004811 \\ 0 \\ 0.004647 \\ 0 \\ 0.004207 \end{bmatrix} = 0.0056 \times \mathbf{Cf_1} = 0.00558 \times \begin{bmatrix} 0 \\ 0.8623 \\ 0 \\ 0.8329 \\ 0 \\ 0.754 \end{bmatrix} \quad (6.18)$$

When disconnecting Actuator 2 (setting Actuator 2 gain to zero) of the system, the experiment result shown in Figure 6.24 validates that the designed operable BJ filter is able to detect Actuator 2 fault successfully.

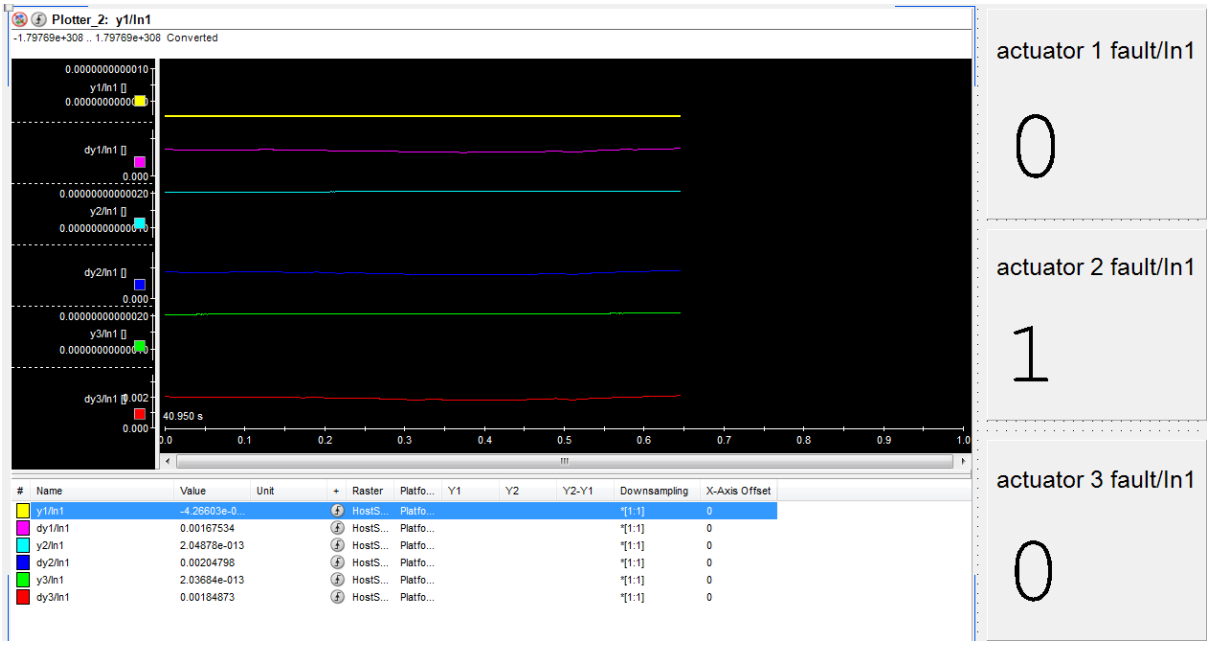

Figure 6.24 The experiment result for Actuator 2 fault of the physical system

In addition, the experiment data of the output residual for Actuator 2 fault can also be extracted to verify the result, which is shown in Figure 6.25.

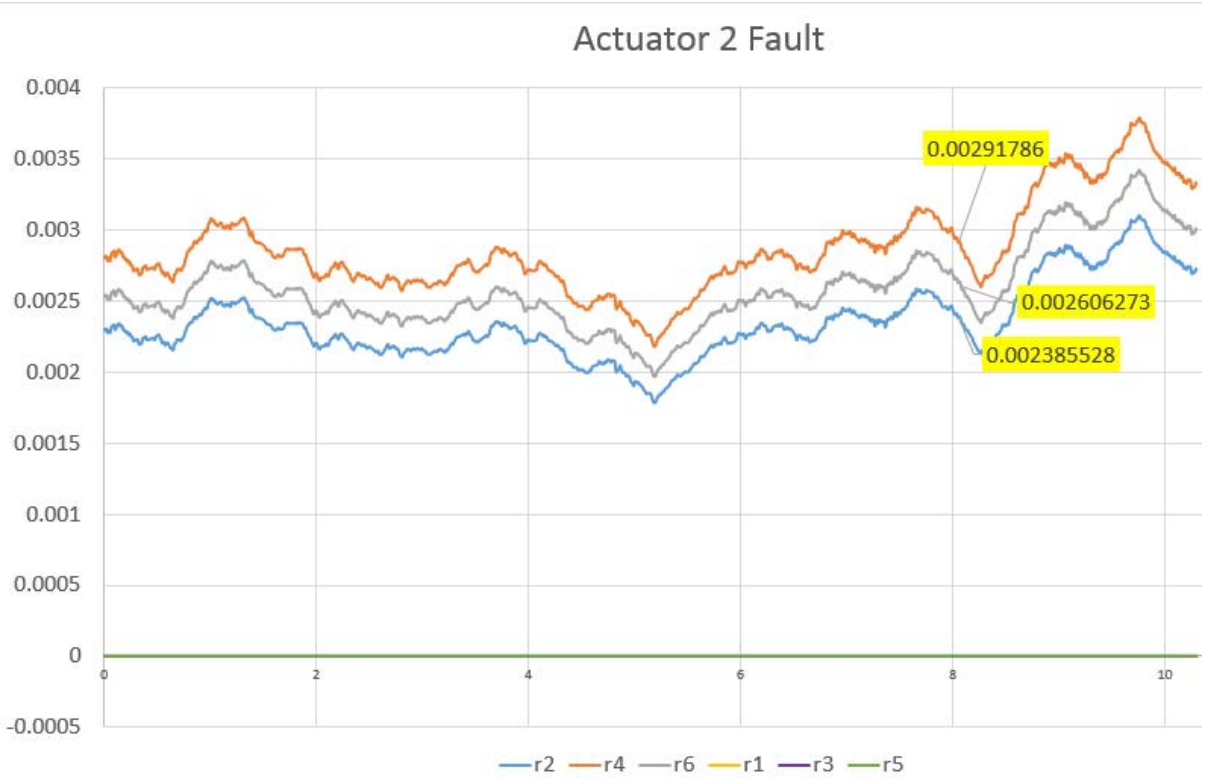

Figure 6.25 The experiment data of the output residual for Actuator 2 fault

From Figure 6.25, it shows that there exists fluctuation in the output residual, so the value of the output residual can be selected at a random time after the system becomes stable. The value of the output residual is therefore selected when system operates to 8th second, and the value is [0; 0.002385; 0; 0.002918; 0; 0.002606], which is proportional to $\boldsymbol{Cf_2}$ as calculated in (6.19). This result also validates that the designed operable BJ filter is able to detect Actuator 2 fault successfully.

$$\text{output residual for Actuator 2 fault} = \begin{bmatrix} 0 \\ 0.002385 \\ 0 \\ 0.002918 \\ 0 \\ 0.002606 \end{bmatrix} = 0.00286 \times \boldsymbol{Cf_2} = 0.00286 \times \begin{bmatrix} 0 \\ 0.8329 \\ 0 \\ 1.0181 \\ 0 \\ 0.9191 \end{bmatrix} \quad (6.19)$$

When disconnecting Actuator 3 (setting Actuator 3 gain to zero) of the system, the experiment result shown in Figure 6.26 validates that the designed operable BJ filter is able to detect Actuator 3 fault successfully.

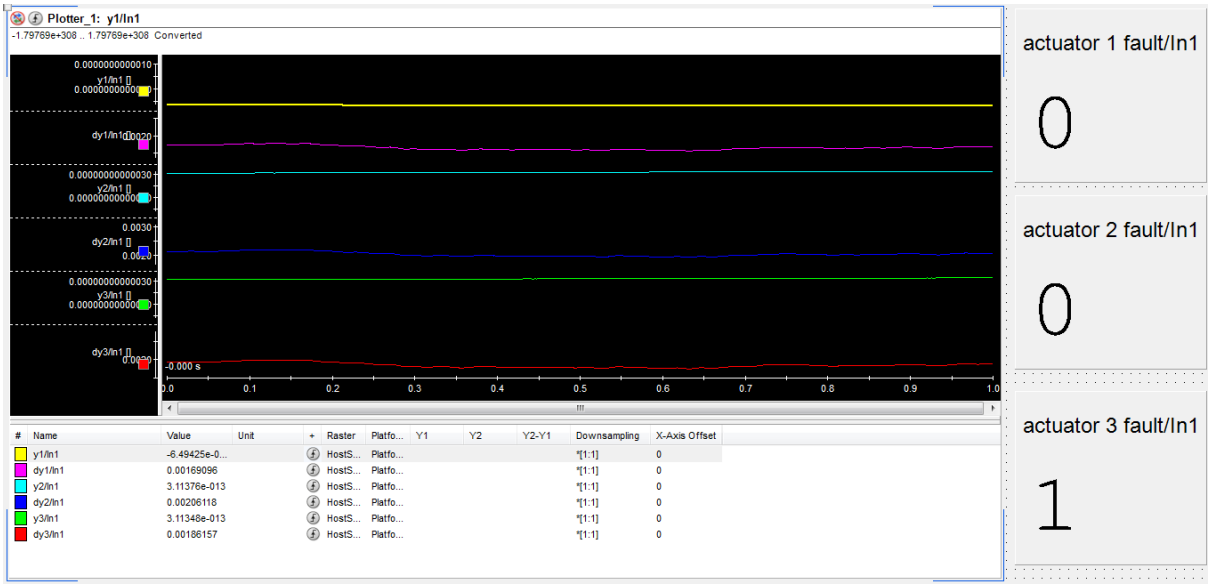

Figure 6.26 The experiment result for Actuator 3 fault of the physical system

In addition, the experiment data of the output residual for Actuator 3 fault can also be extracted to verify the result, which is shown in Figure 6.27.

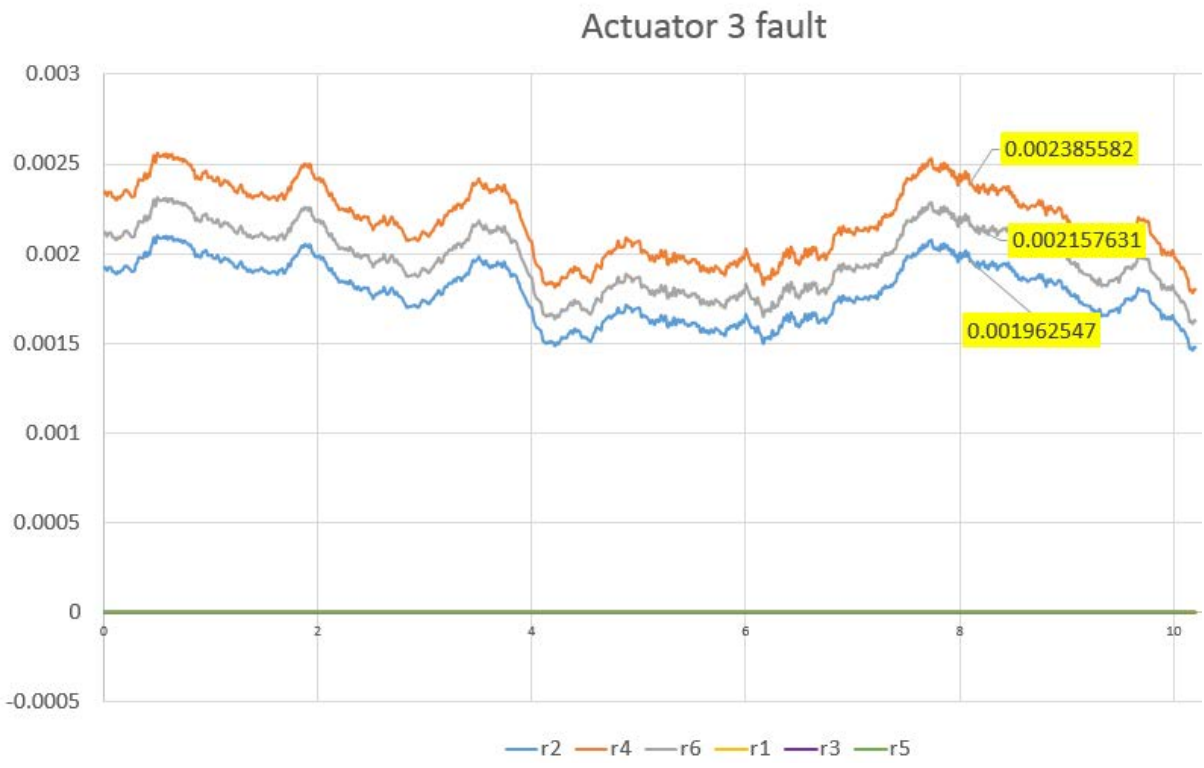

Figure 6.27 The experiment data of the output residual for Actuator 3 fault

From Figure 6.27, it shows that there exists fluctuation in the output residual, so the value of the output residual can be selected at a random time after the system becomes stable. The value of the output residual is therefore selected when system operates to 8th second, and the value is

[0; 0.001963; 0; 0.002385; 0; 0.002158], which is proportional to $\mathbf{Cf_3}$ as calculated in (6.20). This result also validates that the designed operable BJ filter is able to detect Actuator 3 fault successfully.

$$\text{output residual for Actuator 3 fault} = \begin{bmatrix} 0 \\ 0.001963 \\ 0 \\ 0.002385 \\ 0 \\ 0.002158 \end{bmatrix} = 0.0026 \times \mathbf{Cf_3} = 0.0026 \times \begin{bmatrix} 0 \\ 0.754 \\ 0 \\ 0.9191 \\ 0 \\ 0.8301 \end{bmatrix} \quad (6.20)$$

In conclusion, the experiment results validate the design and implementation of the proposed BJ fault detection and diagnosis system for real-time operation of the given MIMO plate control structure.

Chapter 7 : Conclusion

7.1 Project Conclusion

In this project, theoretical analysis and physical experiment are used to generate an acceptable transfer function model of a MIMO mechanical plate structure. Considering the real impact on the plate, a truncated transfer function model which only includes the first three modes is developed and this model can be regarded as a valid simplified mathematical model of the physical system. For the purpose of fault detection, a state-space representation of the system is developed based on the truncated transfer function model. Based on the BJ filter theory, a fault detection system is constructed by designing the detection gain **L** in one-fault case and multiple-fault case, and the BJ filter design principle and procedure are validated through simulating a random system with pre-defined fault vectors in MATLAB SIMULINK.

A conceptual BJ filter for the underlying plate control system is then designed and tested in MATLAB SIMULINK via different configurations (namely, SISO configuration – considering one pair of the inputs and outputs of the real system only, 2I2O configuration – considering two pairs of the inputs and outputs of the real system only, and MIMO configuration – considering all three pairs of the inputs and outputs of the real system, respectively). Simulation results show that the output residual associated with each fault vector $\boldsymbol{f_i}$ is indeed proportional to $\mathbf{C}\boldsymbol{f_i}$, thus, the designed conceptual BJ filters are able to detect the pre-defined faults in the real plate system successfully.

Upon the validation of the conceptual BJ filter design principle and procedure, an operable BJ filter is designed specifically for actuator fault detection of the given plate control system in real-time operations. In order to simulate each actuator fault, a specific fault matrix **F** ($[\boldsymbol{f_1} \quad \boldsymbol{f_2} \quad \boldsymbol{f_3}]$), where $\boldsymbol{f_i}$ (i=1, 2 and 3) equals to the corresponding column of matrix **B** and represents the i^{th} actuator fault of the i^{th} sensor/actuator pair, is developed for the real plate system. However, by simply setting matrix **F** equals to matrix **B**, the rank of **CF** will become zero which makes the faults non-separable. An extended 3I6O model is therefore proposed to replace the initial model of the real plate system for the BJ filter design purpose. The derivative of each output $Y_i(t)$ (i=1, 2 and 3) is introduced and extends the original 3I3O model into a 3I6O model. Benefiting from this alternation, the output matrix **C** is extended which makes the rank of **CF** non-zero. It is proven that the output residual (especially for the residual associated with $\dot{Y}_i(t)$ because the residual associated with $Y_i(t)$ are all zero**)** is proportional to $\mathbf{C}\boldsymbol{f_i}$ through

two simulation processes in MATLAB SIMULINK (introducing each fault vector to the system and artificially disconnecting each actuator). This result validates the design of the operable BJ filter as well as the construction of fault vectors. In addition, an improved fault detection system using operable BJ filter is successfully developed to achieve the online fault detection and identification.

After the designed operable BJ filter is successfully validated in the simulation, it is finally tested via experiment. For effective actuator fault detection and diagnosis, a dual BJ filter configuration is implemented where one BJ filter acts as an online observer of the given plate system by producing the extended system output $\dot{\boldsymbol{Y}}$ from the truncated model of the true plant, and another BJ filter acts as a fault detector and identifier by producing the required residual proportional to $\boldsymbol{Cf_i}$. This arrangement takes into account the inevitable modelling errors between the real plant and the modelled plant used for the BJ filter design purpose, and increases the accuracy of the fault detection and identification in practice. During the experiment, each actuator fault can be detected and identified online successfully, and three sets of experimental data also verify the design and implementation of the proposed BJ fault detection and diagnosis system for real-time operation of the given MIMO plate control structure.

7.2 Recommendations

The current experiment can be improved by designing a PCB board which enables the connecting wire between each actuator and dsPACE to be disconnected artificially. Rather than adding actuator gain into the SIMULINK model, this practice provides a more practical approach to simulate each actuator fault in real-time operation.

Due to time constraints, this thesis mainly focuses on the design of the fault detection system using BJ filter techniques for the actuator faults. However, there is a possibility for the future researchers to improve the fault detection system for sensor-fault detection.

Appendix A: MATLAB Code

The MATLAB codes for each section are kept within the Advanced Control Research Group, Flinders University. The MATLAB codes can be provided upon request.

Bibliography

[1] Edwards, C., Alwi, H. and Tan, C. (2012). Sliding mode methods for fault detection and fault tolerant control with application to aerospace systems. International Journal of Applied Mathematics and Computer Science, 22(1).

[2] Isermann, R. and Ballé, P. (1997). Trends in the application of model-based fault detection and diagnosis of technical processes. Control Engineering Practice, 5(5), pp.709-719.

[3] Zolghadri, A., Henry, D., Cieslak, J., Efimov, D. and Goupil, P. (2013). Fault Diagnosis and Fault-Tolerant Control and Guidance for Aerospace Vehicles. Advances in Industrial Control, pp.216.

[4] Mark, P. (2011). Chernobyl's legacy: twenty-five years after the nuclear disaster, the clean-up grinds on and health studies are faltering. Are there lessons for Japan?

[5] Mahmoud, M., Jiang, J. and Zhang, Y. (2003). Active fault tolerant control systems. Berlin: Springer.

[6] NTSB. (1979). Aircraft accident report - American airlines.

[7] Van Overschee, P. and De Moor, B. (1994). N4SID: Subspace algorithms for the identification of combined deterministic-stochastic systems. Automatica, 30(1), pp.75-93.

[8] Sinha, N. (1989). System identification—Theory for the user. Automatica, 25(3), pp.475-476.

[9] Verhaegen, M. (1994). Identification of the deterministic part of MIMO state space models given in innovations form from input-output data. Automatica, 30(1), pp.61-74.

[10] Wisnewski, P. and Doyle, F. (2001). Model-based predictive control studies for a continuous pulp digester. IEEE Transactions on Control Systems Technology, 9(3), pp.435-444.

[11] Luo, D. (2006). System Identification and Fault Detection of Complex Systems. Ph.D. University of Central Florida.

[12] Chen, Q. (2016). Vibration Cancellation in Plate Structures. Flinders university

[13] Stoer, J. and Bulirsch, R. (2013). Introduction to numerical analysis (Vol. 12). Springer Science & Business Media.

[14] Ogata, K. (2002). Modern control engineering. Upper Saddle River, NJ: Prentice Hall.

[15] Noura, H., Theilliol, D. and Ponsart, J. (2009). Fault-tolerant control systems. Dordrecht: Springer.

[16] Zhang, K. (2016). Performance Assessment for Process Monitoring and Fault Detection Methods. [S.l.]: MORGAN KAUFMANN.

[17] Michel, V., Stoyan, K., Redouane, H., Colin, J. and Hafid, S. (2010). Fault Tolerant Flight Control - A Survey. Lecture Notes in Control and Information Sciences.

[18] Chen, R. (2000). Fault detection filters for robust analytical redundancy. ph.D. University of California.

[19] Ferdowsi, H. and Jagannathan, S. (2013). A unified model-based fault diagnosis scheme for non-linear discrete-time systems with additive and multiplicative faults. Transactions of the Institute of Measurement and Control, 35(6), pp.742-752.

[20] Frank, P. (2009). Fault diagnosis for linear system. Control system, Robotics and Automation.

[21] Isermann, R. and Füssel, D. (1999). Supervision, Fault-Detection and Fault-Diagnosis Methods. Boston, MA: Springer.

[22] Hwang, I., Kim, S., Kim, Y. and Seah, C. (2010). A Survey of Fault Detection, Isolation, and Reconfiguration Methods. IEEE Transactions on Control Systems Technology, 18(3), pp.636-653.

[23] Blanke, M., Kinnaert, M., Lunze, J. and Staroswiecki, M. (2015). Diagnosis and fault-tolerant control. 3rd ed. Springer.

[24] Jones, H.L. (1973). Failure detection in linear systems. Ph. D. Massachusetts Institute of Technology.

[25] Beard, R. V. (1971). Failure accommodation in linear systems through self-reorganization. Ph. D. Purdue University

[26] Isermann, R. (2006). Fault diagnosis systems: an introduction from fault detection to fault tolerance. Berlin: Springer.

[27] Chen, J. and Patton, R. (1999). Robust model-based fault diagnosis for dynamic systems. Kluwer Academic.

[28] David, F., Beck, J. and Arnold, K. (1977). Parameter Estimation in Engineering and Science. Biometrics, 33(4), p.768.

[29] Chiang, L., Russell, E. and Braatz, R. (2002). Fault Detection and Diagnosis in Industrial Systems. Measurement Science and Technology, 12(10).

[30] Milliken, G., Bates, D. and Watts, D. (1990). Nonlinear Regression Analysis and Its Applications. Technometrics, 32(2), p.219.

[31] Ron, P., Frank, M. and Clark, N. (2000). Issue of Fault Diagnosis for Dynamic Systems. London: Springer-Verlag.

[32] Mehra, R. and Peschon, J. (1971). An innovations approach to fault detection and diagnosis in dynamic systems. Automatica, 7(5), pp.637-640.

[33] Basseville, M. and Benveniste, A. (1986). Lecture Notes in Control and Information Sciences: Detection of Abrupt Changes in Signals and Dynamical Systems. International Journal of Electrical Engineering Education, 24(1), pp.93-94.

[34] Gertler, J. (1997). Fault detection and isolation using parity relations. Control Engineering Practice, 5(5), pp.653-661.

[35] Isermann, R. (1994). On the applicability of model-based fault detection for technical processes. Control Engineering Practice, 2(3), pp.439-450.

[36] Patton, R. and Chen, J. (1994). Review of parity space approaches to fault diagnosis for aerospace systems. Journal of Guidance, Control, and Dynamics, 17(2), pp.278-285.

[37] Gertler, J. (1991). Analytical Redundancy Methods in Fault Detection and Isolation - Survey and Synthesis. IFAC Proceedings Volumes, 24(6), pp.9-21.

[38] Wunnenberg, J. (1990). Observer-based fault detection in dynamic systems. ph.D. University of Duisburg.

[39] Patton, R. and Chen, J. (1994). Review of parity space approaches to fault diagnosis for aerospace systems. Journal of Guidance, Control, and Dynamics, 17(2), pp.278-285.

[40] Clark, R., Fosth, D. and Walton, V. (1975). Detecting Instrument Malfunctions in Control Systems. IEEE Transactions on Aerospace and Electronic Systems, AES-11(4), pp.465-473.

[41] Simani, S., Fantuzzi, C. and Patton, R. (2003). Model-based fault diagnosis in dynamic systems using identification techniques, Springer: London.

[42] Ding, S. (2013). Model-based fault diagnosis techniques. London: Springer-Verlag.

[43] Chakradhar, B. (2006). Fault-tolerant Active Vibration Control. ph.D. Vanderbilt University.

[44] Tjanyadi, H. (2006). Adaptive Multi Mode Vibration Control of Dynamically Loaded Flexible Structures. M.Eng. Flinders University.

[45] Pratama, G. (2010). Characterization of Vibration of Two-Dimensional Rectangular Plate. B.Eng. Flinders University.

[46] Zhang, P. and He, F. (2017). Experimental implementation of a multi-input multi-output active vibration control on vibration isolation systems. In: 24th International congress on sound and vibration. London: London Calling.

[47] Tao, T., Byreddy, C. and Frampton, K. (2008). Experiments on Fault-Tolerant Active Vibration Control. Journal of Dynamic Systems, Measurement, and Control, 130(6), p.061006.

[48] White, J. and Speyer, J. (1987). Detection filter design: Spectral theory and algorithms. IEEE Transactions on Automatic Control, 32(7), pp.593-603.

[49] Kim, Y. and Park, J. (2003). A condition of the eigenvalues of detection filters for disturbance attenuation: an invariant zero approach. In: 42nd IEEE International Conference on Decision and Control.

[50] Kim, Y. and Park, J. (1999). An Analysis of Detection Spaces using Invariant Zeros. In: Proceedings of the American Control Conference. California.

[51] Kim, Y. and Park, J. (2005). On the approximation of fault directions for mutual detectability: an invariant zero approach. IEEE Transactions on Automatic Control, 50(6), pp.851-855.

[52] White, J. and Speyer, J. (1985). Detection Filter Design by Eigensystem Assignment. In: American Control Conference.

[53] Zhang, P. and He, F. (2017). MIMO PPF Active Vibration Control of Asymmetrical Plate Structures. In: The 13th IEEE Conference on Industrial Electronics and Applications. Wuhan.